Development of a three-dimensional microphysiological Retina-on-a-Chip system

Dissertation

zur Erlangung des Grades eines
Doktors der Naturwissenschaften

der Mathematisch-Naturwissenschaftlichen Fakultät
und
der Medizinischen Fakultät
der Eberhard-Karls-Universität Tübingen

vorgelegt
von

Jasmin Carmen Haderspeck
aus Heidenheim an der Brenz, Deutschland

Dezember - 2019

Tag der mündlichen Prüfung: 25. Juni 2020

Dekan der Math.-Nat. Fakultät: Prof. Dr. W. Rosenstiel

Dekan der Medizinischen Fakultät: Prof. Dr. D. Wallwiener

1. Berichterstatter: Prof. Dr. Stefan Liebau

2. Berichterstatter: Prof. Dr. Bernd Wissinger

Prüfungskommission: Prof. Dr. Stefan Liebau

Prof. Dr. Bernd Wissinger

Prof. Dr. Bernhard Hirt

Jun.-Prof. Dr. Peter Loskill

Erklärung / Declaration

Ich erkläre, dass ich die zur Promotion eingereichte Arbeit mit dem Titel:

„Development of a three-dimensional microphysiological Retina-on-a-Chip system",

selbständig verfasst, nur die angegebenen Quellen und Hilfsmittel benutzt und wörtlich oder inhaltlich übernommene Stellen als solche gekennzeichnet habe. Ich versichere an Eides statt, dass diese Angaben wahr sind und dass ich nichts verschwiegen habe. Mir ist bekannt, dass die falsche Abgabe einer Versicherung an Eides statt mit Freiheitsstrafe bis zu drei Jahren oder mit Geldstrafe bestraft wird.

I hereby declare that I have produced the work entitled

"*Development of a three-dimensional microphysiological Retina-on-a-Chip system",*

submitted for the award of a doctorate, on my own (without external help), have used only the sources and aids indicated and have marked passages included from other works, whether verbatim or in content, as such. I swear upon oath that these statements are true and that I have not concealed anything. I am aware that making a false declaration under oath is punishable by a term of imprisonment of up to three years or by a fine.

Tübingen, den ....

Datum / Date Unterschrift /Signature

Statement of contributions

1. Achberger K*, Probst C*, **Haderspeck J***, Bolz S, Rogal J, Chuchuy J, Nikolova M, Cora V, Antkowiak L, Haq W, Shen N, Schenke-Layland K, Ueffing M, Liebau S, Loskill P. *"Merging organoid and organ-on-a-chip technology to generate complex multi-layer tissue models in a human retina-on-a-chip platform."* Elife. 2019 Aug 27;8. (*contributed equally)

Publication on the retina-on-a-chip model described in this thesis. I contributed to the development of the concept. My contribution to the experiments performed were the generation and culture of all RPE cells, and part of the retinal organoids, loading of chips with RPE cells and culture of loaded chips, immunohistochemistry, visualization, RNA isolation of RPE cells, phagocytosis assay, ELISA assay, and drug treatment. Further, did I participate in the evaluation of the results and wrote parts of the manuscript. Figure 6, 7, 8, 9, 10, 11, 12, 13, 14, 15, 16, 17, 18 and 19 were adapted from this publication.

<u>Detailed contributions of authors to the results described in this thesis:</u>

- Conceptualization was performed by Achberger K, Probst C, Haderspeck J, Shen N, Schenke-Layland K, Ueffing M, Liebau S, Loskill P
- Writing, Review and Editing was performed by Achberger K, Probst C, Haderspeck J, Liebau S, and Loskill P.
- Evaluation of results was performed by Achberger K, Probst C. and Haderspeck J.
- Chip production was performed by Probst C, Rogal J and Chuchuy J at the Fraunhofer Institute for Interfacial Engineering and Biotechnology.
- Differentiation and culture of hiPSC-derived retinal organoids and RPE cells was performed by Haderspeck J, Achberger K, Nikolova M, Cora V and Antkowiak L.
- Loading and culture of chips was performed by Haderspeck J, Achberger K, Nikolova M, Cora V, and Antkowiak L.
- Electron microscopy was performed by Bolz S (Universitätsklinikum Tübingen, Institute for ophthalmic research).
- Immunohistochemistry of RPE cells and RPE chips was performed by Haderspeck J.

- Immunohistochemistry of chips was performed by Haderspeck J and Achberger K.
- RNA isolation of retinal organoids and RPE cells was performed by Haderspeck J and Achberger K.
- qRT-PCR was performed by Conrad S.
- Phagocytosis assays were performed by Haderspeck J and Achberger K.
- ELISA assay was performed by Haderspeck J.
- Drug testing of RPE and chips was performed by Haderspeck J, Achberger K, Nikolova M, Cora V, and Antkowiak L.

2. **Haderspeck JC***, Chuchuy J*, Kustermann S, Liebau S, Loskill P. *"Organ-on-a-chip technologies that can transform ophthalmic drug discovery and disease modeling."* Expert Opin Drug Discov. 2019 Jan;14(1):47-57. (*contributed equally)

Review on recent organ-on-a-chip models in the field of ophthalmology with special focus on existing retinal model system, their advantages, limitations and fields of improvement.
I contributed to the concept and writing of the manuscript, as well as the revision and editing.
Figure 1, 2 and 4 were adapted from this publication.

3. Achberger K*, **Haderspeck JC***, Kleger A, Liebau S *"Stem cell-based retina models*" Adv Drug Deliv Rev. 2019 Feb 1;140:33-50. (*contributed equally)

Review on different stem cell-based retinal models with focus on hiPSC-derived models, especially retinal organoids. I contributed to the concept and writing of the manuscript, as well as the revision and editing.
Figure 3 was adapted from this publication.

Table of content

List of abbreviations

%	Percentage
°C	Degree Celsius
2D	Two-dimensional
3D	Three-dimensional
AA	Antibiotics- antimycotics
AC	Amacrine Cells
AMD	Age-related macular degeneration
AMPA	α-amino-3-hydroxy-5-methyl-4-isoxazolepropionic acid
ANXA4	Annexin A4
ARR3	Arrestin3
ATOH = MATH5	Protein atonal homolog
ATP	Adenosine triphosphate
BC	Bipolar Cells
BEST1	Bestrophin 1
BRDM	B27-based retinal differentiation medium
BRN3	Brain-specific homeobox/POU domain protein 3
CASP3	Cleaved caspase 3
CDL	Chemically defined lipid
cDNA	Complementary DNA
CHX10 = VSX2	Ceh-10 homeodomain containing homolog / visual system homeobox 2
c-MYC	Myc Proto-Oncogene Protein
CNS	Central nervous system
CNTF	Ciliary neurotrophic factor
CO2	Carbon dioxide
CQ	Chloroquine
CRX	Cone-rod homeobox protein
CTRL	Control
d	Day
DAPI	4',6-diamidino-2-phenylindole

DMEM	Dulbecco's modified eagle medium
DNA	Deoxyribonucleic acid
dNTP	Deoxynucleotide
e.g.	Exempli gratia, for example
EB	Embryoid body
EEA1	Early Endosome Antigen 1
EGF	Epidermal growth factor
ELISA	Enzyme-linked Immunosorbent Assay
ESC	Embryonic stem cell
FBS	Fetal bovine serum
FGF	Fibroblast growth factor
g	Gravitational acceleration ~ 9.806 m/s^2
GABA	gamma-Aminobutyric acid
gDNA	Genomic DNA
GC	Ganglion cell
GCL	Gsnglion cell layer
GFP	Green fluorescent protein
GLUL	Glutamine Synthetase / Glutamate-Ammonia Ligase
GM	Gentamicin
GNAT1	G Protein Subunit Alpha Transducin 1
GNGT1	G Protein Subunit Gamma Transducin 1
Gp100	Melanocytes Lineage-Specific Antigen GP100
h	Hour(s)
HC	Horizontal cells
hESC	Human embryonic stem cells
hiPSC	Human induced pluripotent stem cells
HMBS	Hydroxymethylbilane synthase
HSA	Human serum albumin
IGF-1	insulin-like growth factor-1
ILM	Inner limiting membrane
INL	Inner nuclear layer
IPL	Inner plexiform layer

iPSC	Induced pluripotent stem cell
iPSCs	Induced pluripotent stem cells
IRBP	Interphotoreceptor Retinoid-Binding Protein, Retinol Binding Protein 3
ISLET-1	Insulin gene enhancer protein ISL-1
ITS	Insulin-transferrin-selenium
JAM	Junction adhesion molecule
k	Kilo
KLF4	Kruppel Like Factor 4
L-,S-,M- opsin	Long-wave sensitive opsin, short-wave sensitive opsin, middle-wave sensitive opsin
LAMP2	Lysosome-associated marker protein 2
LHX2	LIM/homeobox 2
LIF	Leukemia inhibitory factor / LIF Interleukin 6 Family Cytokine
min	Minutes
MITF	Microphthalmia-associated transcription factor
mJ	Milijoule
miRNA	microRNA
mRNA	Messenger RNA
NDS	Normal donkey serum
NEAA	Non-essential amino acids
NEUROD1	Neuronal Differentiation 1
NFL	Nerve fiber layer
NGF	Nerve groth factor
nl, µl, ml, l	Nanoliter, microliter, milliliter, Liter
nm, µm, mm	Nanometer, micrometer, millimeter
nM, µM, mM, M	Nanomolar, micromolar, millimolar, molar
NRL	Neural retina-specific leucine zipper protein
O2	Oxygen
OCT	Octamer-Binding Transcription Factor
OLM	Outer limiting membrane
ONL	Outer nuclear layer
OoC	Organ-on-a-chip

OPL	Outer plexiform layer
OS	Outer segment
OTX2	Orthodenticle Homeobox 2
OV	Optic vesicle
pmol	Picomole
p	Passage
PAX	Paired-box-gene
PBS	Phosphate-buffered saline w/o magnesium and calcium
PCR	Polymerase chain reaction
PDMS	Polydimethylsiloxane
PEDF	Pigment Epithelium-Derived Factor / Serpin Family F Member 1
PET	Polyethylene terephthalate
PFA	Paraformaldehyde
pH	Potentia hydrogenii
PHAL	Phalloidin
PI	Propidium iodide
PKC-α	Protein kinase C-α
PNA	Peanut
POS	Photoreceptor outer segments
PR	Photoreceptor
PRC	Photoreceptor cell
PRKCA	Protein kinase C-α
PROX1	Prospero homeobox protein 1
PRPH2	Peripherin-2
qRT-PCR	quantitative reverse transcription polymerase chain reaction
RA	Retinoic acid
RHOD	Rhodopsin
RNA	Ribonucleic acid
RO	Retinal organoid
ROs	Retinal organoids
RoC	Retina-on-a-chip
ROM1	Rod/retinal outer segment membrane protein 1

RPC	Retinal progenitor cells
RPE	Retinal pigmented epithelium
rpm	Rounds per minute
RT	Room temperature
RT-PCR	Reverse transcription polymerase chain reaction
RAX (RX)	Retinal homeobox protein Rx
s	Second(s)
S.E.M	Standard error of the mean
SHH	Sonic hedgehog signsling molecule
SIX3	Homeobox protein SIX3
SOX2	SRY-Box Transcription Factor 2
TGF	Transforming growth factor
VEGF	Vascular endothelial growth factor
VEGF-A	Vascular endothelial growth factor A
w/	With
w/o	Without
W	Watt
ZO1	Zonula occludens 1

Summary

The human retina is a complex neurosensory system that features multiple layers of different retinal neurons. Those neurons are arranged in a unique architecture and function to transmit a signal to the human brain that is interpreted as visual perception. Vision impairment is affecting millions of people worldwide while at the same time, for many disorders, pharmacological treatment options are not available or can only ameliorate the symptoms. To be able to investigate underlying disease mechanisms and to find new pharmacologic treatment options, new retina models are urgently required. Up to now, there are several different retinal model systems available, ranging from animal models to in silico as well as *in vitro* cell culture models. These systems differ considerably in their advantages and applicability. However, the limitations of each system lead to the consequence that a new and physiological accurate model system is necessary that is able to represent the human retina biology with all of its cell types as precisely as possible. Retinal organoids (ROs) as miniature "retina in a dish" have the potential to serve as new *in vitro* model system. They feature all retinal layers, can be generated from healthy human cells but also from patient material. Here especially, they can serve as disease model and allow to test potential treatment options. However, standard dish culture of these organoids leads to several limitations since the tissues' natural environment is not considered.

This thesis substantially contributed to the development of a new microfluidic retina-on-a-chip (RoC) system. For this purpose, we combined RO-technology with organ-on-a-chip technology (OoC). OoC technology uses microfluidic devices for cell-culture to simulate an organ-like physiology. We used ROs as well as retinal pigment epithelium (RPE) cells derived from human induced pluripotent stem cells by retinal differentiation to integrate them into a microfluidic chip system.

By first establishing individual culture chips for monoculture of RPE or ROs alone, we verified that both tissues are viable and can be cultured in the chip environment. Using immunohistochemistry and qRT-PCR we showed that characteristic markers expression is not affected and using electron microscopy that the typical morphology is preserved.

The chips were then combined into a co-culture RoC system, enabling the cultivation of ROs in close contact with RPE cells.

We verified that it was possible to bring both tissues into a physiological and close contact by analyzing the distance between RPE and RO inside the chip using live-cell imaging and immunohistochemistry.

Further, we found that the setup inside the RoC leads to improved segment formation in the photoreceptors of the ROs. This was shown in a qualitative fashion using immunohistochemistry and also in a quantitative fashion, using electron microscopic comparisons between dish-cultured and chip-cultured ROs. In this context, we also observed a positive impact of the presence of RPE inside the chip regarding photoreceptor segment formation.

As another functionality test to show a physiological setup, we analyzed the phagocytotic ability of the RPE cells for digestions of shed photoreceptors segments inside the RoC. Using live-cell imaging, immunohistochemistry and electron microscopy, we were able to confirm phagocytosis inside the RPE layer within the RoC.

Lastly, as a proof-of-principle study, we showed that the RoC is suitable as an *in vitro* drug-testing device for analysis of retinal toxicity. The known retinopathic effect of two different drugs, chloroquine and gentamicin, was verified by analyzing cell death with live-cell imaging of treated RoCs and subsequent quantitative comparison to non-treated RoCs. In the case of chloroquine, also the known lysosomotropic effect was verified using immunohistochemistry.

In summary, we have generated a new and physiological microfluidic retina-on-a-chip system that helps to improve RO generation and maturation. This system represents a new retinal model system and is suitable not only for testing of candidate or established drugs regarding retinal toxicity, but it has the outmost potential to serve as a disease model to identify new pharmacological treatment options as well as underlying disease mechanisms.

1. Introduction

1.1. The anatomy of the human eye

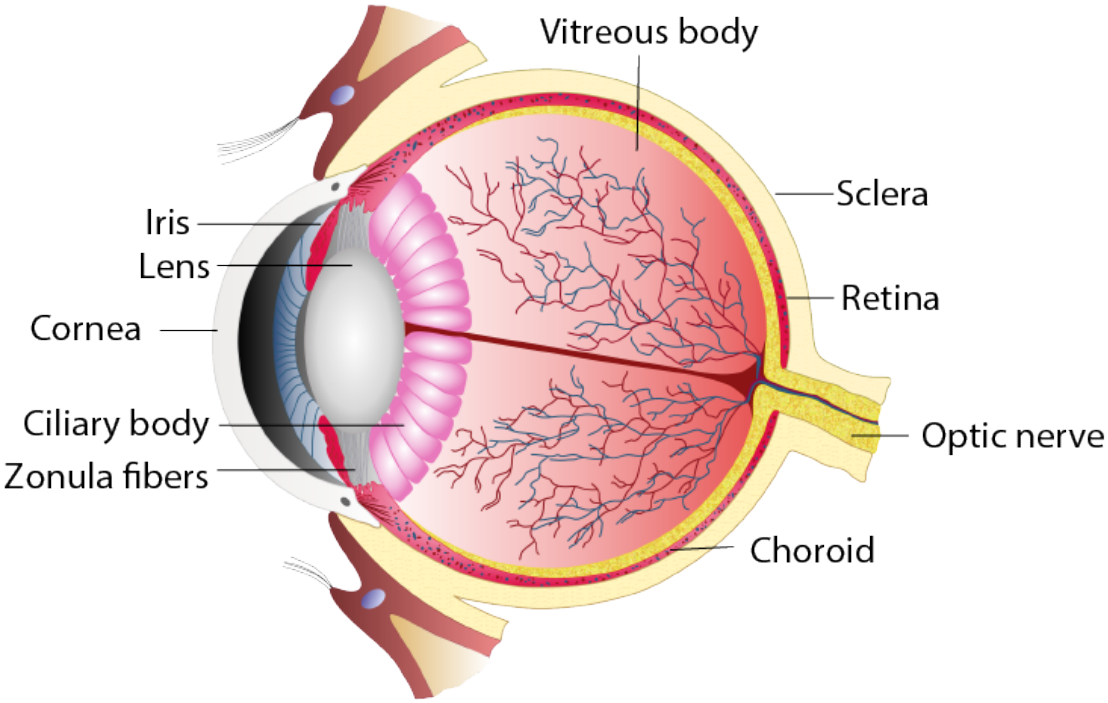

Figure 1: Anatomy of the human eye.

Anatomy of the human eye adapted from (Haderspeck et al., 2019) *showing the most important structures that are part of the three primary layers of the human eye. The external layer is formed by the sclera and the cornea (and conjunctiva). The intermediate layer consists of choroid, iris, ciliary body, zonula fibers and lens. The internal layer of the eye consists of the retina as neurosensory structure. The eyeball is filled by the vitreous body.*

The human eye is a slightly asymmetrical, spherical structure consisting of three primary layers (Kolb, 1995): The external, the intermediate and the internal layer as well as its accessory structures like the eye lids, the lacrimal apparatus, extra- and intraocular muscles (Kolb, 1995; Rehman and Bhimji, 2018). The cavity of this eyeball is filled with a gel-like mass called the vitreous body. For an overview on the anatomy of the human eye, see Figure 1.

The outermost layer consists of a dense and white fibrous tunic and is called sclera. It mainly provides structural stability and a window to the outside environment with the cornea as transparent structure at the anterior side (McCaa, 1982). Its transparency is only possible due to a specialized arrangement of cells and collagenous fibrils, due to the absence of blood

vessels and a state of relative dehydration (McCaa, 1982). Further, the anterior part of the eyeball, where the sclera is visible, is covered with a mucous membrane, called the conjunctiva, that also covers the inner surface of the eyelids (Estlack et al., 2017).

The intermediate layer of the eye is called the uvea and forms a vascularized layer at the posterior side, the choroid, necessary to provide nutrition especially to the inner layer. Moreover, the uvea also includes the iris, that acts as a diaphragm, and the ciliary body which regulates the shape of the lens during accommodation and further also produces aqueous humor (McCaa, 1982).

Finally, the complex neurosensory structure that is responsible for visual perception is found as the innermost layer of the eye and is called retina. Since this thesis focuses mainly on the generation and applicability of retinal cells, this tissue will be highlighted in greater detail within the next section.

1.1.1. Anatomy and physiology of the human retina

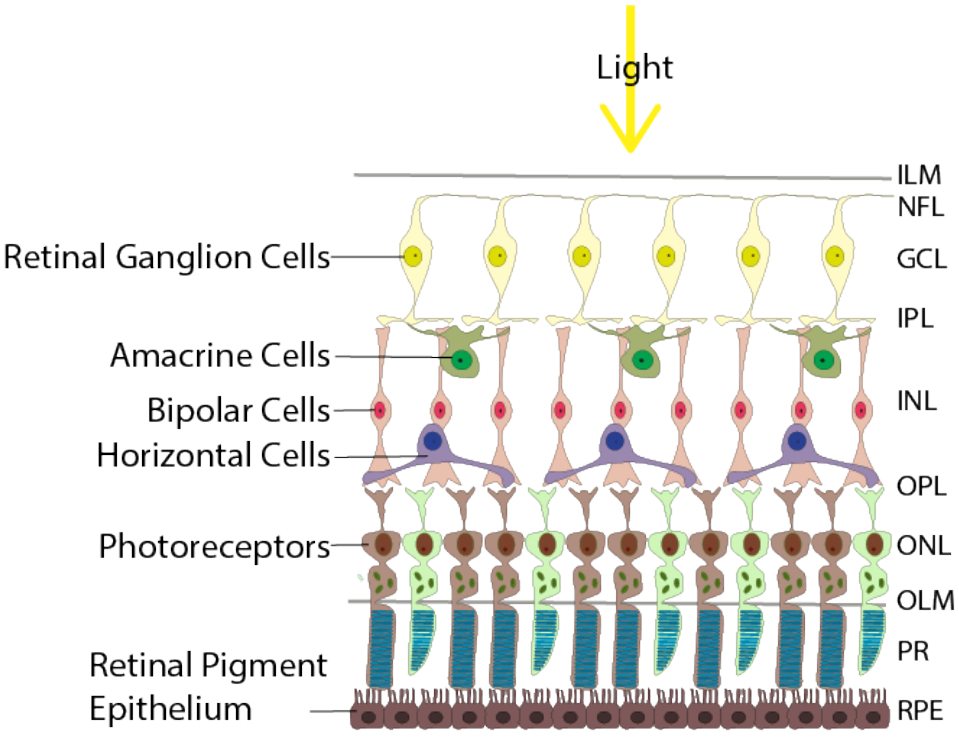

Figure 2: The layers of the human retina.

The layers of the retina adapted from (Haderspeck et al., 2019) *showing the inner limiting membrane (ILM), the nerve fiber layer (NFL), the retinal ganglion cell layer (GCL), the inner plexiform layer (IPL), the*

inner nuclear layer (INL), the outer plexiform layer (OPL), the outer nuclear layer (ONL), the outer limiting membrane (OLM), the photoreceptor (PR) layer and the retinal pigment epithelium (RPE).

The retina consists of three cellular layers with plexiform layers for synaptic transmission in between as well as limiting membranes to border the retinal tissue. A detailed representation of the retina is depicted in Figure 2 including: the inner limiting membrane (ILM); the nerve fiber layer (NFL); the retinal ganglion cell layer (GCL); the inner plexiform layer (IPL); the inner nuclear layer (INL); the outer plexiform layer (OPL); the outer nuclear layer (ONL); the outer limiting membrane (OLM); the photoreceptor (PR) layer. The non-neural part of the retina is formed by the retinal pigment epithelium (RPE) (Hoon et al., 2014; Kels et al., 2015; McCaa, 1982).

The light signal as the visual stimulus enters the eye and is refracted by three structures including the cornea, the lens and the vitreous body, to be then focused onto the retina. It is then absorbed by photopigments in the outer segments of the photoreceptor cells and converted into an electrical stimulus (Purves and Williams, 2001). Further, this signal is passed through the outer plexiform layer (OPL), where synaptic transmission occurs, and then to the inner nuclear layer (INL), where the cell bodies of the three main classes of interneurons reside, that further integrate and modulate the signal (Purves and Williams, 2001). These interneurons are the bipolar cells, the amacrine cells and the horizontal cells (Purves and Williams, 2001). Finally, the modified signal is passed via synapses in the inner plexiform layer (IPL) to the retinal ganglion cells inside the ganglion cell layer (GCL) (Purves and Williams, 2001). These cells have long axons, forming the optic nerve, that is responsible for transmission of the visual information to the brain (Purves and Williams, 2001). Besides the neurons inside the retina, also glial cells can be found, including microglia, astrocytes as well as Müller glia that fulfill a multitude of different functions (Bringmann et al., 2006; de Souza et al., 2016). The non-neural part of the retina is formed by a pigmented layer for light absorption called retinal-pigment epithelium (RPE) that is located distally to the photoreceptor outer segments.

1.1.2. Cell types of the retina

As previously mentioned, the retina consists of five major classes of neuronal cells, as well as additional cell types like Müller glia and RPE cells (Hoon et al., 2014). This paragraph will

discuss the characteristics of the main cell types relevant for this thesis, including their main functions. In addition, each cell type's typically expressed marker proteins are mentioned, which plays an important role for verification of different cell types in this study.

1.1.2.1. Photoreceptor cells

Photoreceptor cells make up the vast majority of cell types in the retina and have a very unique and polarized structure, divided into an inner and outer segment by a connecting cilium (Li et al., 2015; Molday and Moritz, 2015). While the inner segment contains most of the photoreceptor cell's organelles, the outer segment consists of stacks of membrane disks that contain photopigments to absorb light (Molday and Moritz, 2015). The transformation of photons of light into an electrical signal is initiated in the photoreceptor outer segments via conformational change of the vitamin A-derivate retinal, that is bound to an opsin protein leading to a signal cascade (Baylor, 1996; Molday and Moritz, 2015; Purves and Williams, 2001). This process, called phototransduction, ultimately leads to photoreceptor hyperpolarization and therefore to a reduced release of the photoreceptors' neurotransmitter glutamate (Purves and Williams, 2001; de Souza et al., 2016). As a consequence, this graded transmitter release results in action potentials and signal transmission in the downstream retinal neurons (Purves and Williams, 2001).
Photoreceptor cells are classified into rod and cone photoreceptors with both classes differing in light and wavelength-specific sensitivity depending on the opsin-type present (Hoon et al., 2014; de Souza et al., 2016). While rods are very sensitive to light and therefore responsible for dim-light scotopic vision, cones are less sensitive in general, but each cone photoreceptor type has specific wavelength sensitivity (Hoon et al., 2014). Hence, cone photoreceptors are mainly used for photopic vision under bright-light conditions and are capable of high-acuity color vision (Hoon et al., 2014).
Rod and cone photoreceptors also divide the signal pathway through the retina into two separate pathways, the rod and cone pathway, that both involve specific kinds of subtypes of bipolar cells, amacrine cells and ganglion cells and are responsible for processing different kinds of visual stimuli (de Souza et al., 2016).
Photoreceptor cells are often identified using specific markers for the opsin protein they express. For example, the opsin present in rods that is called rhodopsin, is an obvious and

very specific marker for rod photoreceptor cells (de Souza et al., 2016). Cones on the other hand, either express opsins with long (L), medium (M), or short (S) wavelength sensitivity and can be marked accordingly (de Souza et al., 2016). Moreover, all proteins involved in the signal cascade of phototransduction can be used as markers, including e.g. transducin, arrestin, or recoverin (Lerea et al., 1989; de Souza et al., 2016).
As specific marker proteins for photoreceptor outer segments, ROM-1 as well as peripherin-2 (PRPH2), both homologous membrane proteins of the disk rims, can be used (Clarke et al., 2000).

1.1.2.2. Interneurons of the retina

The bipolar cells are the interneurons responsible for vertical signal transmission from the photoreceptors to the ganglion cells (de Souza et al., 2016). As their name implies, they have a bipolar morphology, forming synapses on both sides. Bipolar cells can be further subdivided into several different cone bipolar cell types and one rod bipolar cell type (de Souza et al., 2016), moreover, also according to whether they hyperpolarize (OFF-BCs) or depolarize (ON-BCs) in response to a light stimulus (de Souza et al., 2016). This subdivision presents itself on the level of characteristic marker expression. Protein kinase C-α (PKC-α PRKCA) is a typical marker for rod BCs (Haverkamp et al., 2003). Its colocalization with ISLET-1, a marker for all ON-BCs, allows to discriminate the rod from the cone ON-BCs (de Souza et al., 2016). One typical marker used to label OFF-BCs is calbindin (Haverkamp et al., 2003; de Souza et al., 2016).

Horizontal cells and amacrine cells are the interneurons involved in horizontal signal transmission, also called the “lateral” pathway, responsible for modulating the vertical signal (de Souza et al., 2016).
The role of the horizontal cells in this context is negative feedback to cones and bipolar cells through inhibitory synapses after receiving an excitatory input from photoreceptors (de Souza et al., 2016). Calbindin and ISLET-1 are also markers that can be used for horizontal cell, in addition to bipolar cells. The homeodomain protein PROX1, which regulates progenitor proliferation, was shown to be a marker of developing horizontal cells but for amacrine cells as well (Dyer et al., 2003; Pérez de Sevilla Müller et al., 2017).

Amacrine cells are in contact with bipolar cells and ganglion cells, as well as other amacrine cells (de Souza et al., 2016). This cell type can be identified by markers for inhibitory synapses like GABA and glycine (de Souza et al., 2016). With more than 24 different types, amacrine cells have the highest number of known subtypes that have been identified so far, based on morphology (Kolb et al., 1992). The most common type, the A*II* amacrine cells that mediate the rod pathway, are positive for the marker calretinin in humans (de Souza et al., 2016).

1.1.2.3. Ganglion cells

Ganglion cells are the last neurons of the retina before the visual signal is transmitted to higher visual centers via their long axons that are bundled as the optic nerve (Hoon et al., 2014; Purves and Williams, 2001). The ganglion cells receive input from bipolar cells as well as amacrine cells (de Souza et al., 2016). Different subtypes of retinal ganglion cells are categorized based on their projections to different layers of the lateral geniculate nucleus, or based on their response to light or their morphology (Baden et al., 2016; Farrow and Masland, 2011; Xiang et al., 1995). The existence of these different retinal ganglion cell subtypes that are involved in different pathways is a prerequisite for some of the most complex features of the retina, such as color vision, fine feature analysis, or direction selectivity (Elstrott et al., 2008; Masland, 2012; Shapley and Hugh Perry, 1986; de Souza et al., 2016; Yin et al., 2009).

Since this cell type has long axonal processes, typical neuronal markers, such as the microtubule marker beta-III tubulin, can be used to identify retinal ganglion cells (Jiang et al., 2015). The most common markers for ganglion cells, however, are the POU-domain proteins of the BRN3 family that are essential transcription factors. In addition, the BRN3 expression patterns allow a cell subtype specification (Sajgo et al., 2017; de Souza et al., 2016; Xiang et al., 1995). A very specific subtype of retinal ganglion cells, the intrinsically photosensitive ganglion cells can be marked using antibodies against melanopsin (Dacey et al., 2005).

1.1.2.4. Müller cells

Müller glia are the major glia cell type of the retina, spanning all layers and forming a sheath around all retinal neurons (Bringmann et al., 2006). The processes of Müller glia also form the so-called inner and outer limiting membrane (ILM and OLM) that are essential as distal and proximal barriers of the retina and to separate an ionically distinct compartment (Massey, 2006). Thus, Müller glia keep the structural integrity of the retina through mechanical strength (Omri et al., 2010).

Moreover, Müller cells also play several essential roles for homeostatic and metabolic support e.g. by providing nutrition to retinal neurons, by regulating ion and water homeostasis and recycling of neurotransmitters (Bringmann et al., 2006; Hoon et al., 2014). Glutamine synthetase (GLUL) is an enzyme that is expressed by Müller glia to break-down the neurotransmitter Glutamate released from retinal neurons and is therefore one of the most commonly used markers for this cell type (Bringmann et al., 2006). Further, the annexin family of angiogenic and anti-inflammatory proteins was identified by proteomic profiling of Müller cells and allows them to be distinguished from microglia cells (Grosche et al., 2016). The member of this family used as a marker in this work was Annexin A4 (ANXA4). In the OLM, typical adherens junction and tight junction proteins can be found as marker proteins, such as zonula occludens 1 (ZO1), occludin and junction adhesion molecule (JAM) (Omri et al., 2010).

1.1.2.5. Retinal pigment epithelium

Another part of the retina is the pigmented monolayer of quasi-hexagonal cells, which is located adjacent to the photoreceptor cells, and is referred to as RPE (Kiser et al., 2014). In these cells, the pigment melanin is found in granules called melanosomes and is essential to absorb scattered light. Therefore, it is of obvious importance to improve the quality of the light signal (Purves and Williams, 2001; Strauss, 1995). But besides this central function, the RPE fulfills many other tasks that are especially important for the survival of photoreceptor cells (Molday and Moritz, 2015).

The RPE forms tight junction barriers and in this way, is part of the blood-retinal barrier, allowing selective transport of water and metabolic products coming from the retina, as well as transport of nutrients and vitamin A towards the retina (Steinberg, 1985; Strauss, 1995).

Further, the epithelial transport via the RPE controls ion homeostasis in the subretinal space (Strauss, 1995). Another function of RPE is the communication with both neighboring tissues, the retinal cells on one side and the endothelium of the choroid on the other side (Steinberg, 1985; Strauss, 1995). This communication happens via secretion of different signaling molecules, for example ATP, fibroblast growth factors (FGFs), insulin-like growth factor-1 (IGF-1), vascular endothelial growth factor (VEGF) or pigment epithelium-derived growth factor (PEDF). VEGF is a factor that is released towards the basolateral side of the cell, which means towards the choroid. VEGF as secreted factor mediates paracrine survival signals for the fine fenestrated endothelium of the choriocapillaries (Witmer et al., 2003). A factor that is secreted predominantly to the retinal, apical side of the RPE is PEDF, a neurotrophic factor that even has a protective effect against retinal injury and ischemia (Becerra et al., 2004; Ogata et al., 2001).

This functional polarization also appears as a morphological polarization of the cells, since prominent microvilli processes are only formed on the apical side, to increase surface contact with the outer segments of photoreceptors (Kiser et al., 2014). As a marker for this apical microvilli formation, the membrane protein Ezrin can be used (Kivelä et al., 2000). Further signs of the characteristic RPE polarization is, for example, the basolateral expression of the ion channel Bestrophin 1 (BEST1) (Kay et al., 2013; Marmorstein et al., 2000).

Moreover, a functional interaction of photoreceptors and RPE cells is necessary for the visual cycle. The visual cycle involves the regeneration of the chromophore retinal that is required for light absorption in its 11-cis form in the photoreceptor outer segments (Kiser et al., 2014). Via photoisomerization, 11-cis retinal changes its conformation into all-trans retinal which dissociates from rhodopsin and needs to be isomerized back into its 11-cis conformation via several intermediate steps (Kiser et al., 2014). Part of this enzymatic re-isomerization is performed by the retinoid isomerase RPE65 and takes place in the RPE cells, and therefore retinal needs to be shuttled to and from the RPE (Kiser et al., 2014; Molday and Moritz, 2015; Saari, 2012).

The process of photo-oxidation in the photoreceptor outer segments inevitably leads to damage to the segment tips (Kevany and Palczewski, 2010). Therefore, photoreceptors constantly shed their tips and renew their outer segments from the base to stay functional

(Kevany and Palczewski, 2010). These shed outer segment tips are phagocytosed by the RPE cells and unnecessary material is degraded (Steinberg, 1985).

To summarize, the turnover of outer segments, the maintenance of photoreceptor cells as well as many other interactions between RPE and the neural retina shows the importance of this simple monolayer of pigmented cells for vision.

1.2. Development of the human retina

In this thesis, we used retinal cells that have been derived from stem cells via retinal differentiation. Therefore, it is essential to understand the normal process of retinal development *in vivo* to then be able recapitulate this process *in vitro* and classify the stage of retinal maturity within our model system. A schematic timeline of embryonic development including the formation of the retina is provided in Figure 3.

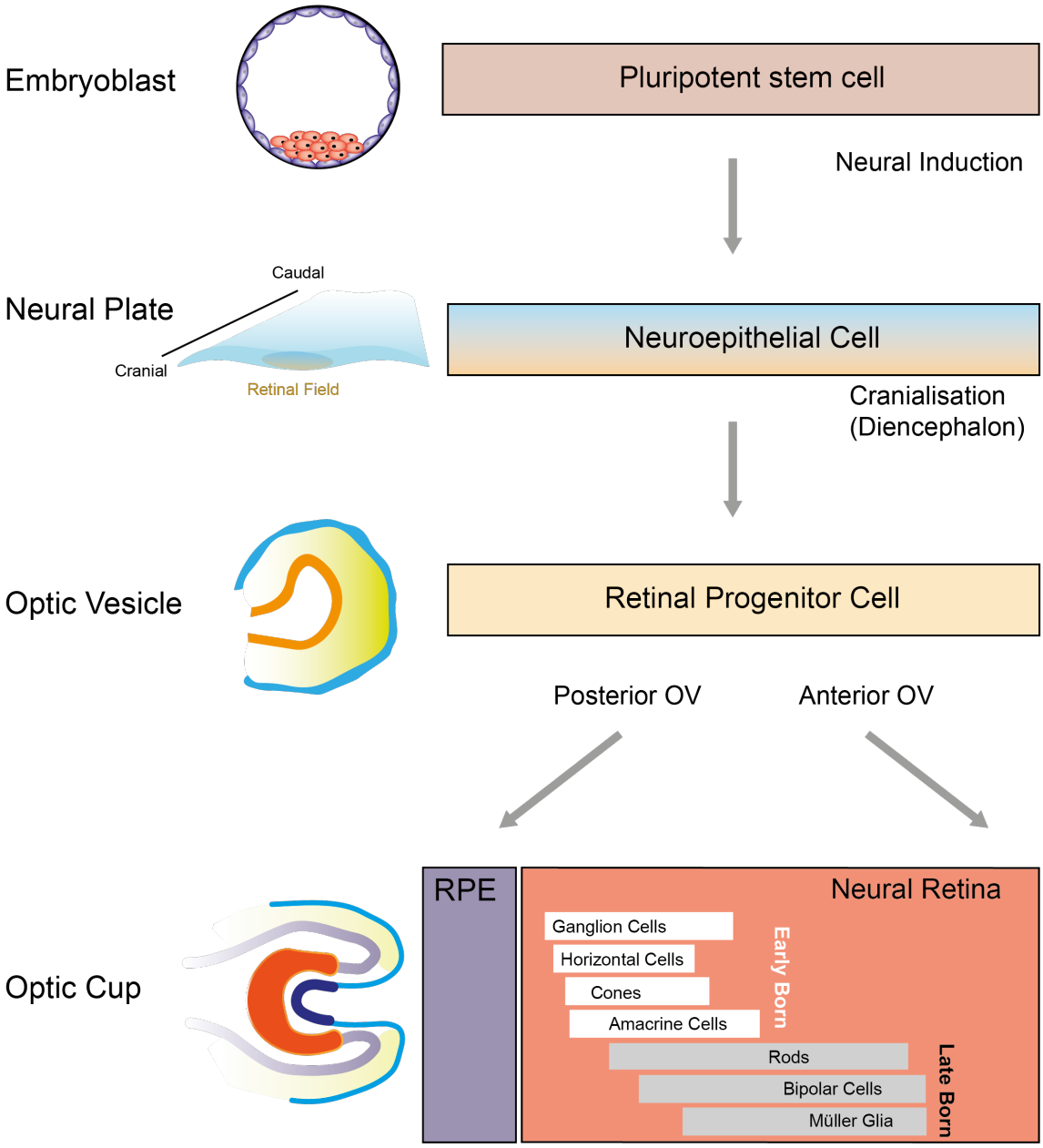

Figure 3: Development of the human retina.

Some of the pluripotent stem cells from the inner cell mass (the embryoblast) of the blastocyst will be directed to become neuroectoderm. Neural induction leads to formation of the neural plate that contains neuroepithelial cells. A retinal field develops at the cranial end of the neural plate. Optic vesicles (OV) appear as evaginations from the retinal field. Retinal progenitor cells can be found in the OV. The anterior part of the OV that will develop into neural retina invaginates to form the optic cup. Posterior parts of the optic cup will develop into RPE. Figure adapted from Achberger et al., 2019a.

Eye development in humans starts around day 22 of embryonic development (Paquette et al., 2009) (Figure 3). The retina is derived from the developing diencephalon during the stage of the neural plate when the neural tube starts to form (Fuhrmann, 2010; Purves and Williams, 2001). At this time, first retinal progenitor cells (RPCs) can be found inside a single retinal field at the cranial end of the neural plate (Li et al., 1997). Towards the rostral side, evaginations are formed that are initially called optic grooves. While the neural tube develops through an upfolding of the neural plate, these optic grooves on each side evaginate further and are referred to as optic vesicles (OV) after that event (Kolb, 1995; Lamb et al., 2007). The developing vesicle is in contact with parts of the surface ectoderm (the lens placode), leading to the induction of further differentiation steps in both tissues (Fuhrmann, 2010; Lamb et al., 2007). Subsequently, the optic vesicles are folding inwards to form a cup-like structure referred to as optic cup. Later, the inner layer of this cup forms the neural part of the retina, while the outer layer forms the RPE (Fuhrmann, 2010). Meanwhile, the surface ectoderm is folding in towards the optic cup and develops the lens. Consequently, retina and lens have different developmental origins. After both layers of the optic cup are in contact, early retinal ganglion cells start to send their axons out crossing the retinal surface. The eye cup continues growing and finally seals at the region of the choroidal fissure (Fuhrmann, 2010; Lamb et al., 2007).

However, the cells of the developing retina are not born at the same time. Moreover, the order in which the different retinal cell classes appear during development seems to be a highly conserved mechanism in all vertebrates (Lamb et al., 2007). Retinal ganglion cells, horizontal cells, amacrine cells, as well as cone photoreceptors are born first and therefore referred to as “early-born” retinal neurons, while rod photoreceptors, bipolar cells, and Müller glia are “late-born” retinal cells (Bassett and Wallace, 2012). Nevertheless, despite their different time points of cell genesis, all retinal neurons, the RPE as well as the Müller glia, are generated from the multipotent retinal progenitor cells (RPCs) mentioned before.

1.2.1. Characteristic marker expression during retinal differentiation

Both, tissue-tissue interactions, as well as intrinsic signals play important roles throughout the process of retinal development (Fuhrmann, 2010). Here, some of the most important

specific extrinsic and intrinsic signals will be described with focus on the transcription factors involved since they also represent important markers for developing retinal cells. Regulatory marker molecules are important within this work to identify retinal cell types and also to stage their maturity and are therefore mentioned in greater detail.

Early retinal progenitor cells at the optic vesicle stage express the transcription factors CHX10 (ceh-10 homeodomain containing homolog, also called VSX2, visual system homeobox 2) and MITF (microphthalmia-associated transcription factor). While the RPE continues to express MITF, its expression is downregulated in the developing neural parts of the retina, predominantly due to FGF signaling (Nguyen and Arnheiter, 2000).
The sequence in which retinal cells are born follows a defined chronological order and a hierarchical gene regulation mechanism (Marquardt, 2003; Mu and Klein, 2004). These RPCs show a multipotent differentiation ability that allows them to generate different retinal cell types (Marquardt, 2003; Wetts and Fraser, 1988). Throughout this process they are adopting a series of defined and irreversible competence states influenced by secreted factors including TGFβ, EGF, SHH, NGF, LIF, and CNTF (Bassett and Wallace, 2012; Marquardt, 2003). At the top of this hierarchical network are homeobox transcription factors like PAX6, RAX, CHX10, SIX3 and LHX2 which are expressed in all retinal progenitors (Marquardt, 2003; Mu and Klein, 2004). PAX6 in this context plays an important role during eye field specification and keeps RPCs in their multipotent state (Marquardt et al., 2001; Mu and Klein, 2004).
For each specific retinal cell type, there are several key intrinsic regulators directing the cell fate. For example, photoreceptor cell fate is determined by transcription factors such as NRL, CRX and OTX2 whereas ATOH7 (MATH5), ISLET-1, NEUROD1 and BRN3 are involved in retinal ganglion cell-differentiation (Bassett and Wallace, 2012).

1.3. Retinal model systems

1.3.1. Overview on existing retinal model systems and their limitations

To highlight the necessity for a new and physiological accurate human retinal model system, this chapter will briefly summarize existing model systems in the field, explain their

applications and point out the limitations of the respective system. Existing systems include animal models (*in vivo*), theoretical models (*in silico*), retinal explants (*ex vivo*), 2D and 3D *in vitro* models.

Figure 4: Overview on existing retinal model systems.

Current retinal model systems include animal models (in vivo), theoretical or mathematical models (in silico), explant cultures (ex vivo), as well as 2D and 3D cell culture models (in vitro). Figure adapted from (Haderspeck et al., 2019).

1.3.2. Animal models

According to J.C. Zeiss, professor of comparative medicine, a suitable animal model *"elucidates some fundamental aspects of a human disease to promote greater understanding of its mechanism"* (Zeiss, 2013).

For disease modeling, where hereditary or transgenic models are usually required, rodents are still one of the most widely used model systems (Kompella et al., 2010). There are many mouse strains available to study retinal disease and development, especially concerning microphthalmia, glaucoma or genetic retinal degeneration (Hafezi et al., 2000; Zeiss, 2013). Besides, for every specific experimental ocular disease, different animal model systems are favored and necessary. For this reason, for example primates are the primarily used species in age-related macular degeneration (AMD) studies (Turgut and Karanfil, 2017). Pharmacokinetic studies for ophthalmic drug development on the other hand, rely on testing animals like dogs, pigs, rabbits or monkeys, mainly because of the size of the eye that is comparable to the human eye (Kompella et al., 2010; Zeiss, 2013). However, pharmacokinetic data require a large number of animals to be tested, consume a large amount of time and money, but still are currently essential for drug approval (Kompella et al., 2010). However, even between these species, ocular drug delivery can differ significantly (Proksch et al., 2009) and scaling or mathematical models can only account for these inter-species differences up to some degree (Amrite et al., 2008). In general, the broader anatomy and physiology of the eye between different vertebrates is preserved, but there are still major differences and unique features that are the reason why animals cannot fully represent the human ophthalmic system (Zeiss, 2013). This is especially true for the retina and its macula where great differences can be observed. Mice, for instance, completely lack a macula (Zeiss, 2013).

To conclude, limitations of animal experiments eventually include ethical issues, cost, and time-consumption and also major differences in anatomy or physiology compared to the human eye (Barar et al., 2009). Further, many countries today have legislative restrictions which confine the number of animals in experiments to be used.

1.3.3. Theoretical model systems

Theoretical model systems include mathematical or computational models. These models are often designed to add value where traditional animal models show weaknesses, or to show ocular phenomena from a totally different perspective and are useful to test hypotheses (Roberts et al., 2016).

The physiology of the healthy retina, retinal development, as well as the retina in a diseased state can be modeled in this regard (Roberts et al., 2016). For example, for disorders like retinitis pigmentosa or AMD, different models were established to test different hypotheses for disease progression or for potential treatment options (Roberts et al., 2016).

In some cases, mathematical and computational models allow the extrapolation from one species to another, for example after testing the pharmacokinetic properties of a drug in an animal model (Amrite et al., 2008). Thus, the use of pharmacokinetic and pharmacodynamic mathematical models can speed up drug discovery and also drug development and might help to reduce the number of animals tested (del Amo et al., 2017).

However, there is still a long way to go until detailed pathomechanisms as well as pharmacokinetic and pharmacodynamic aspects of a drug can be modeled without any living cell to be involved and future work will require cooperation of theorists and clinicians to find useful strategies in this regard.

1.3.4. Explant culture

The term explant culture is used for tissues sections that are removed using surgery and then kept in cell culture for limited periods of time depending on culture conditions like cultivation atmosphere or culture medium composition (Resau et al., 1991). Human or animal explant cultures of the eye have been used for retinal tissue (Johnson and Martin, 2008; Orlans et al., 2018; Osborne et al., 2016; Valdés et al., 2016). They offer advantages for studies regarding differentiation, development, disease modeling like diabetic retinopathy, cell degeneration or therapy testing (Orlans et al., 2018; Osborne et al., 2016; Resau et al., 1991; Valdés et al., 2016). Most importantly, the usage of human donor tissue allows to overcome the limitations of interspecies differences.

However, the survival and long-term culture of these cells is often restricted to a few days and cells also might change their morphology and characteristics during *ex vivo* culture (Denk et al., 2015; Fernandez-Bueno et al., 2012; Rettinger and Wang, 2018).

1.3.5. *In vitro* model systems

An alternative model to *in vivo* and *ex vivo* models for a wide variety of applications can be traditional culture of cells in monolayers, either as primary cells or as immortalized cell lines. There are cell lines available for many different retinal cell types with the purpose of developmental or differentiation studies, toxicology or pharmacologic experiments, as well as disease modeling (Shafaie et al., 2016).

One of the advantages that cell culture models offer, is a more defined experimental environment leading to more reproducible data (Barar et al., 2009; Kaur and Dufour, 2012). Moreover, problems of species-variability can be circumvented by using cells that originate from the desired species (Barar et al., 2009; Combes, 2004). Cell culture experiments in general, especially compared to *in vivo* experiments, are less expensive, have fewer legislative restrictions, are easier to handle and can still provide important insights regarding physiological or pathological functions (Kaur and Dufour, 2012) .

Some of the most prominent examples of retinal cell lines are the immortalized RPE cell lines ARPE-19 and hTERT-RPE. But also other retinal cell lines like Müller glia or ganglion cell-precursors are used in cell culture (Alge et al., 2006; Sarthy et al., 1998; Sayyad et al., 2017).

Nevertheless, cell culture of primary cells or cell lines usually exhibit some limitations and disadvantages. Primary cells from human donors, like explant cultures, have limited availability and can only be cultivated for a few passages before changing their characteristics and passaging then is not possible anymore (Honegger, 2001). On the other hand, immortalized cell lines can be passaged for longer periods and can be easily and rapidly expanded, but this can lead to chromosomal changes or reduced characteristic-marker expression (Honegger, 2001; Shafaie et al., 2016).

Finally, cell monolayers in general do not show all characteristics that cells in a 3D meshwork would, starting from polarized expression of some proteins or communication and influence of neighboring cell types, for example via growth factor secretion (Shafaie et al., 2016). Also, mechanical forces and cell-cell as well as cell-matrix interactions can show differences

compared to 3D networks. Ultimately, the weakness of this system is still the absence of the natural local environment (Kaur and Dufour, 2012).

1.3.6. Stem cell-based retinal model systems

Besides the already mentioned possibilities of using immortalized cell lines or primary cells of retinal tissue, stem cells are another option and further advancement for *in vitro* cell culture experiments. Stem cell-based model systems can include animal or human cells and can make use of either multipotent or pluripotent stem cells which can be differentiated into retinal cell types to study development, physiological function or pharmacologic treatment options.

Adult stem cells (endogenous stem cells) are cells that reside in a specific tissue of the adult body and are responsible for regeneration of specific cell types of this tissue (Montagnani et al., 2016). It should be noted here that endogenous stem cell candidates in the retina have been identified in different animal models but within different vertebrates, the capacity of endogenous stem cells for retinal regeneration can differ substantially (Achberger et al., 2019a; Jeon and Oh, 2015). Even though it is possible to use some of these cell types (like Müller glia and RPE) as retinal progenitor-cell like cells in culture, they still show limited potency and therefore are only able to generate single cell types (Achberger et al., 2019a; Jeon and Oh, 2015).

To achieve a complete retinal model with all cell types, this introduction of stem cell-based retinal models will focus rather on cell types with greater differentiation potential, which are pluripotent stem cells that were also used as starting material for retinal differentiation within this thesis.

1.3.6.1. Pluripotent stem cells

Pluripotent stem cells are (PSCs) defined by an unlimited capacity for self-renewal, and their ability to differentiate into cells of all three germ layers of the human body, i.e. ectoderm, endoderm and mesoderm. During the blastocyst stage of embryonic development, cells from the inner cell mass, also called the embryoblast, are pluripotent (Beddington and Robertson, 1989; Yu and Thomson, 2008). They are referred to as embryonic stem cells

(ESCs) and can be isolated from the inner cell mass (Martin, 1981). This was done for mouse cells in 1981 (Evans and Kaufman, 1981; Martin, 1981) and for human cells in 1998 (Thomson et al., 1998). Using defined culture conditions, the described characteristics of ESCs can then also be maintained *in vitro*. Since this experimental method is possible, human ESCs have opened up new possibilities not only for therapeutic medicine but also for basic research and developmental questions.

Because of their potential to be differentiated into any required cell type, transplantational approaches have been successfully conducted in many areas for example in cell replacement therapy for Morbus Parkinson or diabetes (Bjorklund et al., 2002; Kim et al., 2003; Lumelsky, 2005; Sonntag et al., 2018).

On the other hand, the applicability of ESCs and the necessity for *in vitro* fertilization and subsequent destruction of a human embryo, brings along many ethical concerns and turns this source of pluripotent stem cells very scarce and highly debated. Moreover, many countries today have extremely strict regulations for the usage of those cells and for example in Germany, generation of new ESC lines is not permitted (Bundesministerium der Justiz und für Verbraucherschutz, 2002). Further, the generated human ESC lines usually do not have patient- or disease-specific background, unless genetic-editing technologies are utilized. If transplanted cells with different genetic background would be used, immune rejection due to HLA differences will occur as a consequence (Drukker and Benvenisty, 2004).

Since the description and first generation of so called induced pluripotent stem cells (iPSCs) however, the tide had turned and many of the described limitation of ESCs could be circumvented.

1.3.6.2. Induced pluripotent stem cells

Since it was shown that somatic cells can be reprogrammed into pluripotent cells by fusing them with ESCs (Cowan et al., 2005; Tada et al., 2001), or by transferring their nucleus into oocytes (Wilmut et al., 1997), the question arose whether this was also possible using certain transcription factors.

In 2006, Yamanaka and Takahashi successfully used overexpression of the transcription factors OCT3/4, SOX2, c-MYC and KLF4 to reprogram mouse embryonic fibroblasts (Takahashi and Yamanaka, 2006) and later adult human fibroblasts (Takahashi et al., 2007). The generated cells which they named *induced pluripotent stem cells* (iPSCs), in fact showed the same morphology, surface markers, proliferation, gene expression- and epigenetic profile like ESCs (Takahashi and Yamanaka, 2006; Takahashi et al., 2007). Moreover, the high activity of the enzyme telomerase, allowing the cell to constantly proliferate, is comparable to ESCs levels (Takahashi and Yamanaka, 2006). And, as previously mentioned for ESCs, iPSCs can be differentiated into all cells of the human body which can be shown in teratoma assays and using *in vitro* differentiation for all 3 three germ layers (Takahashi and Yamanaka, 2006; Takahashi et al., 2007).

The group of Yamanaka *et al.* initially used retroviral transfection of cells and first protocols required the cultivation on feeder cells that secrete growth factors and provide attachment for the reprogrammed cells (Takahashi and Yamanaka, 2006).

Since then however, several advancements of their protocol have been achieved. Reprogramming and cultivation of the cells now is possible even without feeder cells on specialized coatings (Nakagawa et al., 2014). Some protocols avoid the integration of the proto-oncogen c-MYC to prevent tumor formation (Yu et al., 2007). The majority of newer protocols are designed to prevent integration into the genome, possibly inducing accidental mutagenesis, either by using viral vectors that do not integrate (for example the Sendai virus (Chen et al., 2013)), or using non-viral strategies of delivery like mRNA, miRNA or plasmid transfection (Malik and Rao, 2013; Okita et al., 2008).

1.3.6.3. 2D retina models from stem cells

Although a variety of differentiation protocols exist, that allow the generation of retinal cell types from adult or pluripotent stem cells, these models usually only feature one cell type in two dimensions. This means that neither the complex interplay and communication with surrounding cell types is represented, nor the actual physiological arrangement in three dimensions. Especially in the retina, where different neuronal and glial cell types are connected to interact, a 2D approach will most certainly not be suitable as a physiological model system. This problem, not only playing a role in retinal models, but in models of any

organ, could be overcome by the generation of 3D models that will be discussed in the next section.

1.3.6.4. Advanced 3D in vitro culture system: Organoids

The term “organoid” refers to *in vitro* structures that are 3-dimensional and can be generated either from progenitor cells or from pluripotent stem cell types (Bartfeld and Clevers, 2017). Most important, they are characterized by a functionality and morphology that closely mimics the organ since these cells are arranged more similar to how they would be arranged *in vivo*. Interestingly, these organ-like structures often self-organize and carry multiple cell types which is a key differentiation point compared to traditional adherent culture systems using cell lines (Achberger et al., 2019a; Lancaster and Knoblich, 2014).
In 2008, first organoids were generated as cortical spheres from mouse embryonic stem cells in suspension (Eiraku et al., 2008). Of note, this first report already used self-organization of cells and highlights that spatial and temporal aspects of organ development can be recapitulated with these aggregates (Eiraku et al., 2008).
Since then, organoids have been generated from human iPSCs and have been developed as model system for almost every tissue, such as pancreas (Hohwieler et al., 2017; Huang et al., 2015), liver (Takebe et al., 2013), brain (Lancaster et al., 2013), cornea (Foster et al., 2017; Susaimanickam et al., 2017), as well as retina (Meyer et al., 2009; Zhong et al., 2014).
Organoid technology not only holds great potential because of the many different tissues that can be generated but also, since organoid generation is possible virtually from every individual. This allows modeling of a disease in the dish and moreover, potential transplantation approaches, drug discovery and personalized drug treatment are possible (Bartfeld and Clevers, 2017). The first case, where organoids were used successfully for a personalized medicine approach was in 2015 when a cystic fibrosis patient was treated based on drug-screening results gained using primary intestinal organoids generated from intestinal adult stem cells of the patient (Dekkers et al., 2013; Saini, 2016).
In addition, pluripotent stem cell-derived organoids have now found applications in drug-screening and toxicity testing. For example kidney and liver-organoids can be tested *in vitro* for superior judgement of side-effects of systemic drugs or environmental toxins (Forsythe et al., 2018; Takasato et al., 2015).

Since the presented work involves usage of retinal organoids, different protocols for generation of this organoid type will be introduced in the following, combined with current limitations of this model system.

1.3.6.5. Retinal organoids

The first report of retinal organoids using human ESCs and iPSCs showed the generation of retinal spheres in a stepwise differentiation process that was able to mimic normal development and generated retinal progenitors as well as some retina-specific cell types (Achberger et al., 2019a; Meyer et al., 2009).

The protocol made use of the fact that human PSCs will develop into anterior neuroepithelial cells under serum-free conditions in proneural medium (Meyer et al., 2009). Consequently, the retinal lineage differentiation seems to be the "default" state if no other extrinsic cues are present. This phenomenon is known as the "default model" also described in other publications (Kamiya et al., 2011; Muñoz-Sanjuán and Brivanlou, 2002; Smukler et al., 2006).

Today, there are several protocols for generation of retinal organoids that mainly differ with regard to adherence and suspension steps. Protocols by the group of Sasai *et al.* for instance, used 3D suspension for every step of the differentiation from embryoid bodies (EBs) up to an optic vesicle and later, an optic cup-like stage (Eiraku et al., 2011; Nakano et al., 2012).

On the other hand, protocols using a combination of 2D and 3D differentiation during organoid formation are described by Zhong et al. (Zhong et al., 2014) and Meyer et al. (Meyer et al., 2011) and were used as a basis for our retinal organoid differentiation protocol. The initial steps of the protocol, during which an undirected neural differentiation is performed, take place as adherent steps after plating of EBs on coated dishes. As soon as eye fields are formed in those adherent cultures, they are manually selected and detached and will self-organize in suspension to form retinal organoids and can be kept in suspension (Meyer et al., 2011; Zhong et al., 2014). If specific RPE-enriched differentiation is intended, they can later be plated again (Ohlemacher et al., 2016). These protocols however, do not aim to form optic cups, but will yield optic vesicle-like structures (Meyer et al., 2011; Zhong et al., 2014).

In this context, the ration of RPE vs. neural retina in cultures seems to play an important role in whether or not optic cups are formed (Nakano et al., 2012). Therefore, the optic cup-

protocols use Wnt signaling to improve MITF expression and RPE differentiation to achieve the correct ratio (Nakano et al., 2012). Even though it might seem that optic cups represent a more mature stage and show the correct apposition of RPE vs. neural retina, they lack a full retinal layering compared to optic vesicle-protocols and can therefore be regarded as less mature (Achberger et al., 2019a; Nakano et al., 2012).

To conclude, while the first protocols published only showed some retinal cell types, still lacking complex retinal layering, the differentiation process was continuously improved in several protocols and today, it is possible to generate retinal organoids that show all major retinal neurons and also Müller glia cells (Achberger et al., 2019a).

Further, retinal organoids show retinal layering including an outer and inner nuclear layer, ganglion cell layer, as well as a synaptic outer plexiform layer. Furthermore, light-responsiveness of the photoreceptor cells could be shown as a functional proof of maturity (Zhong et al., 2014).

Retinal organoids have found broad applications in disease modeling for example to study glaucoma, or Leber congenital amaurosis (Ohlemacher et al., 2016; Parfitt et al., 2016) but they have also been used for toxicology screenings and pharmacological studies (Ito et al., 2017; Jin et al., 2011).

However, the organoid system as retinal model still features some specific limitations. First, organoids often still miss tissue-tissue interactions and contact with surrounding parenchymal tissues that is essential for a normal organ function *in vivo* (Bhatia and Ingber, 2014). For retinal organoids, this means an absence of blood vessels or immune cells in the organoid (Clevers, 2016). Further, cell types that would normally integrate from other tissues like cells that originate from the CNS and mesodermal cell types are missing (Achberger et al., 2019a).

Second, organoids usually show a high variability in size and shape mainly due to variability in media supply in the standard culture dish. Cell degeneration, low maturity (for example of photoreceptor outer segments of retinal organoids), low throughput and low reproducibility are some major drawbacks of using organoids as a model system (Achberger et al., 2019a; Takebe et al., 2017).

Third, organoids in standard dish culture are difficult to be analyzed for functionality, partially because cells cannot be kept in a constant position for long-term analysis and partially because cells in the inside of the sphere are usually hard to reach for visual or functional monitoring (Bhatia and Ingber, 2014).
Consequently, it seems necessary to improve the current retinal organoid system with new options for cultivation.

1.3.7. Microfluidic organ-on-a-chip systems

As described in the previous section, one of the major limitations of the organoid system is centered around the way they are cultured. Therefore, new culture systems aim to improve this aspect.
"Organ-on-a-chip" (OoC) systems are microfluidic devices usually made of biocompatible plastics that allow the cultivation of cells or cell sheets with the goal of achieving a more organ-like physiology (Bhatia and Ingber, 2014). They can be generated using a combination of different microfabrication methods including, for example, photolithograph, replica molding and microcontact printing (Huh et al., 2011). The material used in most cases today is polydimethylsiloxane (PDMS) which is inexpensive, easy to handle, transparent and has high gas permeability, as opposed to other materials like silicon, glass or plastic that require additional oxygenation (Huh et al., 2011).
Microfluidic systems include microscopic structures to simulate the cells natural environment in the human body, and are often used to recapitulate the multicellular architecture of a tissue, cell-cell as well as cell-matrix interactions (Bhatia and Ingber, 2014; Huh et al., 2010; Takebe et al., 2017).
Furthermore, they usually include microchannels for a controlled and steady fluid flow to simulate the body's vascular perfusion for a better oxygen and nutrient supply (Bhatia and Ingber, 2014). Different levels of complexity of these systems can be designed, including one or several cells types in different chambers and additionally, one or several microchannels that can be separated by porous membranes or substrates for simulation of a tissue barrier function.
In this way, microfluidic systems increase reproducibility since they offer control over many parameters and, due to a more physiological culture, have the potential to increase maturity

and survival of the cultured cells or tissue (Takebe et al., 2017). Moreover, physiological stimuli can be integrated into the chip system, for example chemical or electrical stimulation, mechanical movements or stretching (Huh et al., 2012).
Another important aspect is that these chips can be used as a screening platform for *in vitro* analyses, for example they enable real-time imaging, or in the case of neurons, electrophysiological monitoring as well as other tests of functionality with the help of integrated microsensors (Bhatia and Ingber, 2014; Huh et al., 2011).
Consequently, microfluidic organ-on-a-chip systems can produce a level of simulated organ functionality that cannot be achieved using standard 2D or 3D culture systems (Bhatia and Ingber, 2014; Huh et al., 2011). Concerning drug discovery and toxicity testing, these systems have the potential to serve as a platform for a near-physiological testing that can not only help reduce the number of animals to be tested and therefore make the process cheaper and faster, but it might also offer totally new options and insights when no suitable other model is available (Huh et al., 2010; Mathur et al., 2015; Viravaidya and Shuler, 2008). Especially the combination of the organoid technology with the organ-on-a-chip system holds the promise of a synergistic engineering approach, potentially leading to enhanced fidelity, reproducibility, maturity and higher throughput (Takebe et al., 2017).
Organ-on-a-chip systems have been developed for a variety of cell types and for modeling of different organs, including lung (Huh et al., 2010), heart (Mathur et al., 2015, 2016), liver (Carraro et al., 2008), cornea (Puleo et al., 2009), as well as retina (Dodson et al., 2015a; Mishra et al., 2015; Su et al., 2015). Existing microfluidic retina-on-a-chip models will be described in greater detail within the next section.

1.3.7.1. Existing microfluidic retina-on-a-chip systems

There are several retina-on-a-chip models available that were designed to replicate and observe the effects of retinal cell replacement after implantation of retinal progenitor cells (Haderspeck et al., 2019). Such microfluidic systems might help to improve the outcomes of regenerative cell transplantation in disorders that involve retinal degeneration like age-related macular degeneration or retinitis pigmentosa.
A chip designed for retinal synaptic regeneration by the group of Su *et al.* was developed by integrating two microchambers connected by a number of microchannels (Su et al., 2015).

This allows to analyze axonal outgrowth between two different retinal cell populations seeded into the cell chambers and thus, to observe synaptogenesis and factors that can help to improve retinal regeneration (Su et al., 2015).

Another chip integrating retinal cells was designed to analyze cell migration patterns after transplantation (Mishra et al., 2015). This system, called μRetina, was rather focused on replication of the geometric properties of the human and the mouse retina, respectively and was realized by an arch-shaped chamber for cell cultivation (Mishra et al., 2015).

While these two systems can help to find useful factors to improve cell transplantation and retinal axon outgrowth, they are very limited for this very specific application. They only include some retinal cell types and are not able to replicate more complex pathophysiological questions and the sophisticated human retinal architecture.

On the other hand, there are also retina-on-a-chip systems that include whole organs or tissue slices like the chip developed by Dodson *et al.* (Dodson et al., 2015a). Mouse retinal explants can be cultivated *ex vivo* allowing the testing of different chemical substances (Dodson et al., 2015a). As mentioned before for other retinal explants, in this system the viability of cells and the usability of human material is limited.

2. Aim of this thesis

The aim of this thesis was to generate a microphysiological retina-on-a-chip system by integrating retinal organoids as well as RPE derived from human induced pluripotent stem cells (iPSCs) into a microfluidic chip system.

In a first step, retinal organoids had to be differentiated from human iPSCs and retinal pigment epithelium (RPE) cells had to be cultured as monolayers. Next, different variants of a microfluidic chip system had to be developed to test the integration of the organoid as well as the RPE, and further, to show that the respective cell types are still expressed and able to survive in the system. Characteristic marker expression was shown on protein level using immunohistochemistry, and on mRNA level using qRT-PCR. Morphological features were analyzed with electron microscopy.

In a second step, a co-culture retina-on-a-chip (RoC) system was developed that allowed the integration of retinal organoid as well as RPE to be able to cultivate them in a physiological manner. To test whether the RoC actually showed retinal functionality, some key retinal features were analyzed, including phagocytosis of photoreceptor outer segments and improvement of outgrowth of photoreceptors outer segments.

Finally, as a proof-of-principle study, the suitability of the retina-on-a-chip system as drug testing device was analyzed. Chemicals with known retinopathic side-effects were tested and effects were monitored.

3. Material

3.1. Machines, tools and labware

Table 1: List of machines and tools

Machine	Company
Analytical Balance BP2218-0CE	Sartorius, Göttingen, Germany
BioMark HD	Fluidigm, South San Francisco, CA, USA
BioTek ELx800 Absorbance Microplate Reader	BioTek Instruments, Winooski, USA
Cryostat, Microm HM 560	Thermo Fischer Scientific, Waltham, MA, USA
Evos FL Cell Imaging System	Thermo Fischer Scientific, Waltham, MA, USA
Fluidigm BioMark HD	Fluidigm, South San Francisco, CA, USA
Freezer -20°C	Liebherr, Biberach, Germany
Freezer -80°C	Thermo Fischer Scientific, Waltham, MA, USA
Fridge 4°C	Liebherr, Biberach, Germany
Heraeus Megafuge 16 Centrifuge	Thermo Fischer Scientific, Waltham, MA, USA
Heraeus Fresco 17 Centrifuge	Thermo Fischer Scientific, Waltham, MA, USA
Ice machine, AF103	Scotsman, Great Blakenham, UK
Incubator 37°C, Heracell 240i	Thermo Fischer Scientific, Waltham, MA, USA
Legato 210 pump	KD Scientific, Holliston, MA, USA
Microscope (Axioskop 2 mot plus, Primo Vert)	Zeiss, Oberkochen, Germany
Multipipette Stream	Eppendorf, Hamburg, Germany
NanoPhotometer P330	Implen, München, Germany
Nitrogen Tank, CryoPlus 2	Thermo Fischer Scientific, Waltham, MA, USA
PCR Thermocycler, peqStar	Peqlab Biotechnologie, Erlangen, Germany
Pipette research plus (2.5 µl ,10 µl, 100 µl, 200 µl, 1000 µl, 5 ml)	Eppendorf, Hamburg, Germany

Pipette F1 Clip-Tip (10 µl, 100 µl, 1000 µl)	Eppendorf, Hamburg, Germany
Pipettus	Hirschmann, Eberstadt, Germany
Reichert Ultracut S	Leica, Wetzlar, Germany
StepOnePlus real-time PCR systems	Thermo Fischer Scientific, Waltham, MA, USA
Sterile Bench, MSC-Advantage	Thermo Fischer Scientific, Waltham, MA, USA
SU8 developer	Micro Resist Technology, Berlin, Germany
Ultra-Fine-Clipper-Scissors-II	Fine Science Tools, Heidelberg, Germany
Upright fluorescence microscope BX50WI	Olympus, Tokio, Japan
UV developer Quantum ST4	Vilber Lourmat, Eberhardzell, Germany
Vacuum Pump, Integra Vacusafe	Integra Biosciences, Biebertal, Germany
Vortexer	Bender+ Hobein, Zürich, Switzerland
Water bath, Lab Line waterbath	Thermo Fischer Scientific, Waltham, MA, USA
Zeiss EM 900 transmission electron microscope	Zeiss, Jena, Germany

Table 2: List of labware

Labware	Company
6-, 12-, 24- well-plates (Tissue treated, Non treated)	Becton Dickinson, New York, NY, USA
96 Well-V-shaped culture plates	Sarstedt, Nümbrecht, Germany
Cell scraper	Thermo Fischer Scientific, Waltham, MA, USA
Cell strainer 70 µm	Becton Dickinson, New York, NY, USA
Coverslips, Menzel (24 mm x 24 mm, 24 mm x 40 mm)	Thermo Fischer Scientific, Waltham, MA, USA
Fluidigm 96.96 Dynamic Array IFC	Fluidigm, South San Francisco, CA, USA
Dako pen	Dako, Hamburg, Germany
Gloves Peha-Soft nitrile	Hartmann, Heidenheim, Germany
PET membranes	Sabeu, Northeim, Germany
Petri dishes (10 cm, 6 cm)	Greiner Bio-One, Frickenhausen, Germany

Pipette tips (10 µl, 100 µl, 200 µl, 1 ml, 5 ml)	Eppendorf, Hamburg, Germany
Pipettus	Hirschmann, Eberstadt, Germany
QiaShredder	Qiagen, Hilden, Germany
Reaction tubes (15 ml, 50 ml)	Becton Dickinson, New York, NY, USA
Reaction tubes small (0.5 ml, 1.5 ml, 2.0 ml)	Sarstedt, Nümbrecht, Germany
Serological Pipettes (5 ml, 10 ml, 25 ml, 50 ml)	Sarstedt, Nümbrecht, Germany
Sterile filters (0.22 µm, 0.45 µm)	Merck Millipore, Darmstadt, Germany
Super FrostPlus object slides	R. Langenbrinck, Emmendingen, Germany
Syringes BD Plastipak 50 ml	Thermo Fischer Scientific, Waltham, MA, USA
Syringes, BD Syringe with Luer-Lok Tips (5 ml, 10 ml, 20 ml)	Thermo Fischer Scientific, Waltham, MA, USA
Syringes, BD 1 ml Insulin Syringe with Slip Tip	Thermo Fischer Scientific, Waltham, MA, USA
T25-flasks (Culture treated)	Greiner Bio-One, Frickenhausen, Germany

3.2. Media, chemicals, supplements

Table 3: List of cell culture media

Machine	Company
Antibiotic-antimycotic 100 x liquid	Thermo Fischer Scientific, Waltham, MA, USA
CryoStem	Biological Industries, Beit Haemek, Israel
DMEM, high glucose	Thermo Fischer Scientific, Waltham, MA, USA
DMEM/F12 + GlutaMAX	Thermo Fischer Scientific, Waltham, MA, USA
Fetal bovine serum (FBS)	Thermo Fischer Scientific, Waltham, MA, USA
GlutaMax 100 x liquid	Thermo Fischer Scientific, Waltham, MA, USA
KnockOut -DMEM	Thermo Fischer Scientific, Waltham, MA, USA
KnockOut serum replacement	Thermo Fischer Scientific, Waltham, MA, USA

Non-essential amino acids	Thermo Fischer Scientific, Waltham, MA, USA
Normal donkey serum (NDS)	Sigma-Aldrich, St. Louis, MO, USA
OptiMEM	Thermo Fischer Scientific, Waltham, MA, USA
PeproGrow hESC embryonic stem cell media	PeproTech, Hamburg, Germany
Phosphate-buffered saline (PBS) w/o magnesium and calcium	Thermo Fischer Scientific, Waltham, MA, USA
Synth-A-Freeze cryopreservation medium	Thermo Fischer Scientific, Waltham, MA, USA

Table 4: List of chemicals and supplements

Chemical	Company
9-cis-retinal	Sigma-Aldrich, St. Louis, MO, USA
Activin A	Cell Guidance Systems LLC, St. Louis, MO, USA
Agarose	AppliChem, Darmstadt, Germany
All-trans-retinoic acid	Sigma-Aldrich, St. Louis, MO, USA
Apotransferrin	Serologicals, Atlanta, GA, USA
Araldite resin	Serva, Heidelberg, Germany
B-27 without vitamin A	Thermo Fischer Scientific, Waltham, MA, USA
Bis-[3-trimethoxysilypropyl]amine	Sigma-Aldrich, St. Louis, MO, USA
(-)- Blebbistatin	Sigma-Aldrich, St. Louis, MO, USA
Bovine insulin	Sigma-Aldrich, St. Louis, MO, USA
Bovine outer segments	InVision BioResources, Seattle, WA, USA
Chemically defined lipid (CDL) concentrate	Thermo Fischer Scientific, Waltham, MA, USA
Chlorotrimethylsilane	Sigma-Aldrich, St. Louis, MO, USA
Chloroquine	Sigma-Aldrich, St. Louis, MO, USA
Collagen IV	Sigma-Aldrich, St. Louis, MO, USA
DAPI	Thermo Fischer Scientific, Waltham, MA, USA
Dorsomorphin dihydrochloride	Tocris Bio-Techne, Wiesbaden-Nordenstadt, Germany

Ethanol	Serva, Heidelberg, Germany
Gentamicin	Sigma-Aldrich, St. Louis, MO, USA
Glutaraldehyde	Electron Microscopy Sciences, Munich, Germany
Heparin sodium salt	Sigma-Aldrich, St. Louis, MO, USA
Human recombinant EGF	Cell Guidance Systems LLC, St. Louis, MO, USA
Human recombinant FGF-2	Cell Guidance Systems LLC, St. Louis, MO, USA
Human serum albumin (HSA)	Biological Industries, Cromwell, CT, USA
HOECHST 33342	Thermo Fischer Scientific, Waltham, MA, USA
HyStem-C- hydrogel	EsiBio, Alameda, CA, USA
Isopropanol	VWR, Radnor, PA, USA
ITS	BD Bioscience, San Jose, CA, USA
L-Ascorbic acid	Sigma-Aldrich, St. Louis, MO, USA
Lenti-X concentrator	Takara Bio, Kusatsu, Japan
Paraformaldehyd	Roth, Karlsruhe, Germany
Polybrene (Hexadimethrine bromide)	Sigma-Aldrich, St. Louis, MO, USA
Polydimethylsiloxane (PDMS) Sylgard 184	Dow Corning, Midland, MI, USA
Polyethylenimine	Polysciences, Warrington, PA, USA
Progesteron	Sigma-Aldrich, St. Louis, MO, USA
ProLong gold antifade mountant with DAPI	Thermo Fischer Scientific, Waltham, MA, USA
Propidium iodide	Sigma-Aldrich, St. Louis, MO, USA
Putrescine dihydrochlorid	Sigma-Aldrich, St. Louis, MO, USA
Rock-inhibitor Y-27632	Ascent Scientific, Avonmouth, UK
Saponin	Merck Millipore, Darmstadt, Germany
Sodium cacodylate buffer, pH 7.4	Electron Microscopy Sciences, Munich, Germany
SU8-50 photoresist	MicroChem, Westborough, MA, USA

Sucrose	Roth, Karlsruhe, Germany
Taurine	Sigma-Aldrich, St. Louis, MO, USA
TGFβ1	Cell Guidance Systems LLC, St. Louis, MO, USA
Tissue-Tek O.C.T. compound	Sakura, Alphen aan den Rijn, NL
Triton X-100	Roth, Karlsruhe, Germany
Uranyl acetate	Serva, Heidelberg, Germany

Table 5: List of cell culture coatings

Coating	Company
Collagen IV	Sigma-Aldrich, St. Louis, MO, USA
Laminin	Roche, Basel, Switzerland
Matrigel, hESC-Qualified	Corning, New York, NY, USA
Matrigel, Growth factor reduced	Corning, New York, NY, USA
Poly-L-ornithine	Sigma-Aldrich, St. Louis, MO, USA

Table 6: List of enzymes

Enzyme	Company
AccuMax	Sigma-Aldrich, St. Louis, MO, USA
Dispase	Stem Cell Technologies, Vancouver, Canada
TrypLE Express	Thermo Fischer Scientific, Waltham, MA, USA

3.3. Antibodies and vectors

Table 7: List of primary antibodies

Antibody	Dilution	Company
CASP3	1:200	Thermo Fisher Scientific, USA
EEA1	1:500	eBioscience, Thermo Fisher Scientific, USA
EZRIN	1:200	Cell Signaling, USA
LAMP2	1:50	Santa Cruz Biotechnology, USA
Melanoma gp100	1:100	Abcam, USA
MITF	1:500	Exalpha Biologicals, USA
Phalloidin Alexa Fluor 647	1:500	Thermo Fisher Scientific, USA
PAX6	1:100	Santa Cruz Biotechnology, USA
PNA lectin-Alexa Fluor 568 or 647	20 mg/ml	Thermo Fisher Scientific, USA
Rhodopsin	1:200	Santa Cruz Biotechnology, USA
ROM1	1:200	Proteintech, USA
ZO1	1:100	Thermo Fisher Scientific, USA

Table 8: List of secondary antibodies

Enzyme	Dilution	Company
Alexa Fluor 488 Donkey anti mouse IgG	1:1000	Abcam, Cambridge, UK
Alexa Fluor 568 Donkey anti mouse IgG	1:1000	Abcam, Cambridge, UK
Alexa Fluor 647 Donkey anti mouse IgG	1:1000	Abcam, Cambridge, UK
Alexa Fluor 488 Donkey anti goat IgG	1:1000	Abcam, Cambridge, UK
Alexa Fluor 568 Donkey anti goat IgG	1:1000	Abcam, Cambridge, UK
Alexa Fluor 647 Donkey anti goat IgG	1:1000	Abcam, Cambridge, UK
Alexa Fluor 488 Donkey anti rabbit IgG	1:1000	Abcam, Cambridge, UK
Alexa Fluor 568 Donkey anti rabbit IgG	1:1000	Abcam, Cambridge, UK
Alexa Fluor 647 Donkey anti rabbit IgG	1:1000	Abcam, Cambridge, UK

Table 9: List of plasmids

Plasmid	Origin
pJG-IRPB-eGFP Vector	Gift from Deepak Lamba & Thomas Reh (Lamba et al., 2010)
psPAX2 lentiviral packing plasmid	gift from Didier Trono, Addgene plasmid # 12260
pMD2.G envelope expressing plasmid	gift from Didier Trono, Addgene plasmid # 12259

3.4. Kits and assays

Table 10: List of kits

Kit	Company
CellLight Early Endosomes-GFP, BacMam 2.0	Thermo Fischer Scientific, Waltham, MA, USA
PreAmp Master Mix	Fluidigm, San Fransisco, USA
RNeasy Plus Micro Kit	Qiagen, Hilden, Germany
RNeasy Plus Mini Kit	Qiagen, Hilden, Germany
VEGF-A Human ELISA Kit	Thermo Fischer Scientific, Waltham, MA, USA

Table 11: List of Taqman assays for Fluidigm.

All Taqman assay were purchased from Thermo Fisher Scientific, Waltham, USA

Gene	Companies' article number
ANXA4	Hs00154040_m1
BEST1	Hs04397293_m1
CRX	Hs00230899_m1
GAPDH	Hs99999905_m1
GLUL (GLU1)	Hs00365928_g1
GNAT1	Hs00181100_m1
GNGT1	Hs00184207_m1

HMBS	Hs00609297_m1
LHX2	Hs00180351_m1
MITF	Hs01117294_m1
NRL	Hs00172997_m1
PMEL (GP100)	Hs00173854_m1
PRKCA (PKCA)	Hs00925193_m1
PROX1	Hs00896294_m1
PRPH2 (PERIPHERIN2)	Hs00165616_m1
RAX (RX)	Hs00429459_m1
RPE65	Hs01071462_m1
SERPINF1 (PEDF)	Hs01106937_m1
TJP1 (ZO1)	Hs01551861_m1
VSX2 (CHX10)	Hs01584047_m1

3.5. Software

Table 12: List of software

Software	Company
Adobe Illustrator	Adobe Systems Software Ireland Limited, Dublin, Republic of Ireland
AxioVision SE64 Rel 4.9	Carl Zeiss AG, Oberkochen, Germany
Fluidigm Real-Time PCR Analysis Software v.3.0.2.	Fluidigm, San Fransisco, USA
Gen5 Microplate Reading & Data Analysis	BioTek Instruments, Winooski, USA
ImageJ v1.51w	https://imagej.nih.gov/
Microsoft Office	Microsoft Corporation, Redmond, USA
Prism 8.2.0	Graphpad Software, La Jolla, UA
StepOne Software V 2.3	Thermo Fisher Scientific, Waltham, USA
ZEN	Carl Zeiss AG, Oberkochen, Germany

4. Methods

4.1. Cell culture methods

Cultivation of stem cells as well as of derived differentiation products was performed under sterile conditions at a sterile bench. For medium change, cultivation media were heated to 37°C before usage. Standard incubation was performed at 37°C in an incubator with 5% CO_2 and 5% O_2 for stem cell cultivation and 5% CO_2 and 20% O_2 for retinal organoid (RO) and retinal pigmented epithelium (RPE) or chip cultivation.

Stem cells used in this work were human induced pluripotent stem cells (hiPSCs) that have been derived from keratinocytes of plucked human hair roots. Written consent of the donating persons was documented. The experiments were performed in accordance with the Helsinki convention and approval of the Ethical Committee was granted (Nr. 678/2017BO2) at the Eberhard Karls University Tübingen.

4.1.1. Human induced pluripotent stem cell culture

Starting material for this work were hiPSCs derived from keratinocytes from healthy individuals as previously described (Linta et al., 2012). Briefly, lentiviral vectors were used to deliver a pluripotency cassette carrying the 4 pluripotency factors: OCT4, SOX2, KLF4 and c-MYC. Reprogramming of keratinocytes was performed on mouse embryonic fibroblasts as feeder cells. Growing colonies of hiPSCs were transferred and kept in feeder-free conditions. The hiPSCs were characterized for their stem cell characteristics as described before using immunohistochemistry to stain for pluripotency markers and by performing germ layer differentiation to proof the ability of hiPSCs to generate cells from ectoderm, endoderm as well as mesoderm.

For standard cultivation, hiPSCs were grown as colonies on matrigel coating in 6-well plates. For passaging, 1 dense well of cells was detached by washing once with PBS, adding 500 µl stem-cell dispase (diluted in DMEM/F12 1:6), incubating for 1 min at room temperature and washing again twice with PBS. Then, 1 ml of FTDA-medium was added to the well and cell colonies were detached gently by using a cell scraper. The cells were then transferred onto freshly coated wells after incubation with matrigel for 1 h at 37°C.

The passing usually was performed once a week and cells were split 1:5 or 1:6 onto new 6-wells. Cells were then incubated at 37°C, 5% CO_2 and 5% O_2 and medium. Medium was changed daily with 1.5 ml FTDA medium.

FTDA medium:

- DMEM/F12+GlutaMAX
- 1:100 Human serum albumin (HSA)
- 1:100 Chemically defined lipids (CDL)
- 1x Antibiotic-Antimycotic (100x) (Anti-Anti)
- 1:1000 Insulin-transferrin-selenium (ITS)
- 10 ng/ml FGF2
- 5 ng/ml Activin A
- 0.5 ng/ml TGFβ1
- 50 nM Dorsomorphin

4.1.1.1. Freezing and thawing of hiPSCs

For cryo-freezing, hiPSC colonies were allowed to grow 80% dense and colonies were detached using stem-cell dispase as described before for the procedure of passaging. After stopping the reaction, cell colonies were collected in FTDA medium and centrifuged at 1500 rpm, 2 min. Supernatant was discarded, and the cell pellet was carefully dissociated in 0.8 ml/well CryoStem and transferred to the corresponding number of cryovials. Attention was paid that cell colonies were not fully dissociated. Cryovials were moved into a cryo-container with isopropanol at -80°C and on the next day, moved to liquid nitrogen storage at -196°C for long-term freezing.

For thawing of hiPSCs, cryovials were quickly heated in a water bath of 37°C and then gently transferred to pre-warmed FTDA-medium in a 15 ml-tube for centrifugation at 1500 rpm, 2 min. The cell pellet of one cryovial was resuspended in 1.5 ml FTDA-medium and distributed onto a matrigel pre-coated well of a 6-well plate.

4.1.2. Differentiation protocols

4.1.2.1. Retinal organoid differentiation protocol

The differentiation protocol for generation of retinal organoid (ROs) was adapted from the protocol by Zhong et al. (Zhong et al., 2014) with some processes modified. To initiate differentiation (defined as day 0), embryoid bodies (EBs) were generated by detaching and dissociating $2.88*10^6$ hiPSCs of a 6-well plate using treatment with TrypLE for 6-8 min at 37°C and by stopping the reaction with PeproGrow hESC embryonic stem cell medium. After centrifugation (1500 rpm, 2 min), the cell pellet was resuspended in PeproGrow hESC embryonic stem cell medium supplemented with 1% Antibiotics- Antimycotics, 10 µM Y-27632, 10 µM blebbistatin. The cells in suspension were distributed in a volume of 100 µl/well on a v-shaped 96-well plate and centrifuged again (400 g, 4 min) to allow re-aggregation of cells. Plates were then cultivated at 37°C, 5% CO_2 and 20% O_2.

On the following day (defined as day 1 of differentiation), 80% of the medium was replaced with a neural induction medium (N2-medium, see below). On day 4, medium was again changed with N2-medium.

On day 7, EBs were collected carefully from the 96-well plate and then plated equally onto a 6-well plate coated with growth-factor reduced matrigel for 1 h at 37°C. Approximately 32 EBs were plated per well of the 6-well plate. Medium was then changed daily with 1.5 ml of N2-medium/well.

On day 16, cultivation medium was switched from N2 to a B27-based retinal differentiation medium (BRDM, see below) and changed daily with 1.5 ml of BRDM-medium.

On day 24, retinal fields were detached: First, medium was changed with fresh BRDM. Then, retinal field areas were identified morphologically and detached with a 10 µl pipette tip under a bright-field microscope. Detached cell clusters were collected in 10 cm-dishes (uncoated), medium was filled up to 10 ml and 10 µM Y-27632 was added overnight. Cultivation medium was changed twice a week with BRDM-medium. For each medium change, cells were allowed to sink to the bottom of the dish, before half of the medium was replaced.

When formation of the spheres was completed, ROs were manually sorted from non-retinal spheres by their morphological appearance. If non-retinal cells were attached to a retinal part, the parts were manually isolated using Ultra-Fine-Clipper-Scissors-II under the bright-

field microscope. Retinal spheres were collected, and morphology was checked regularly before medium change.

From day 40, the cultivation medium was switched to BRDM supplemented with 10% FBS and 100 µM taurine and changed twice a week.

From day 70, the medium was additionally supplemented with 1 µM retinoic acid which was reduced to 0.5 µM retinoic acid from day 100 onwards.

After day 190, retinoid acid was removed, but addition of FBS and taurine was continued.

N2-medium:

- DMEM/F12 + GlutaMAX supplement
- 24 nM sodium selenite
- 16 nM progesterone
- 80 µg/ml human apotransferrin
- 20 µg/ml human recombinant insulin
- 88 µM putrescin
- 1x non-essential amino acids (100x)
- 1x antibiotics-antimycotics (100x)

BRDM-medium:

- DMEM/F12 + GlutaMAX supplement : DMEM, high glucose (1:1)
- 2% B27 (w/o vitamin A)
- 1x non-essential amino acids (100x)
- 1x antibiotics-antimycotics (100x)

4.1.2.2. Retinal pigment epithelium differentiation protocol

Retinal pigment epithelium (RPE) cells were derived from RO-differentiation as a by-product and cultivated according to protocols by Zhong *et al.* (Zhong et al., 2014) and Ohlemacher *et al*. (Ohlemacher et al., 2015) with some modifications.

Retinal spheres in suspension (as described above) after day 40 can show parts which become increasingly pigmented over time. These pigmented areas were manually dissected from non-pigmented retinal areas using Ultra-Fine-Clipper-Scissors-II and collected in a 1.5

ml Eppendorf tube. After washing with PBS, cell aggregates were treated for 90 min with AccuMax at 37°C at 5% CO_2 for dissociation into single cells. To improve dissociation, every 30 min cells were carefully resuspended. After complete dissociation, the enzyme was stopped with BRDM-medium supplemented with 10% FBS, to be then centrifuged at 1500 rpm, 2 min.

RPE single cells were then plated on pre-coated wells, either 6-well plates, 24-well plates with glass coverslips, or 24-well transwell plates. In each case, coating was performed by a 30 min incubation with 0.01% Poly-L-Ornithine at room temperature, followed by a 4 h incubation with 20 µg/ml Laminin at 37°C and 5% CO_2 with a PBS-washing step in between. For plating freshly dissociated RPE cells, 20 ng/ml EGF, 20 ng/ml FGF2, 2 µg/ml heparin, 10 µM Y-27632 were added to BRDM medium. For the first day, the medium was additionally supplemented with 10% FBS to improve survival and adherence of cells.

As soon as RPE cells reached confluence, all supplementation to BRDM was omitted.

For splitting of RPE cells, the same supplementation steps were used.

4.1.3. Generation of pJG-IRBP-eGFP lentiviral particles

Lentiviral particles were generated using Lenti-X cells purchased from Takara. Cultivation medium was Lenti-X medium (DMEM with 10% FBS. Cells were grown in 10 cm-petri dishes (culture treated) to 80% density to be then transfected. The following transfection mix was prepared per 10 cm-dish of cells to be transfected.

- 400 µl OptiMEM
- 12 µg Target vector pJG-IRBP-eGFP
- 5.5 µg psPAX2-Vector, lentiviral packing plasmid (gift from Didier Trono, Addgene plasmid # 12260)
- 2 µg pMD2.G-Vector, envelope expressing plasmid (gift from Didier Trono, Addgene plasmid # 12259)
- 70 µg Polyethylenimine

The mix was incubated for 10 min at RT. 1 ml of DMEM was then added to the mix and dropwise pipetted onto the cells in the petri dish.

Cells were then incubated for 4 h in the incubator at 37°C, 5% CO_2 and 5% O_2.

Medium in the petri dish was replaced with 8 ml Lenti-X medium. On day 2 and day 4 after transfection, medium was collected in 50 ml-tubes to be then used for lentivirus concentration.
First, the medium in the tubes was centrifuged (1500 rpm, 2 min) to separate the cell pellet from virus supernatant. Next, the virus supernatant was sterile filtered using 0.45 µm filters. Lenti-X concentrator was added in a ratio of 1:3 (Lenti-X concentrator : virus supernatant). The solution was mixed and stored at 4°C overnight, then centrifuged again at 1500 g, 45 min, at 4°C and supernatant was discarded. The final pellet of virus particles was then dissolved in DMEM/F12 (1 ml/ petri dish) and stored at -80°C.

4.1.4. Transduction of RPE cells

RPE cells in adherent cultures were transfected with pJG-IRBP-eGFP lentiviral particles by incubating them in BRDM with 10% FBS overnight, washing three times with PBS on the next day and cultivation with BRDM, as previously mentioned. Successful transduction was checked by monitoring green fluorescence under the microscope.

4.1.5. Loading of RPE cells into the retina-on-a-chip

First, individual chips were moved into 10 cm petri dishes and excess liquid was removed using a vacuum pump. Attention was paid that the wells and channels are still filled with liquid and no air bubbles can enter the system. Chips were then coated for 2 h at 37°C with 50 µg/ml laminin diluted in DMEM/F12. Directly before loading cells, the coating solution was removed and wells were washed and then filled with BRDM supplemented with 20 ng/ml EGF, 20 ng/ml FGF2, 2 µg/ml heparin, 10 µM Y-27632 and 10% FBS.
RPE cells loaded into the chips system were confluent, pigmented and had been starved for at least 2 weeks, unless mentioned otherwise.
Wells of RPE to be loaded were dissociated by first washing with PBS once and then adding warm AccuMax to the well (500 µl / 6 Well). Cells were incubated at least 10 min at 37°C and 5% CO_2, (depending on how long the RPE had been starved before, up to 40 min) until cells were detaching completely. To achieve a single-cell solution, cells were additionally resuspended in AccuMax 1-2 times before stopping the reaction with warm BRDM medium.

To avoid incomplete dissociation and cell clumps, the cell solution was additionally applied onto cell strainers, first onto a 70 µm, then onto a 40 µm cell strainer. Cells were then collected in a 15 ml tube and additional BRDM medium with 10% FBS was added before centrifugation at 1500 rpm, 2 min. The cell pellet was then resuspended in 1 ml BRDM medium with all supplements mentioned above and cells were counted in a Neubauer counting chamber. For each chip loaded, 108 000 cells were calculated and diluted in the appropriate volume of BRDM plus supplements (see above) including FBS for overnight attachment of the cells. 27 000 cells were then loaded in 4.5 µl per well by pipetting slowly, allowing the cells to sink to the bottom of the well. After loading, density per well was again checked at the microscope and corrected if necessary. Cells were then allowed to attach in the small volume of the well for 2 h in the incubator. Afterwards, 500 µl of medium were added on top of the chip for complete attachment overnight. The day after loading of RPE (unless mentioned otherwise), RPE chips were either connected directly to a syringe pump for cultivation or retinal organoids were loaded first before chips were connected to a pump.

4.1.6. Loading of retinal organoids into the retina-on-a-chip

Before loading ROs into the chips, medium was removed from the wells almost completely. 8 µl of HyStem-C, a hyaluronic acid-based hydrogel that had been prepared before according to the manufacturer's protocol, was then added to each well by pipetting. ROs which had been manually chosen before regarding their retinal morphology and size, were placed into the well by pipetting them into the liquid hydrogel on top of the membrane covered with RPE cells. One RO was placed per well. ROs were then gently moved into the center of the well and positioned with minimal distance to the RPE. Chips were incubated for 30 min at 37°C without any medium added, to allow the hydrogel to become solid. Afterwards, chips inside the incubator were connected to a Legato 201 syringe pump for automatic medium supply with BRDM, supplemented with 100 µM taurine and 10% FBS at a constant rate of 20 µl/h for 3-7 days. To further improve media flow and prevent evaporation, wells of the chips were covered using sterile adhesive tape (optical adhesive covers).

4.2. Chip production

4.2.1. PDMS chip production

Details of chip production are further described in (Achberger et al., 2019b).

The retina-on-a-chip (RoC) was fabricated from polydimethylsiloxane (PDMS) in 2 layers (media layer + tissue layer), carrying a polyethylene terephthalate (PET) membrane in between.

As a first step, 2 wafers (master molds) had to be produced. To generate the wafer for the media layer, SU8-50 photoresist was spin-coated onto a 4'' silicon wafer that had been cleaned before. A height of 100 µm was achieved. The substrate was exposed to UV light and allowed to develop for 6 min in SU8 developer.

The second wafer, required for RO culture (tissue layer), involves structures for an additional channel that will be referred to as tissue channel. The second wafer was generated in a 2-step process: The base layer, intended for the membrane insert, with a height of 25 µm was generated by spin-coating SU8-3025 photoresist, subsequent exposure to UV light, and development for 4 min. A cleaning step was inserted before the next layer was fabricated on top of the first (as molds for the tissue channels). Therefore, SU8-3025 was spin-coated with a height of 40 µm and exposed to UV light and final development for 4 min.

Both wafers were then silanized using chlorotrimethylsilane, to be used in a next step as negative master molds for Sylgard 184 PDMS (ratio 10:1, prepolymer:curing agent) that was poured onto the wafers.

Generation of the lower layer (media layer) was achieved using exclusion molding and overnight curing at 60°C. Generation of the tissue layer including the wells and tissue channels, was achieved with 25 g PDMS that was poured onto the master mold and overnight curing at 60°C.

After carefully removing both PDMS layers from their master molds, holes were punched into the tissue layer with a 2 mm biopsy puncher to generate 4 wells for later cultivation of cells and RO. Further, holes were punched with a 0.75 mm biopsy puncher to generate an inlet and an outlet for the medium.

PDMS layers and glass slide (170 µm) were cleaned. Next, the media layer bottom side and the surface of the glass slide were treated with oxygen plasma (50 W for 30 s) to be then bonded. Next, the PDMS-tissue layer needed to be bonded to a membrane:
Porous PET membranes with a diameter of 20 mm (pore size: 3 µm, thickness 10-20 µm) were used for this purpose that had been treated previously with bis-[3-trimethoxysilypropyl]amine for functionalization, to be then treated with oxygen plasma. Positioning of the membrane on the plasma-treated tissue layer was performed under the microscope.
To achieve plasma bonding between both PDMS layers, the surfaces of both layers were again treated with oxygen plasma (50 W, 30 s) and the setup was carefully aligned under the microscope. Stabilization was achieved by baking at 60°C overnight. For transportation and storage, the chips were plasma-activated (50 W, 5min) and then placed in sterile PBS to prevent air from entering the system.

4.2.2. Production of an agarose chip version

For cryo-sections, we build a specialized version of the RoC, made of 4% agarose in BRDM + 10% FBS. As the standard version of the RoC, this version contains four wells for cultivation of the ROs, as well as a semipermeable PET membrane, for cultivation of the RPE cells. The loading of RPE and ROs was performed as described before. Agarose RoCs were fixed using 4% PFA and 10 % sucrose in PBS for 2 h at RT. Cryoprotection was achieved using a sucrose gradient (10% sucrose for 10 min, then 20% sucrose for 1h) and storage overnight in 30% sucrose at 4°C. For cryoembedding, tissue-tek O.C.T. cryomatrix was used to cover the agarose RoC, before freezing it in liquid nitrogen. Cryosections of 14 µm thickness were cut using a cryostat and collected on superfrost glass slides, to then be stored at -20°C for immunohistochemistry.

4.3. Readouts

4.3.1. Purification of total RNA

Isolation of total RNA was performed using the Qiagen RNeasy Plus Mini Kit or the RNeasy Plus Micro Kit, depending on the expected RNA amount. Purification steps were performed according to the manufacturer's protocol. For adherent cells, for organoids in suspension

culture, as well as for chip-cultured cells or organoids, the same protocol was applied. Briefly, cells or organoids were washed twice with PBS before lysis buffer (RLT buffer) was applied. Resuspension was performed inside the lysis buffer. In the case of adherent cells in standard dish culture, cell scrapers were used in addition to help to detach all cells. QiaShredder columns were used for homogenization and centrifugation was performed at 13 300 rpm, 2 min. To eliminate genomic DNA, gDNA eliminator spin columns were used to centrifuge the homogenized lysate at 10,000 rpm for 30s. For precipitation of RNA, 70% ethanol were applied to the flow-through, mixed and transferred to RNeasy spin columns for centrifugation at 10,000 rpm for 15 s. Three washing steps followed with RW1 and RPE buffer (10,000 rpm for 15 s, 15 s, 2 min). Finally, total RNA was eluted using 30 µl of RNase-free water, directly applied to the spin column membrane and centrifugation at 10,000 rpm, 1 min. Flow-through was kept on ice for measurement of the RNA concentration and then stored at -80°C.

4.3.2. Gene expression analysis

Gene expression analysis was performed on the Biomark Fluidigm for an automated qRT-PCR reaction with Taqman assays as probes for quantification of the genes of interest.
80 ng of purified RNA was used as template for cDNA synthesis with the following material:

- 1 µl 5x RT Buffer
- 0.25 µl dNTPs
- 0.313 µl Hexanucleotide Mix
- 0.25 µl MMLV RT
- 0.438 µl H2O

The mixture was incubated for 1 h at 37°C, followed by 10 min at 85°C.
Taqman assay plates (96 well) were loaded according to the manufacturer's protocol, to be then placed in the Fluidigm machine.

4.3.3. Quantification of fluorescence intensity after PI treatment

The intensity of the PI signal was quantified with the help of the open source software ImageJ (https://imagej.nih.gov/) for ROI selection and calculation of mean intensity pixel values of this area.

To avoid confounding effects of background fluorescence, an image of the fluorescent signal was taken before and after PI treatment. For calculation of the real PI signal, ROI were selected and were calculated. Intensities before PI-treatment were then subtracted from intensities after PI-treatment.
Since the images were taken from underneath the RPE, RO signals should be regarded as a combination of RO signals with signals from the RPE directly underneath. Therefore, the calculation of the RO signal required to subtract the RPE signal. The RPE signal had to be calculated from the surrounding area (RoC minus RO).

The following calculation was performed:
I[RPE] =(I[RoC]*A[RoC]- I[RO+RPE]*A [RO]) / (A [RoC]- A [RO])
I[RO] = I[RO+RPE]- I[RPE]

A[X]: Area of [X]
I[X]: Mean Intensity of X

[RO]: only RO without RPE underneath
[RoC]: the complete Retina-on-a-Chip (RO + underlying RPE + surrounding RPE)
[RPE]: RPE in the RoC (not underneath the RO)

4.3.4. ELISA VEGF-A assay

To able to measure apical vs. basal secretion, we produced specialized chip versions made of PDMS with an additional apical media channel to connect the 4 chip compartments. These double channel RoC allowed the collection of the apical media (from above the RPE layer) and the measurement of VEGF-A secretions. Further, it allowed the comparison to the basal secretion from the media flow below the RPE.
RPE loading was performed as described before and cultivated with media flow generated from a syringe pump. After 14 days, media from the apical and basal channel were collected over 24h and frozen at -20°C.
For measurement of the VEGF-A amount, a VEGF-A Human ELISA Kit was used. The ELISA assay was performed according to the manufacturer's protocol. The media were collected

from (apical and basal) channels from 3 different RoCs. For calculation of the total VEGF-A amount per side, the starting volumina were measured.

4.3.5. Transmission electron microscopy

For transmission electron microscopy, either agarose RoCs or RoC without glass slide were used. The protocol is described in detail in (Achberger et al., 2019b).
RoC were fixed within the chip using Karnovsky buffer (2.5% glutaraldehyde, 2% paraformaldehyde, 0.1 M sodium cacodylate buffer, pH 7.4) overnight at 4°C. Chips were then washed for 30 min with 0.1 M sodium cacodylate buffer and placed for 1.5 h in OsO_4 for postfixation. Samples were then washed three times in cacodylate buffer and dehydrated in 50% ethanol. For counterstaining, 6% uranyl acetate (in 70% ethanol) were used and final dehydration was achieved in graded ethanol solutions.
Samples were then gradually infiltrated with Epon resin, starting with a 2:1 solution of aceton and Epon for 1 h, then with a 1:1 solution for 1 h and finally with pure Epon. Polymerization of the resin was achieved by overnight incubation at 60°C.
After polymerization, the RPE-RO co-culture on the PET membrane could then be removed from the chip setup using biopsy punchers. The removed samples in Epon were embedded in fresh Epon in molds for subsequent sectioning and were then incubated for 12 h at 60°C and 2 h at 90°C.
Ultrathin sectioning into 50 nm sections was performed using a Reichert Ultracut S and samples were collected on copper grids. Reynolds lead citrate was used for counterstaining. Finally, a Zeiss EM 900 transmission electron microscope was used for sample analysis.

4.3.6. Immunohistochemistry

<u>Staining of cells on coverslips and transwells:</u>
RPE cells on coverslips or on transwell inserts were fixed in the culture plate with 4% PFA and 10% sucrose in PBS for 20 min at RT. In case of transwell insert, the membrane was cut out and transferred into a 24 well plate. Blocking and permeabilization was performed in a combined step using 5% normal donkey serum (NDS) and 0.2% triton-X in PBS for 1 h at RT. Primary antibodies were diluted in blocking solution and applied to the coverslips or membranes in the plate for overnight incubation at 4°C. A washing step was performed with

PBS, three times for 5 min at RT. Secondary antibodies were diluted in blocking solution and incubation was performed for 2 h at RT. A washing step was performed with PBS, three times for 5 min at RT. For mounting, ProLong Gold antifade with DAPI was used.
In case of LAMP2 stainings, permeabilization was performed with 0.5% saponin instead of triton-x. In this case, all washing steps and antibody dilutions included 0.1% saponin in PBS.

Staining of cryo-sections:

For cryo-sections, the specialized agarose-version of the RoC was used and 14 µm thick cryo-sections were cut as described above. After thawing of frozen slides, the tissue was rehydrated using PBS for 15 min at RT. Blocking and permeabilization was performed in a combined step using 5% NDS and 0.2% triton-X in PBS for 1 h at RT.
Primary antibodies were diluted in blocking solution and applied to the cryo-sections for overnight incubation at 4°C. A washing step was performed with PBS, three times for 3 min at RT. Secondary antibodies were diluted in 1:1 blocking solution : PBS and incubation was performed for 2 h at RT. A washing step was performed with PBS, three times for 3 min at RT. For mounting, ProLong Gold antifade with DAPI was used.

In situ chip staining:

Immunohistochemistry of the whole RoC was performed using a syringe pump as follows: RoCs were fixed in 4% PFA in PBS for 20 min at RT. Blocking and permeabilization was performed in a combined step using 5% normal donkey serum (NDS) and 0.2% triton-X in PBS for 1 h at RT. This step was repeated for an additional 1 h with fresh solution. Primary antibodies were diluted in blocking solution for 1-2 days at 4°C. A washing step was performed with PBS, three times for 2 h at RT. Secondary antibodies were diluted in blocking solution and incubation was performed overnight at 4°C. A washing step was performed with PBS, three times for 2h at RT. For counterstaining of the nuclei, HOECHST 33342 was applied for 10 min at RT. An additional washing step was performed with PBS, three times for 2 h at RT.
In case of LAMP2 stainings, permeabilization was performed with 0.5% saponin instead of triton-x. In this case, all washing steps and antibody dilutions included 0.1% saponin in PBS.

4.3.7. Phagocytosis assay

Phagocytosis of bovine photoreceptor outer segments (POS):

HiPSC-derived RPE was plated on coated coverslips in 24 well plates. After 1 day, RPE was incubated with POS in BRDM for 2 h at 37°C (at a density of 10 POS per RPE). RPE cells were washed three times with PBS to remove residual POS and plates were moved back to the incubator for additional 2 h. Then, cells were fixed with 4% PFA and 10% sucrose in PBS for 20 min at RT.

4.3.8. Drug treatment

Drug treatment in the RPE dish:

HiPSC-derived RPE p2 cells that had been grown in standard dish culture on coated cover slips in 24 well plates for 1 day were treated with different concentrations of chloroquine (0, 20, 40, 80 µg/ml in BRDM) over 24 h. Afterwards, vacuolization was monitored under the phase-contrast microscope and, following fixation with 4% PFA, immunohistochemistry was used to stain for the lysosomal membrane protein lysosome-associated marker protein 2 (LAMP2) and cleaved caspase 3 (CASP3).

Drug treatment in the RoC:

RPE and ROs were co-cultivated in the RoC for 3 days. Then, the co-culture RoCs were either treated for 3 additional days with chloroquine (at 20 µg/ml or 80 µg/ml diluted in BRDM) or treated for 6 additional days with gentamicin (at 0.5 mg/ml and 2.5 mg/ml in BRDM). For both treatments, control RoCs only supplied with BRDM and the solvent we used.
RoCs were then analyzed using live cell imaging directly after treatment with 3 µM propidium iodide (PI) and HOECHST. In case of chloroquine treatment, RoCs were then fixed with 4% PFA, and immunohistochemistry was performed with the marker LAMP2 for lysosomal imaging.

4.4. Statistical analysis

Statistical analyses were performed using Graphpad Prism software version 8.2.0. Statistical tests used were students t-test (Figure 6d, Figure 7f, Figure 9d), one-way ANOVA with Bonferroni post-hoc test (Figure 14e), one-way ANOVA with Dunnet post-hoc test (Figure 18b, Figure 19b) and two-way ANOVA with Bonferroni post-hoc test (Figure 19c).

Results are provided as mean values ± standard error of the mean (S.E.M.). Statistical significance was represented as follows: $p < 0.05$ = * ; $p < 0.01$ = ** ; $p < 0.001$ = ***.

5. Results

5.1. Retinal organoid and RPE differentiation protocol

The first step for establishing a retinal model system, was to generate retinal tissue in the form of retinal organoids (ROs).

The starting material for this differentiation were human induced pluripotent stem cells (hiPSCs) derived from healthy donors by lentiviral reprogramming of keratinocytes.

Retinal differentiation was performed according to the protocol by Zhong *et al.* (Zhong et al., 2014) with several adaptations. An overview of the differentiation with the corresponding characteristic steps as observed under the bright-field microscope is provided in Figure 5.

In an initial step, embryoid bodies (EBs, Figure 5b) were generated from hiPSCs (Figure 5a). This step was used to initiate the differentiation and was defined as day 0 of differentiation. After 7 days of culture in suspension, EBs were plated on coated dishes and cultured adherent (Figure 5c). Neural rosettes started to form during this process. By day 24, neural retina areas could be identified morphologically by a bright appearance (Figure 5d, red circles) and were manually detached using a pipette tip. The detached retinal areas were then again cultured in suspension and started to form spherical structures within 1-2 days, referred to as retinal organoids (ROs), (Figure 5e). ROs can be identified by a bright appearance and a striped outer rim, indicating development of retinal cells. Moreover, pigmented dark parts could be identified, which are RPE cells and were detached from the neural retinal part of the organoid using fine scissors (Figure 5e).

The removed RPE cell clump was dissociated into single cells and cultured as an adherent mono-cell-layer (Figure 5g) while the remaining ROs (Figure 5f) can be kept in suspension culture for an extended amount of time.

After differentiation, RO-characterization out-of-chip was performed. Results are provided in detail in Achberger, Probst and Haderspeck et al., 2019.

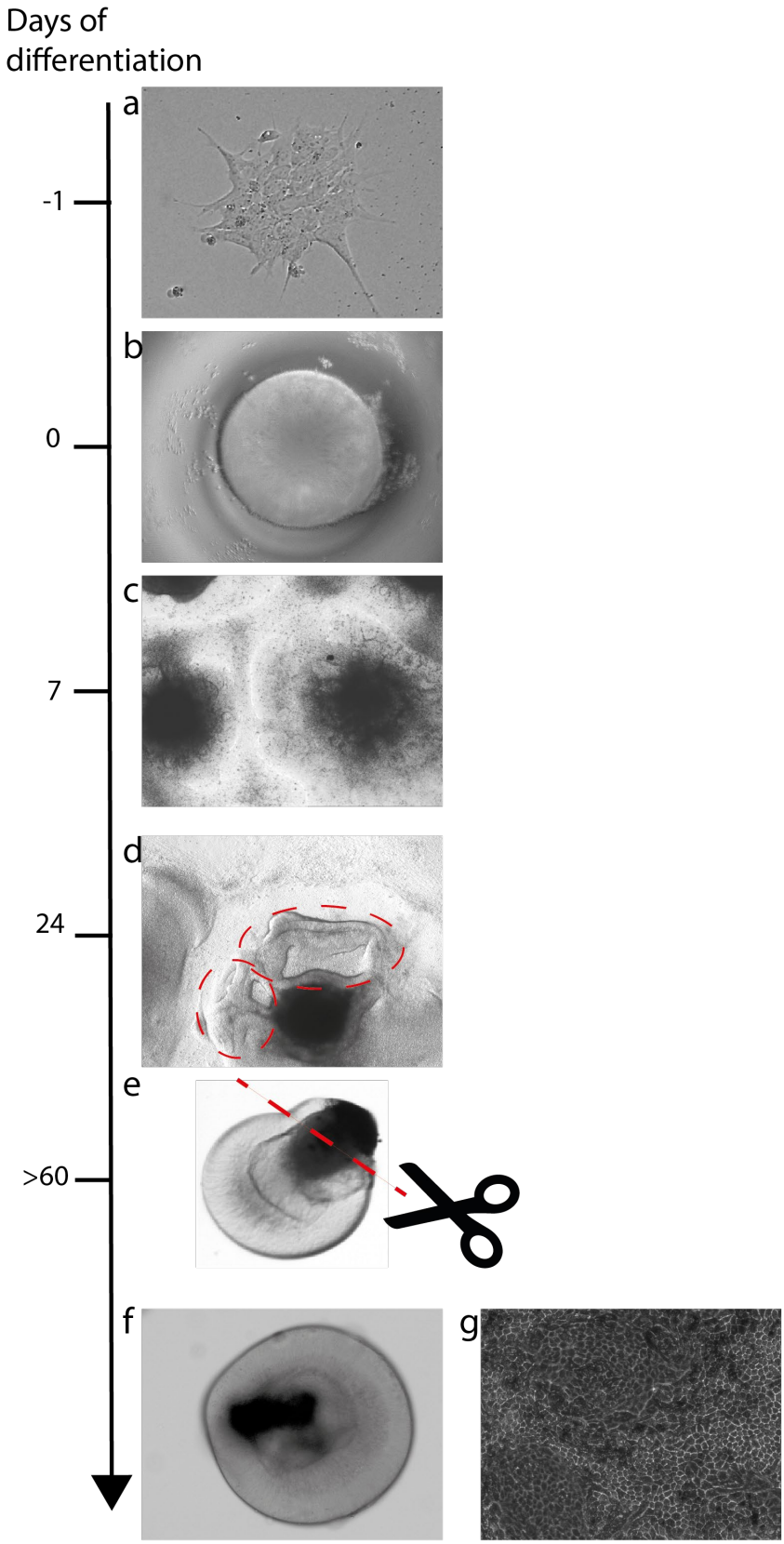

Figure 5: Steps of retinal organoid differentiation.

Number of days of differentiation is indicated on the left. Characteristic steps are shown under the bright-field microscope, including a) hiPSC colony, b) embryoid body (EB) formation, c) plating of EBs and

formation of neural rosettes, d) retinal field formation and area to be detached in red, e) retinal organoid in suspension culture with pigmented RPE are to be dissected along the line shown in red, f) retinal organoid in suspension culture, g) RPE cells as adherent culture.

5.2. Establishment and characterization of individual culture chips

5.2.1. The retinal organoid chip

To analyze whether the cells keep their morphology and characteristics also inside the chip environment, the ROs and RPE tissue were first examined separately in individual monoculture chips made of polydimethylsiloxane (PDMS). The concept of the individual-culture chips is shown in Figure 6a and Figure 7a. The culture chip for ROs consisted of 4 individual chambers (Figure 6a), each for the culture of one RO. Media supply was achieved by pipetting medium on top of each organoid onto the chamber (Figure 6b).

First, ROs were loaded into the specialized chips inside a hyaluronic acid-based hydrogel and morphology was monitored over a period of 3 days. As depicted in Figure 6c, the morphology did not change during that time and the ROs did not show any signs of cell degeneration since appearance of organoids under the bright-field microscope was constant over the examined period of 3 days. After this cultivation period, the organoids were retrieved from the chip, total RNA was isolated and mRNA expression levels analyzed and compared relative to dish-cultured ROs (Figure 6d). Typical retinal cell markers for retinal progenitor cells (RAX, LHX2, VSX2), Müller glia (GLUL, ANXA4), bipolar cells (PRKCA), horizontal cells (PROX1), photoreceptor cells (CRX, NRL GT1), photoreceptor outer segments (PRPH2), as wells as for the outer limiting membrane (ZO1) were analyzed in this context. The mRNA expression levels in none of the measured characteristic retinal cell types or structures changed significantly compared to dish cultured organoids, except for the outer limiting membrane-marker ZO1, where expression was increased significantly under chip-culture (Figure 6d).

Next, retinal organoids were analyzed for key structures and morphology on electron microscopic-level (Figure 6e). Fine microscopic structures characteristic for photoreceptors of retinal organoids at that stage were compared between standard dish-cultured organoids and chip-cultured organoids. For both conditions, the same characteristic structures could

be identified, such as segment-like structures, indications of membrane disc formation, and the typical ribbon synapse structures (Figure 6e).
Consequently, we can conclude that ROs maintain their morphology and typical marker expression inside the chip environment.

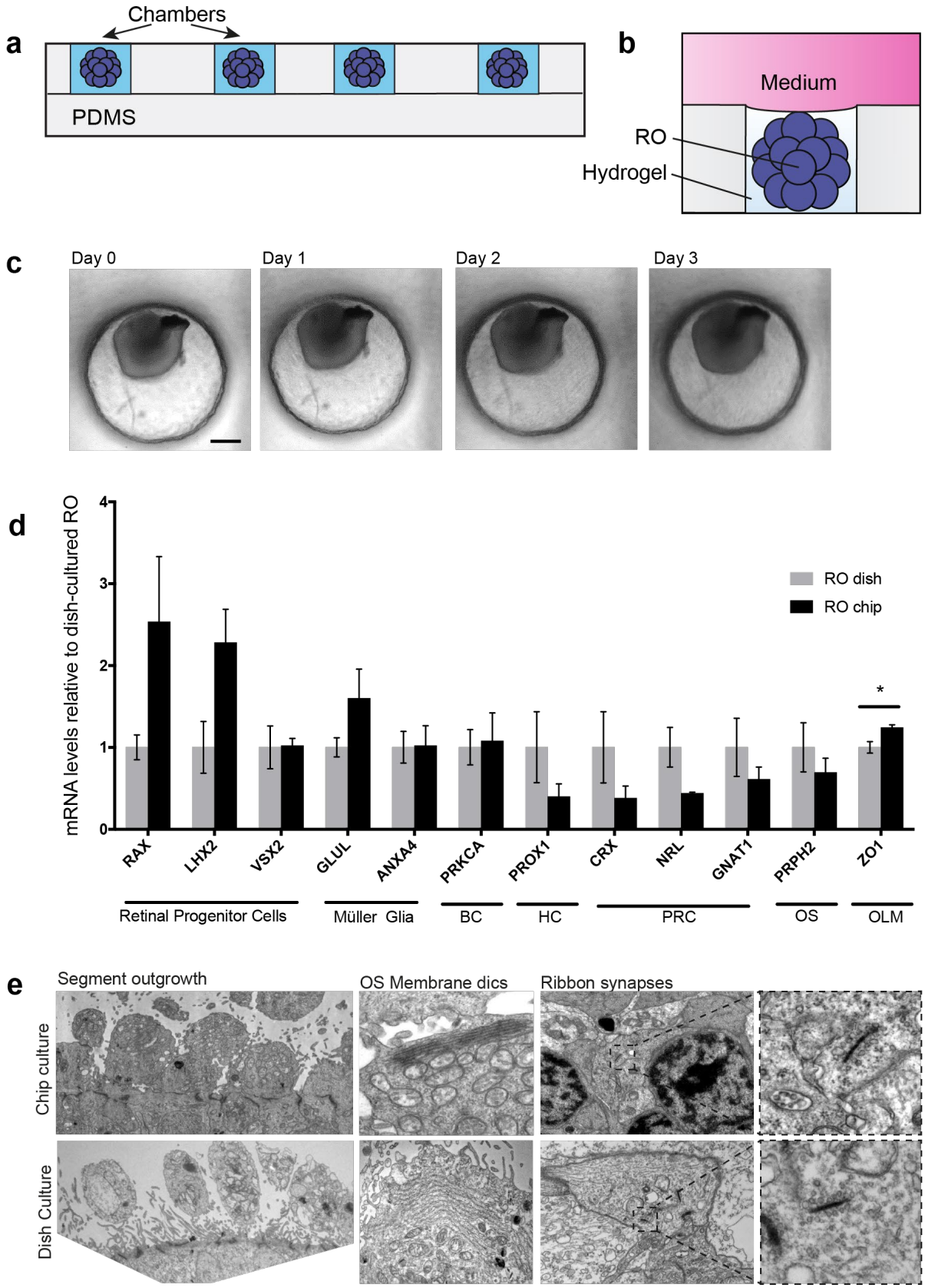

Figure 6: Retinal organoid-individual culture-chip.

a) Scheme of RO-chip as seen from the side. The chip is made of PDMS and consists of 4 chambers that form wells for the culture of one RO per chamber. b) *Scheme of RO-chip culture. ROs were embedded inside hyaluronic acid-based hydrogel into the chambers. ROs were supplied with medium from on top of the chamber. c) ROs were cultured in the chip for 3 days and observed under the bright-field microscope for morphologic changes. d) After culture in the chip for 3 days, ROs were retrieved from the chip and mRNA expression levels of characteristic markers for retinal progenitor cells (RAX, LHX2, VSX2), Müller glia (GLUL, ANXA4), bipolar cells (PRKCA), horizontal cells (PROX1), photoreceptor cells (CRX, NRL, GT1), outer segments (PRPH2) and outer limiting membrane (ZO1) were analyzed. Expression levels were compared to standard-dish cultured ROs. Statistical analysis was performed of RO chip vs. RO dish. e) Electron microscopic images of chip-cultured and dish-cultured ROs, showing characteristic structures of photoreceptor cells, including segment outgrowth, outer segment membrane discs and ribbon synapses. ANXA4=Annexin A4; BC=bipolar cells; CRX= Cone-Rod Homeobox; GLUL= Glutamine Synthetase; GNAT1=G protein subunit alpha transducin 1; HC=horizontal cells; OS=outer segments; LHX2= LIM Homeobox 2; NRL= Neural Retina Leucine Zipper; OLM=outer limiting membrane; OS=outer segments; PRC=photoreceptor cells; PRKCA= Protein Kinase C Alpha; PROX1= Prospero Homeobox 1; PRPH2=Peripherin 2; RAX= Retinal Homeobox Protein Rx; RO=retinal organoid; VSX2= Visual System Homeobox 2; ZO1=Zonula Occludens 1. Error bars: S.E.M. *p-value<0.05 (Two-sided student's t-test). Figure adapted from Achberger, Probst and Haderspeck et al., 2019 (CC BY 4.0).*

5.2.2. The RPE chip

To monitor cell morphology and characteristics of the RPE cells inside the chip environment, another monoculture chip was established, only containing a confluent layer of RPE cells. The RPE chip, also made of PDMS, consisted of 4 individual chambers with a polyethylene terephthalate (PET) membrane at the bottom and a medium-channel underneath (Figure 7a). The concept of a single chip chamber is represented in Figure 7b. RPE cells were grown adherent to the PET membrane.

RPE cells that were used for culture in the chip were cultured initially in standard dish-culture and were starved (cultured without addition of FBS) for at least 2 weeks (Figure 7c). While cells lost their pigmentation during proliferation steps, dark pigmented areas were again starting to form if RPE cells were starved over several months (Figure 7d). Consequently, RPE cells can regain these characteristics, which could also be identified under the electron microscope (Figure 7f). The RPE cells were dissociated before they were loaded in a defined cell number into the chip chambers and given 24 h for attachment. The cells were monitored over a period of 7 days. After 7 days, the morphology of the cells was cobblestone-like and cell borders were again visible (Figure 7e). The cells were then retrieved again from the chip, total RNA was isolated and mRNA expression levels of characteristic RPE markers were analyzed (Figure 7f). The chip-cultured RPE (RPE chip) was compared to dish-cultured RPE after 14 days of starvation in dish-culture (RPE dish starved).

Further, we also analyzed RPE cells directly after dissociation (passage 0, RPE dish p0) to monitor the effect of starvation (Figure 7f). All RPE-markers analyzed (RPE65, BEST1, ZO1, MITF, GP100, PEDF) were significantly higher expressed in starved RPE cells compared to p0 RPE cells. Moreover, chip-culture of 7 days led to comparable expression levels of all RPE markers as in 14 day-starved dish-cultured RPE, except for the tight junction-marker ZO1, where chip-cultured RPE cells showed significantly higher expression levels (Figure 7f). We can conclude that the starvation episode is important for RPE cells with regard to the expression of characteristic markers and further, that RPE cell keep their characteristics in the chip environment and that this culture can even help to improve tight junction formation.

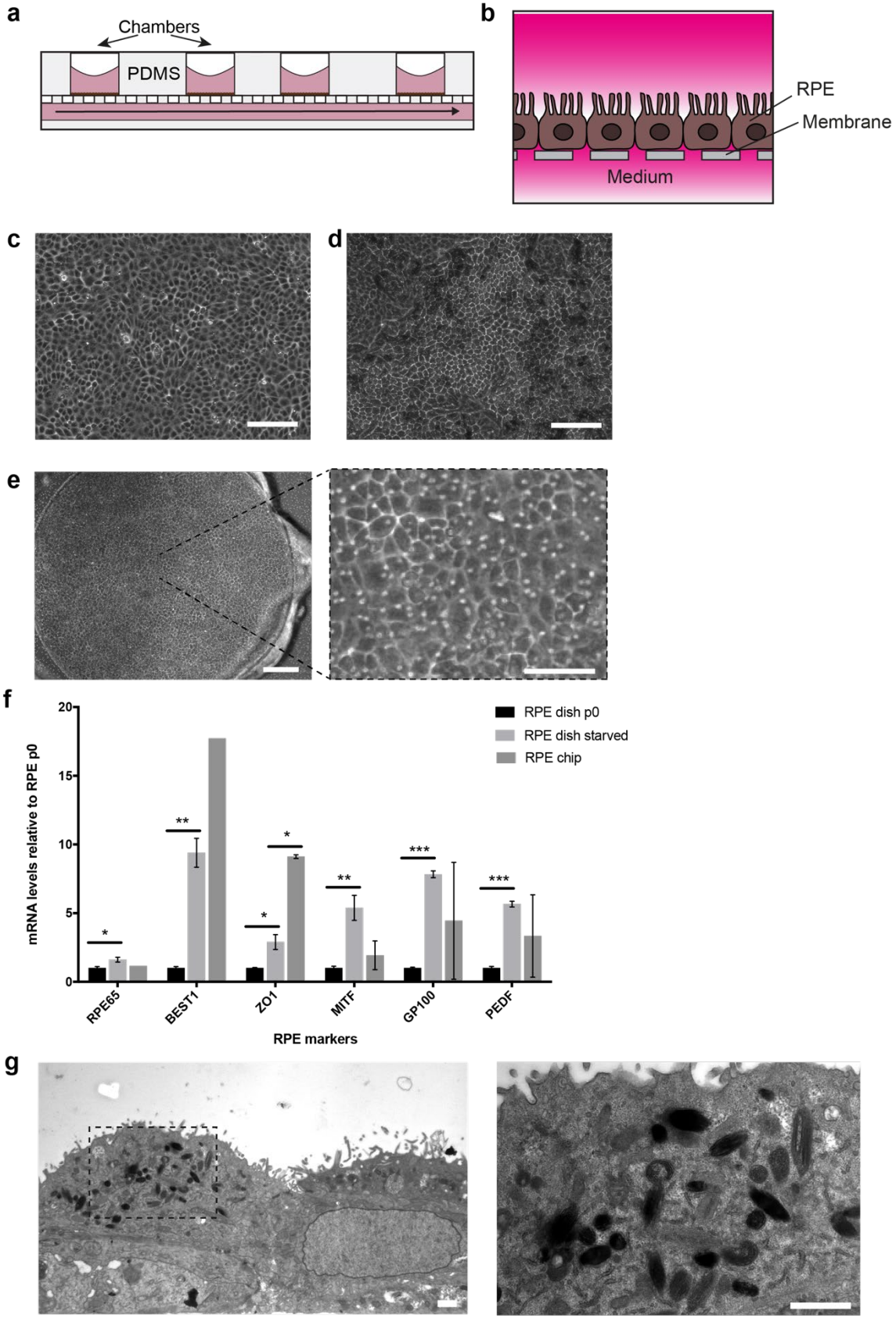

Figure 7: RPE-individual culture-chip.

a) *Scheme of RPE-chip as seen from the side. The chip is made of PDMS and consists of 4 chambers that form wells for the culture of a monolayer of RPE cells. b) Scheme of RPE-chip culture. RPE cells were*

*cultured adherent to the PET membrane. Medium was supplied from on top and via a medium channel underneath that can be connected to a syringe pump. c) Image of RPE cells after 2 weeks of starvation in dish-culture. d) Image of RPE cells after several months of starvation in dish-culture. Dark pigmented areas started to form. e) RPE after 7 days of chip culture. f) mRNA expression levels of RPE cells directly after dissection from the RO, dissociation into single cells and subsequent dish-culture (RPE dish p0), RPE cells at passage 3 after 2 weeks of starvation in dish-culture (RPE dish starved) and RPE cultured in the RPE chip for 7 days (RPE chip). mRNA expression levels are shown relative to RPE p0. Characteristic RPE markers were analyzed including RPE65, BEST1, ZO1, MITF, GP100 and PEDF. Statistical analysis was performed of starved vs. p0 RPE cells and of chip vs. starved RPE cells. BEST1= Bestrophin 1; GP100= Melanocytes Lineage-Specific Antigen GP100; MITF= Microphthalmia-Associated Transcription Factor; PEDF=Pigment Epithelium-Derived Factor; RPE65=Retinoid Isomerohydrolase RPE65; ZO1=Zonula Occludens 1. Scale bars: c) 100 µm, d) 100 µm, e) 100 µm, g) 1 µm, Error bars: S.E.M. *p-value<0.05, **p-value<0.01, ***p-value<0.001 (Two-sided student's t-test). Figure adapted from Achberger, Probst and Haderspeck et al., 2019 (CC BY 4.0).*

5.2.2.1. Immunohistochemistry of the RPE chip

As a next step, we aimed to verify characteristic marker expression inside the RPE chip on protein level using immunohistochemistry (Figure 8). Expression of RPE cell markers, including MITF and ZO1 was first compared between 7-day dish-cultured (Figure 8a) and 7-day chip-cultured (Figure 8b) RPE cells.

The transcription factor MITF which is expressed in the nucleus and is an early RPE marker during differentiation, was found to be equally expressed in the nucleus of almost every cell after 7 days in chip-culture (Figure 8b left). This was comparable to the situation after 7 days in the dish (Figure 8a left). The tight junction marker ZO1, which usually can be found in more mature RPE cells, was not equally expressed in the chip environment (Figure 8b right) but rather found in clusters. This was however, still comparable to dish-cultured RPE at 7 days, even though in the dish, the cell shape was more regular than in the chip at that time point. We concluded that longer cultivation of RPE cells in the chip might be necessary. Therefore, we decided to extent the cultivation period before monitoring marker expression again after 14 days in chip-culture and also before analyzing other markers characteristic for mature RPE cells (Figure 8c,d). On day 14, the tight junction marker ZO1 was found to be expressed in every cell and colocalization with the cytoskeletal marker phalloidin could be observed (Figure 8c left).

The melanosomal marker Melanoma GP100 (also called Glycoprotein 100, GP100 or Melanocyte protein PMEL) was found in the majority of cells with positive vesicles filling the cell bodies (Figure 8c right). This additional indication of pigmentation also verified the results gained from mRNA expression levels in the previous section (Figure 7f).

Further, the transcription factors PAX6 and MITF which are both necessary during RPE differentiation were also analyzed again after 14 days in chip-culture (Figure 8d). For both markers, a positive staining in the nucleus of the cells could be observed. However, intensity of expression was found to be variable between cells.
Consequently, observations made on mRNA level could be verified on protein level. We found the RPE markers MITF, PAX6, ZO1 and Melanoma GP100 to be expressed in RPE cultured in the chip environment.

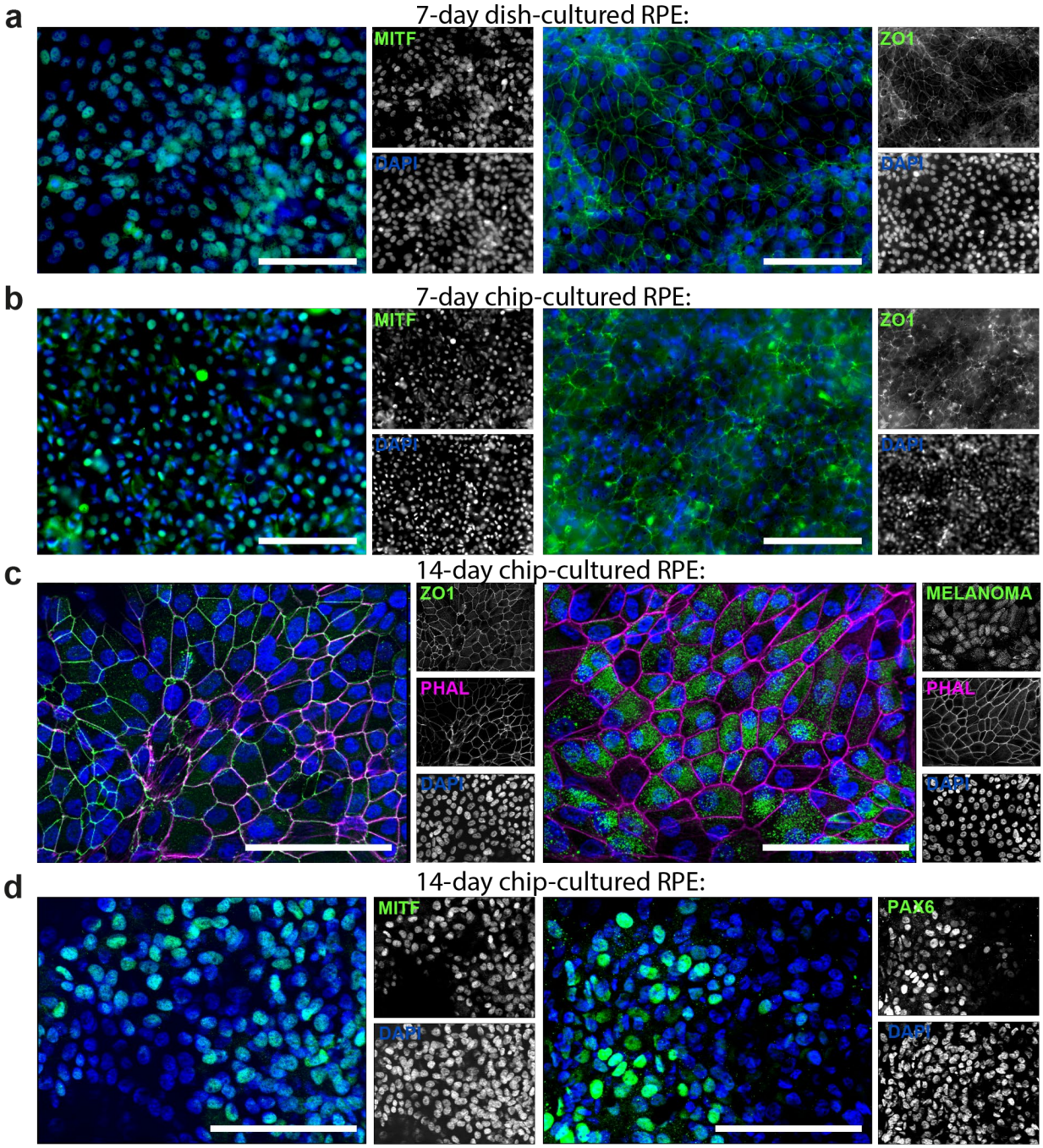

Figure 8: Immunohistochemistry characterization of RPE chips and comparison to dish-cultured RPE.

a-b) Comparison of characteristic RPE-marker expression between (a) 7-day dish-cultured and (b) 7-day chip-cultured RPE cells stained for the nuclear RPE marker MITF (green, left) and for the tight junction-marker zonula occludens 1 (ZO1, green, right). c) Immunohistochemistry of the 14-day chip-cultured RPE cells stained for the tight junction-marker zonula occludens 1 (ZO1, green, left) or for the melanosomal-marker melanoma GP100 (MELANOMA, green, right) as well as for the cytoskeleton marker phalloidin (PHAL, magenta). d) Immunohistochemistry of the 14-day chip-cultured RPE cells stained for the nuclear RPE markers MITF (green, left) and PAX6 (green, right). Scale bars: 100 µm. Figure adapted from Achberger, Probst and Haderspeck et al., 2019 (CC BY 4.0).

5.2.2.2. Polarization of RPE cells inside the RPE chip

RPE cells *in vivo* are polarized cells since they grow as an adherent monolayer. Morphologically, polarization is verified by the apical formation of microvilli and a basal lamina on the basal side.

To analyze whether the RPE cells in the chip show signs of polarization, we used immunohistochemistry to stain for ezrin, which is a marker protein for microvilli formation. Already on day 3 in chip-culture, this marker was found to be expressed in RPE cells inside the chip. The z-stack of an optical section in Figure 9a shows that the ezrin signal is polarized to one side of the cell, as it can also be seen in the 3D reconstruction in Figure 9b. The top view of the cell layer (Figure 9b, left) compared to the bottom view (Figure 9b, right) shows that ezrin is only expressed at the apical side of the cells and that expression is regular throughout the cell layer.

The formation of microvilli was also analyzed using electron microscopy of RPE cells after 7 days of chip-culture. In Figure 9c on the left, an RPE cell can be found with the upper side facing away from the membrane, consequently being the apical side. On the right, close-ups of the apical and the basal side of the cell are shown. We observed that the apical side of the RPE cell is carrying microvilli, whereas no microvilli can be found at the basal side. Here, signs of basal lamina formation can be found instead (Figure 9c).

Polarization of RPE cells also manifests as polarized secretion of certain growth factors. One example is the vasculature endothelial growth factor (VEGF-A) which is predominantly secreted to the basolateral side of the RPE cell, since this is also the side of the cells facing the choroid layer *in vivo*. This factor plays an important role in the maintenance of choriocapillaries. Using ELISA assays, we measured the amount of VEGF-A secreted to the basal and to the apical side over 24 h in RPE cells cultured in transwells or chips for 14 days (Figure 9d). Whereas in transwell-cultured RPE cells, significantly higher concentrations of VEGF-A at the basal side could be measured (Figure 9d left), we found a strong tendency towards a higher basal secretion in chip-cultures, which was however, not significant (Figure 9d right).

Taken together, these results indicate that the RPE cells inside the chip environment show polarization on a morphological and functional level.

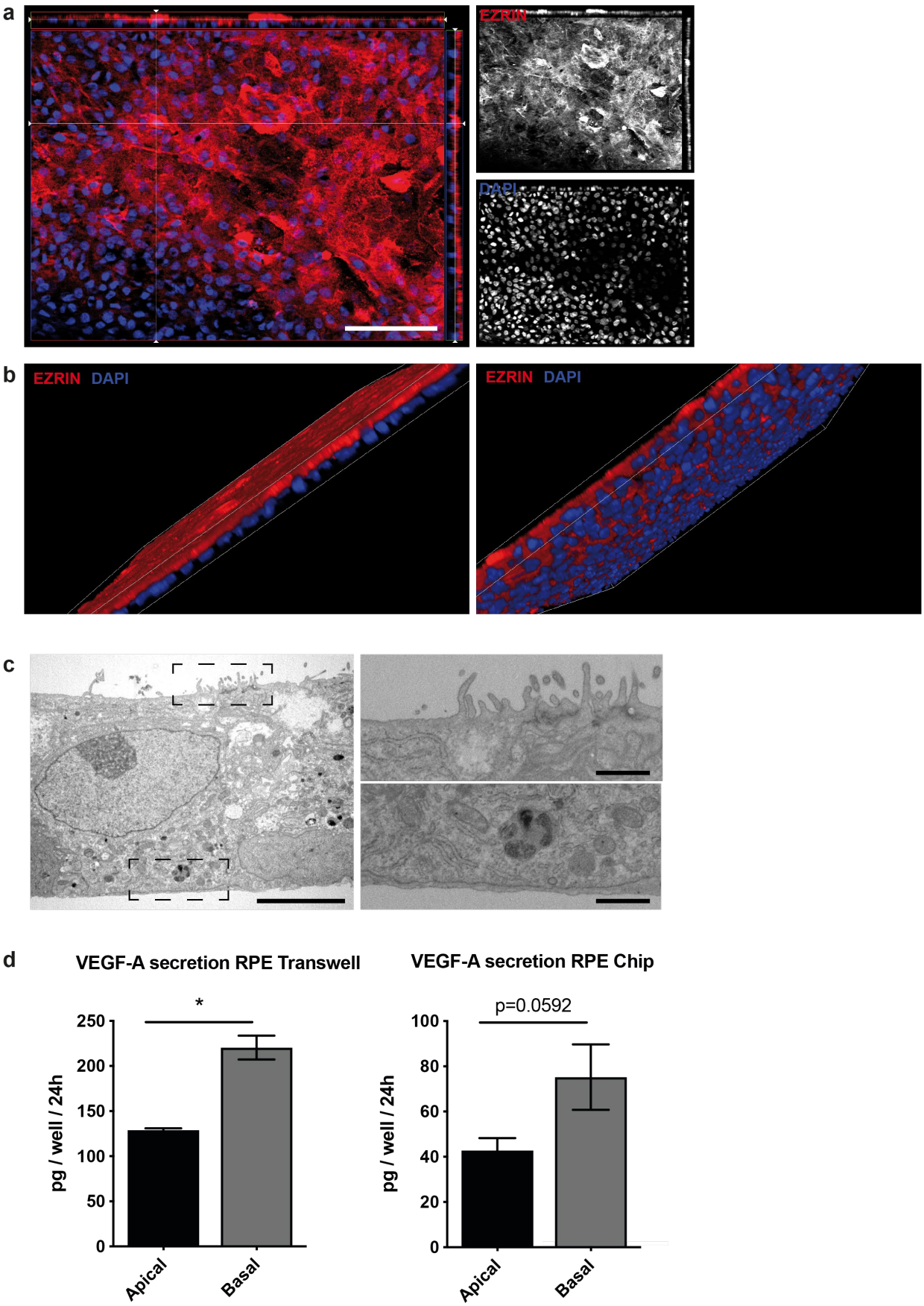

Figure 9: Characterization of polarization of RPE cells inside the RPE chip.

*a) Immunohistochemistry of day 3 RPE chips, stained for the microvilli marker ezrin (red). X-y-projection of an 0.55 µm-thick optical section. b) 3D reconstruction in a side-angle of (a), from above (left) and below (right) the RPE cell layer. c) Electron microscopy of RPE cells cultured in the chip for 7 days. On the right, close ups of the left image are showing the apical side of the RPE cells forming microvilli and the basal side of the RPE cells forming a basal lamina. d) ELISA assay of secreted VEGF-A amount measured over 24h from the apical and basal side of RPE cultured over 14 days in transwells (apical n=3, basal n=3) and RPE cultured over 14 days in the RPE chips (apical n=4, basal n=3). Blue: DAPI. Scale bars: a) 100 µm, c) left 5 µm, c) right 1 µm. Error bars: S.E.M. p= value, *p-value<0.05 (Two-sided student's t-test). Figure adapted from Achberger, Probst and Haderspeck et al., 2019 (CC BY 4.0).*

5.3. The retina-on-a-chip as a co-culture device for retinal organoids and RPE

5.3.1. Description of chip-setup

After individual culture chips had been analyzed, we combined both tissues in a retina-on-a-chip (RoC). The aim was to bring the ROs into close and physiological contact to the RPE, to replicate the situation of the retina *in vivo* as it is shown schematically in Figure 10a. Figure 10b and c show the setup of the RoC. The chips features 4 individual chambers (Figure 10b). Each chamber forms a well for the cultivation of one RO and a layer of RPE cells underneath. A side-view schematic representation of the chambers including ROs and RPE is provided in Figure 10c and a corresponding bright-field image is provided in Figure 10d. The chip is made of 2 layers of a biocompatible and optically clear plastic called PDMS, as used before for the individual-culture chips. The upper thick layer of PDMS forms the well for cell cultivations, whereas the lower layer forms a channel for media supply. Both PDMS layers are separated by a semipermeable and porous membrane made of PET with a pore size of 3 µm. This membrane allows attachment of the RPE cells while at the same time protecting the cells from shear forces generated by the media flow underneath. The chip further features an inlet and an outlet channel (Figure 10b) for medium supply. The chip can then be positioned onto a thin glass slide to be placed into a petri dish during cultivation which also allows microscopic analysis at a later point. Medium is solely supplied via a syringe pump (except for the day after RPE loading). For loading of cells, the wells are accessible from above, while during cultivation, the wells are sealed on top.

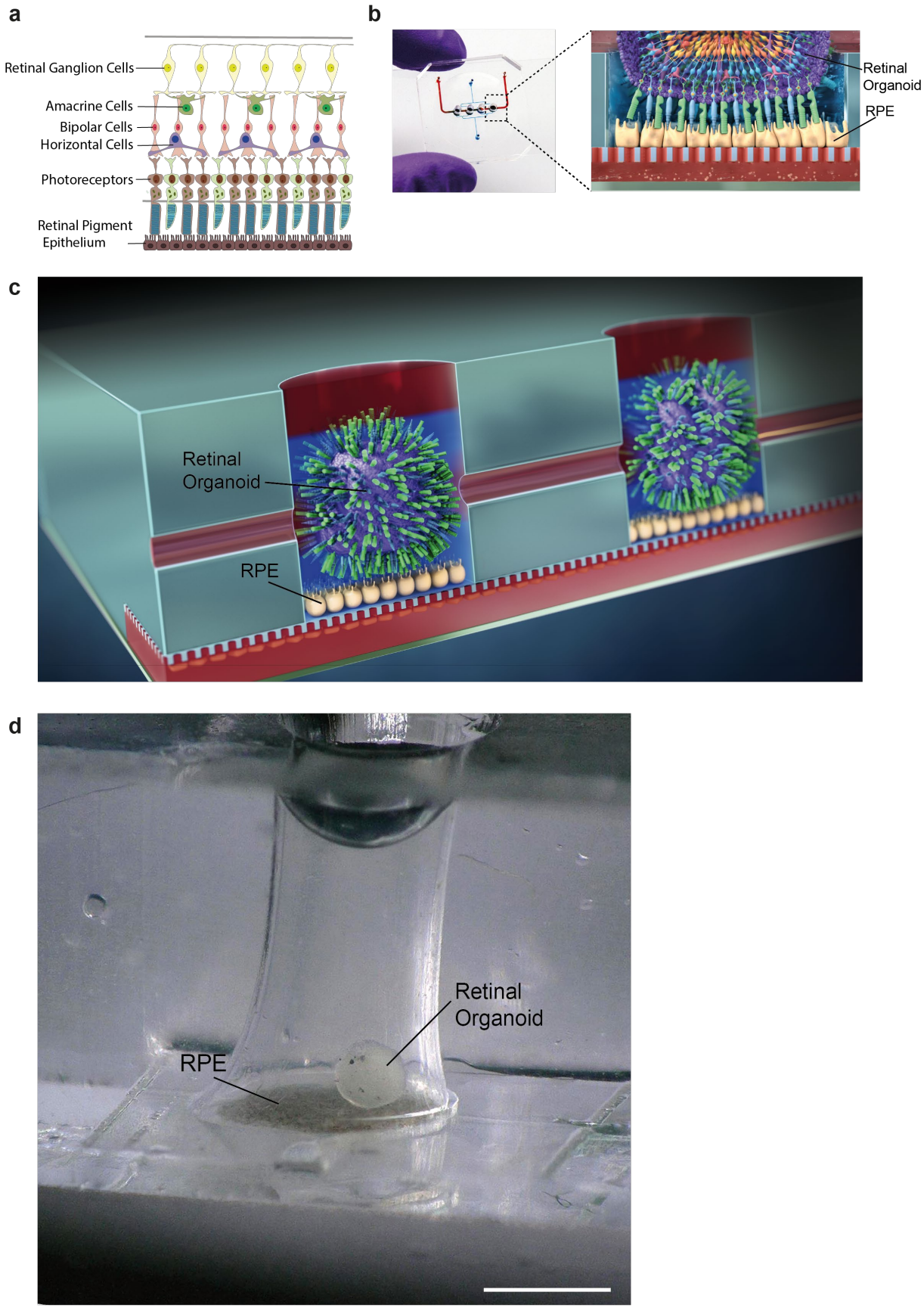

Figure 10: Setup of the retina-on-a-chip.

a) Schematic representation of the retinal layers inside the human eye, showing the close contact of photoreceptor outer segments and RPE cells. b) left: image of the RoC, which is hold in a person's hand for a better impression of the dimensions. The bottom (medium) channel is filled with a red fluid, the optional upper (culture) channel is filled with blue fluid. b) right: schematic representation of the RoC including one RO and RPE cells. c) 3D-schematic representation of the RoC (© Fraunhofer IGB). d) Side view image of one loaded well of the retina-on-a-chip to provide a better impression of the dimensions. At the bottom of the well, the RPE layer is visible as cells with pigmentation. On top, the retinal organoid can be found. Scale bar = 1000 µm. Figure adapted from Achberger, Probst and Haderspeck et al., 2019.

5.3.2. Loading of RPE and RO into the retina-on-a-chip

In the following, the several steps of the loading process of the RoC are described and depicted in Figure 11. The first step was the loading of RPE cells into the RoC. RPE cells were dissociated into single cells and could then be loaded in a defined cell number from the top of the chamber onto the coated PET membrane. This step is shown schematically in Figure 11a and d, as well as under the bright-field microscope in Figure 11g. RPE cells were then allowed to attach to the membrane overnight to form a confluent monolayer. During that time, medium was supplied from above, by pipetting a single media drop onto the chip. After 1 day, RPE cells usually form a dense monolayer of cells, if seeded at the correct cell density. This step is shown schematically in Figure 11b and e, as well as under the bright-field microscope in Figure 11h. The RPE cells were then supplied with medium via the medium channel underneath the PET membrane using a syringe pump connected to the chip. The chambers were sealed from on top, to prevent evaporation or contamination. Between 1-3 days after RPE seeding, ROs were then loaded into the chip. For this step, the sealing of the chamber was removed again to make them accessible from the top. One RO was transferred into each well and the well was filled with hyaluronic acid-based hydrogel. This hydrogel allowed nutrition of the organoid through small pores, while at the same time keeping the RO in place and preventing the RO-cells from direct attachment onto the RPE cells which would result in outgrowth of cells. Via this loading protocol, a defined space between RO and RPE should be achieved. This step is shown schematically in Figure 11c and f, as well as under the bright-field microscope in Figure 11i. Chips were then again connected to the syringe pump and chambers were sealed from the top.

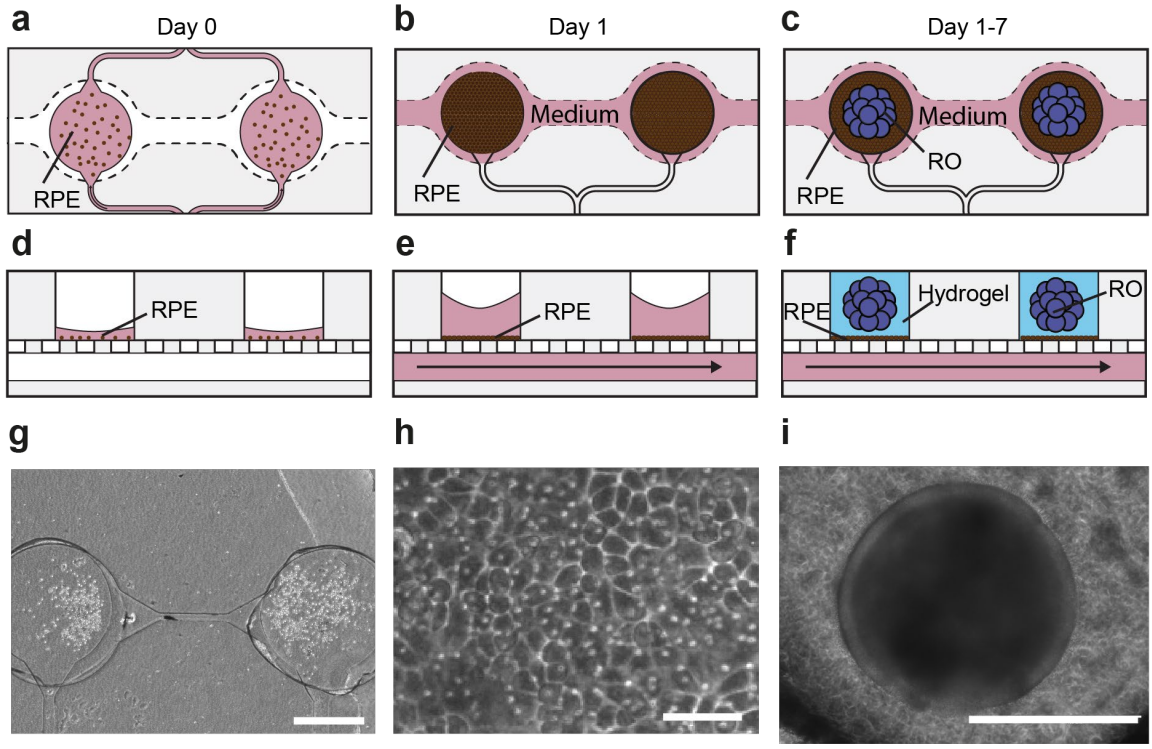

Figure 11: Scheme and images showing steps of loading procedure of the retina-on-a-chip.

a-c) Scheme of top view of chip: during RPE loading (a), 1 day after RPE loading (b), and during RO loading (c). d-f) Scheme of side view of chip: during RPE loading (d), 1 day after RPE loading (e), and during RO loading (f). g-i) Bright-field images: taken during RPE loading (g), 1 day after RPE loading (h), and during RO loading (i). a,d,g) On day 0, RPE cells were loaded as single cells after coating of the membrane. RPE cells can either be loaded via channels or from on top of the well in a defined cell number. After loading of RPE cells, medium was supplied via pipetting from on top of the well. Medium is shown in magenta. b,e,h) 1 day after loading, RPE cells grew adherent to the membrane and formed a dense monolayer. Cell borders became visible. Medium was now supplied via the medium channel below the RPE. c,f,i) After 1-3 days, ROs were loaded into each chamber, inside a hyaluronic acid-based hydrogel (blue). Medium was again supplied via the medium channel (see arrow). Scale bars are g) 500 µm, h) 100 µm, i) 500 µm. Figure adapted from Achberger, Probst and Haderspeck et al., 2019 (CC BY 4.0).

5.3.3. Analysis of the distance between RPE and retinal organoid inside the chip

After the behavior of individual tissues during cultivation had been evaluated, the co-culture RoC was examined. One important aspect to state whether a physiological setup inside the chip can be achieved, is the distance between RPE and RO. In a physiological setting, a close proximity of both tissues is necessary for the RPE to fulfill is functions of phagocytosis, nutrient-, as well as oxygen supply (Kurihara et al., 2016; Sparrow et al., 2010).

To answer this question, both tissues were labeled for fluorescence-imaging before loading them into the chip. RPE cells were labeled using viral transduction with an IRBP-GFP

construct that marks all RPE cells in green (Figure 12a, left) while photoreceptor outer segments of the RO were labeled using PNA-lectin. This lectin protein binds to outer segments of photoreceptors (Blanks and Johnson, 1984). It was coupled with the Alexa-fluor chromophore 568 that would mark all segments in red (Figure 12a, right).
After labeling, RPE as well as ROs were loaded into the chips as described before and live-cell imaging was used to visualize the position of both tissues (Figure 12b,c). In Figure 12b, a 3D-rendering shows the position and approximate distance between marked RO-segments and RPE. However, to gain more precise information on the distance, we used x-y-projections from optical sections (exemplarily shown in Figure 12c) and measured the distance over 12 images from different chip compartments. The calculated mean distance measured was 5 µm (± 3.19 µm) (Figure 12e). Consequently, we concluded that a defined setup with a small distance could be achieved with the RoC, as monitored directly after culture setup.
To analyze how culture over several days impacts the setup and respective positions of tissues in the chip, we used whole-mount immunohistochemistry of chips co-cultivated for 7 days to mark whole rod photoreceptors with rhodopsin, as well as whole RPE cells and whole organoids with the cytoskeleton marker phalloidin (Figure 12d). In this case, live cell imaging was not possible since it only allowed tracking of marked cells over short periods. An x-y-projection of a chip compartment after immunohistochemistry is shown in Figure 12d. This image provides the impression that photoreceptor segment tips and RPE cells were in close apposition, possibly even closer compared to directly after setup. Rhodopsin-positive signals were found not only connected to the RO (identified by a phalloidin-signal) but also within the layer of RPE cells (identified by DAPI and phalloidin).
The question whether on-chip-culture in the RoC actually leads to improved segment formation was analyzed in greater detail within the next section.

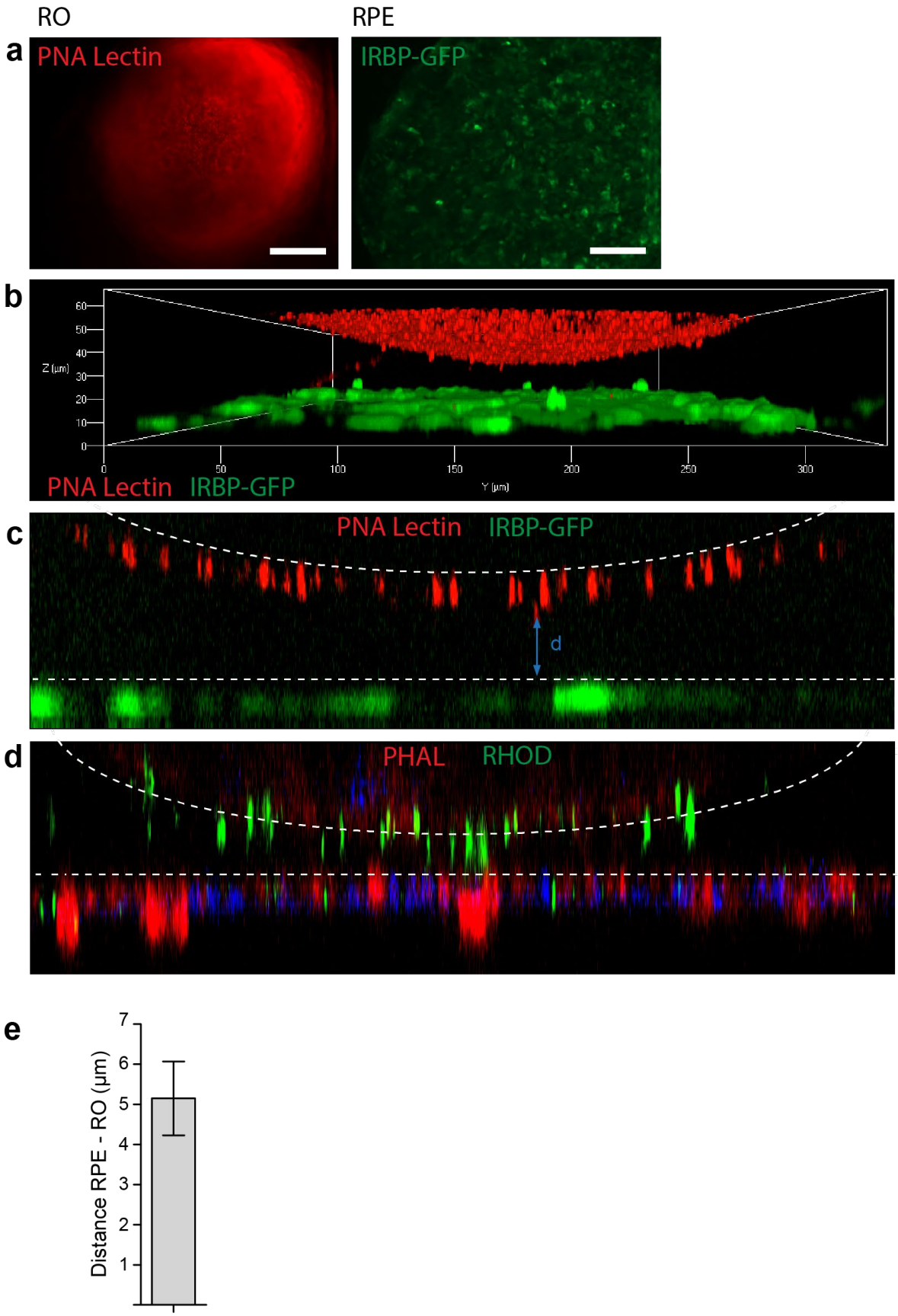

Figure 12: Analysis of distance between RO and RPE in the RoC.

a) *Photoreceptor segments from ROs were labeled with PNA-lectin Alexa Fluor 568 (red), RPE cells were labeled with an IRBP-GFP viral vector (green) construct before insertion into the chip. Live-cell imaging shows successful labeling. b-c) Live-cell imaging of co-culture chips after introduction of labeled ROs and RPE from a). b) 3D rendering of co-culture chip showing position of RO-segment tips vs. RPE cells. c) x-y-projection from optical sectioning as exemplary image to measure distance (d, blue arrows). d) Whole-mount in situ immunohistochemistry of day 181-RO and RPE co-cultured for 7 days in the RoC, stained for rhodopsin (green, rods) and phalloidin (red, cytoskeleton). Nuclei were stained with DAPI (blue). c-d) White dotted lines mark the surface of the RO (at the level of the OLM) and the surface of the RPE, respectively. e) Calculated mean distance between RO-segment tips and RPE over n=12 different chip compartments as shown in c). Figure adapted from Achberger, Probst and Haderspeck et al., 2019 (CC BY 4.0).*

5.4. Functional analysis of retinal organoids and RPE in the retina-on-a-chip

5.4.1. Analysis of photoreceptor segment formation and maturation

To be able to state whether the close proximity of both tissues, the ROs and the RPE, actually results in a functional interaction, we looked at some of the key functions as they would be observed *in vivo*. The first was to analyze if the presence of the RPE in the chip-setup leads to improvement of photoreceptor-segment outgrowth from the organoid. Therefore, we used immunohistochemistry to stain for the typical segment marker proteins. However, to be able to use immunohistochemistry, we built a specialized chip-setup, made of agarose, that would allow cryosectioning of the organoid and RPE inside the chip without destroying or moving the tissue.

We found that the space between ROs and RPE was filled with punctae positive for the rod marker rhodopsin and the outer segment marker ROM1 indicating that the photoreceptors facing the RPE possess these segments (Figure 13a). At higher magnification (Figure 13b), the positive punctae seem to form long processes of segment-like structures.

Next, we aimed to quantify the number of outer segments from organoids cultured in our standard PDMS chips together with RPE (RoC w/ RPE), relative to organoids cultured in the chip without RPE (RoC w/o RPE) and also in comparison to standard dish-cultured organoids (dish RO). For this purpose, electron microscopic slides from organoids (cultured for 7 days under the respective condition) were analyzed and outer segment structures per slide were counted manually. Exemplary pictures of each condition can be found in Figure 14a-c. Segment-like structures were identified by organized membrane-stack formations that are

shown in Figure 14d. The number of segment structures per 100 µm was compared between each condition (Figure 14e).

The mean number of outer segments was significantly higher in the organoids from co-culture chips, compared to standard dish-cultured organoids (Figure 14e) and also in comparison to RoC cultured without RPE (Figure 14e). We concluded that the chip setup leads to improved segment outgrowth and that especially the co-cultivation with RPE cells in a physiological manner can improve the formation of photoreceptor segments.

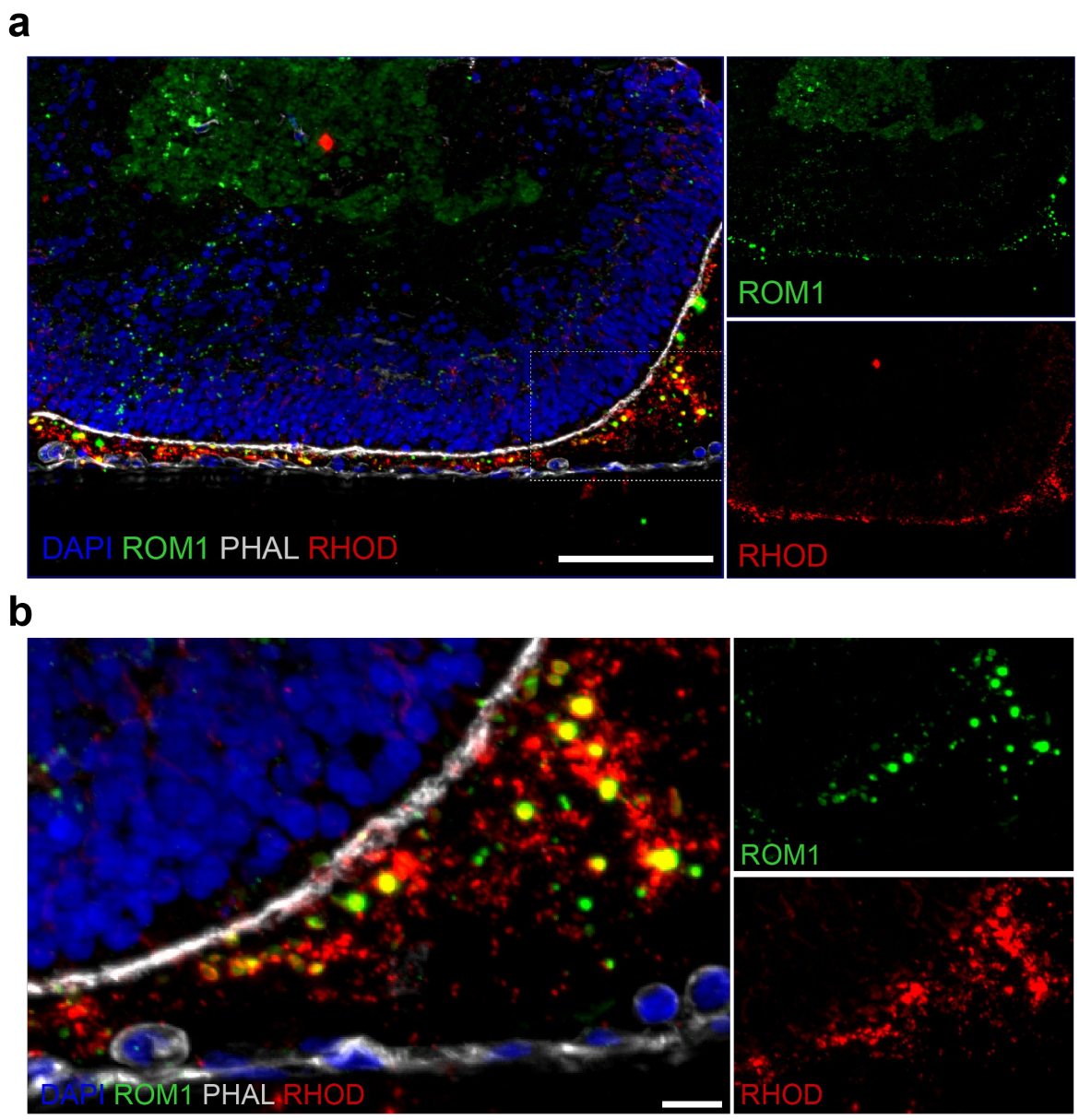

Figure 13: Photoreceptor segment-formation.
Immunohistochemistry of cryosections from a specialized agarose-chip-version cultured 7 days with d260 ROs and RPE. Markers stained for included the outer-segment marker ROM1 (green), the cytoskeleton-

marker phalloidin (PHAL, white) and rhodopsin as a marker for rod photoreceptors (RHOD, red). Nuclei were stained with DAPI (blue). B is an area from A (indicated by white box). Scale bars are a) 100 µm and b) 10 µm. Figure adapted from Achberger, Probst and Haderspeck et al., 2019 (CC BY 4.0).

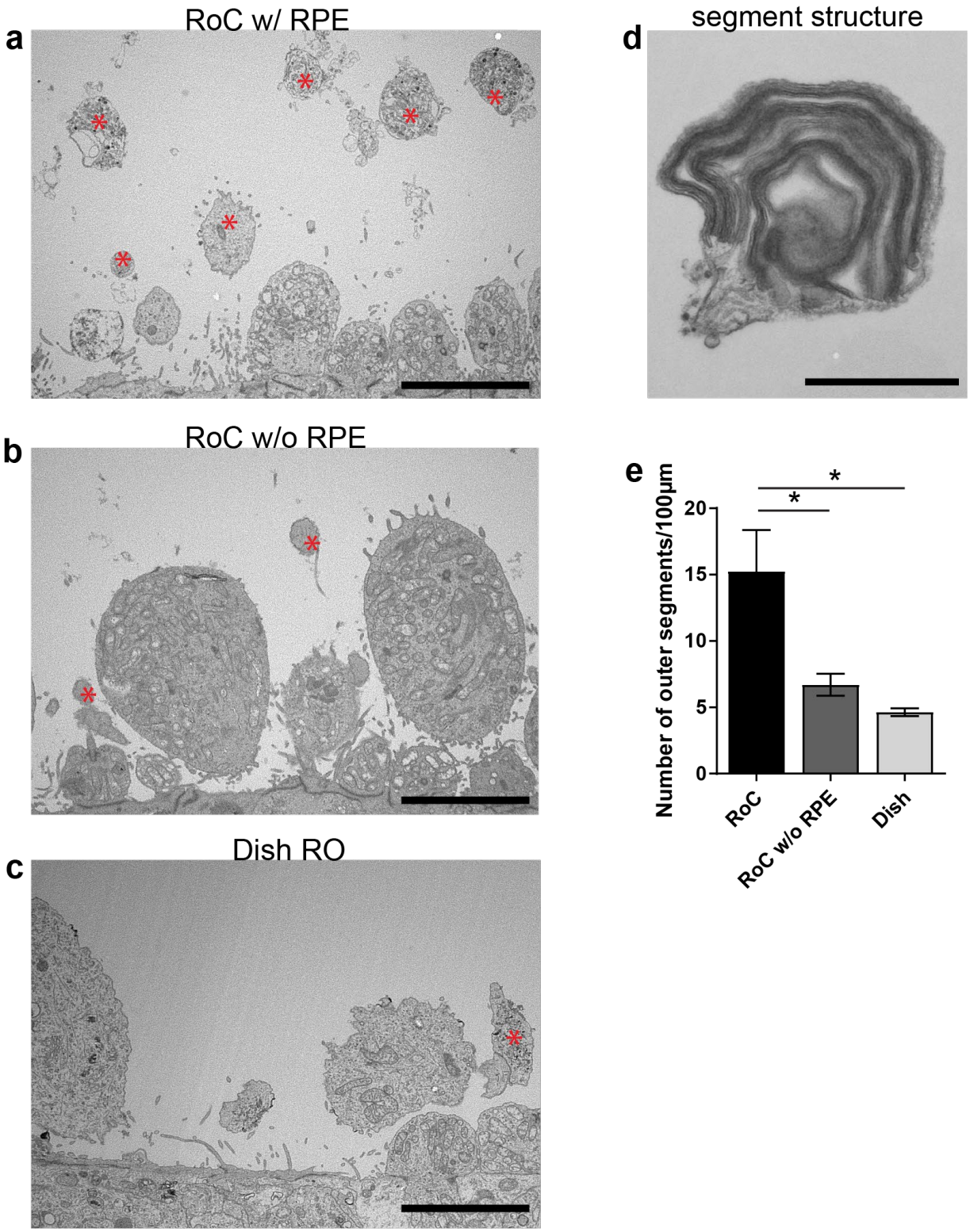

Figure 14: Photoreceptor segment-formation under the EM.
Electron microscopic sections from a) a RO cultured in the RoC with RPE (RoC w/ RPE), b) a RO cultured in the RoC without RPE (RoC w/o RPE), and c) a dish-cultured RO (dish RO). All ROs were 181 days old,

*cultured for 7 days under the respective condition. Red stars indicate outer segment-like structures that were identified by the formation of membrane stacks as shown exemplarily in higher magnification in d). The number of outer segments per imagine was counted on different images and the number of segments per 100 µm was calculated in e) (RoC w/ RPE n=3; RoC w/o RPE n=4; Dish RO n=3). Statistical analysis was performed of RoC w/ RPE vs. RoC w/o RPE as well as of RoC w/ RPE vs. dish RO. Scale bars are a-c) 5 µm, d) 1 µm. Error bars = S.E.M. *p-value < 0.05 (one-way-ANOVA with Bonferroni post-hoc test). Figure adapted from Achberger, Probst and Haderspeck et al., 2019 (CC BY 4.0).*

5.4.2. Functional analysis of interaction using phagocytosis assay

5.4.2.1. Phagocytosis of bovine outer segments out-of-chip

Another major function of RPE cells *in vivo* is the phagocytosis and digestion of shed photoreceptors outer segment (POS) discs (Sparrow et al., 2010). The first step to verify this function was to test whether our hiPSC-derived RPE cells were actually able to phagocytose outer segments in culture. Therefore, we performed a preliminary phagocytosis assay with hiPSC-derived RPE cells out-of-chip, in standard dish culture with cells seeded on cover slips. Cells were incubated for 2 h with bovine photoreceptor outer segments. Then, immunohistochemistry was performed using the early endosomal antibody EEA1, to observe endosomes and using rhodopsin as marker for rod photoreceptors to monitor phagocytotic uptake of photoreceptor segments into the RPE cells. After the 2 h incubation, we found a clear increase in EEA1 signal (Figure 15a), indicating an increase in early endosome formation. Further, rhodopsin-positive signals could be observed inside the RPE cells (Figure 15b). We concluded that our hiPSC-derived RPE cells were indeed able to take up bovine outer segments.

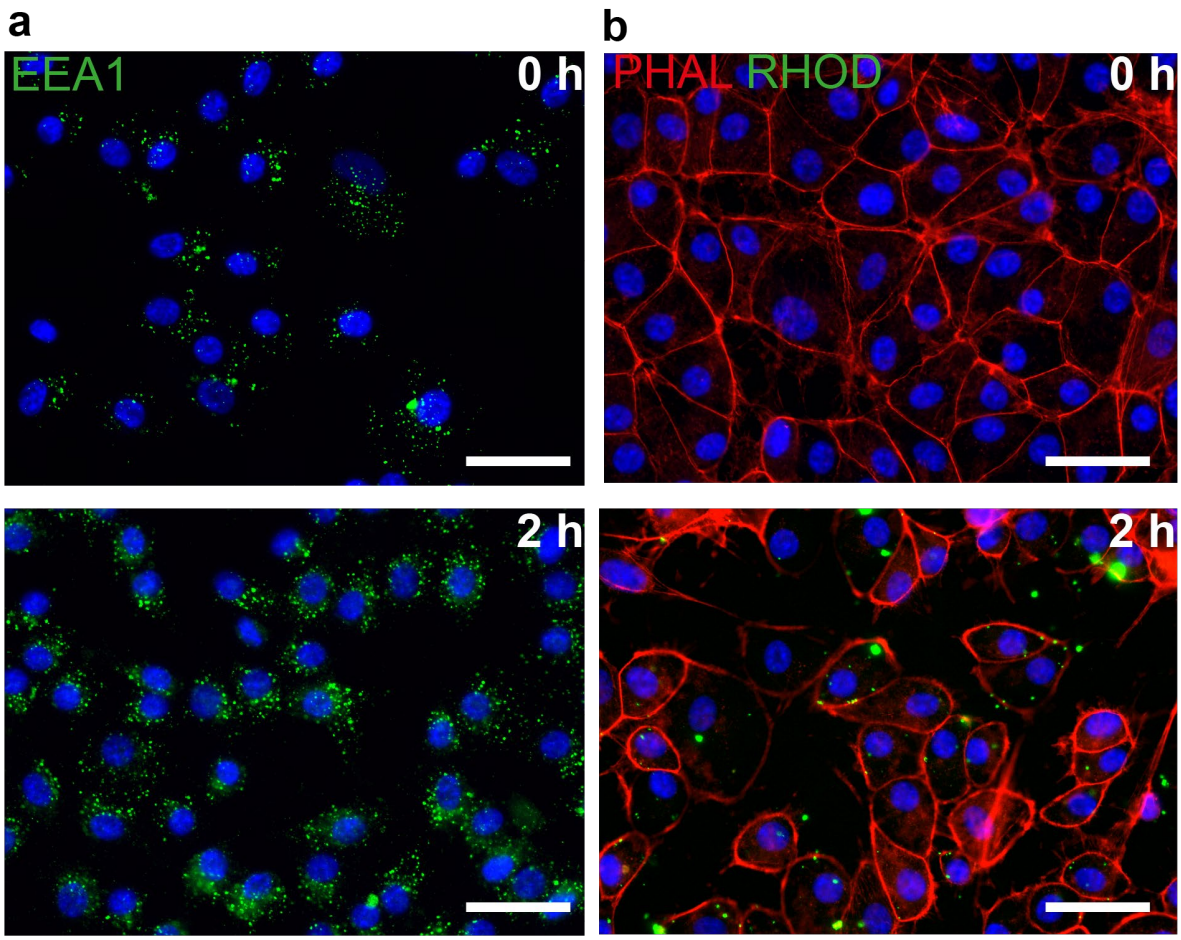

Figure 15: Phagocytosis assay with bovine outer segments on hiPSC- derived RPE cells out-of-chip.

hiPSC-derived RPE cells in standard dish culture grown on cover slips were incubated for 2h with bovine photoreceptor outer segments and then stained using immunohistochemistry for the early endosome marker EEA1 (a, green) or stained for the photoreceptor-marker rhodopsin (b, green) and the cytoskeleton marker phalloidin (b, red). Images at the top show untreated RPE cells, images at the bottom show RPE cells after the 2h incubation. DAPI (blue) was used to mark the cell nuclei. Scale bar = 40 µm. Figure adapted from Achberger, Probst and Haderspeck et al., 2019 (CC BY 4.0).

5.4.2.2. Phagocytosis of shed photoreceptors in the retina-on-a-chip

As a next step, co-culture chips were analyzed for signs of phagocytotic activity. For that purpose, segments of ROs were again labeled with PNA-lectin before co-culture was initiated. If RPE cells were able to phagocytose RO-segments also inside the chip setup, then PNA-lectin positive signals should be found inside the RPE cells. Prior to this experiment, RPE cells were labeled with an IRBP-GFP construct in green, for identification. Co-culture was initiated, and chips were cultivated for 1 day before the setup was analyzed using live-cell

imaging and optical sectioning. The x-z-projection as well as a 3D-projection of respective localization of POS and RPE in Figure 16a, showed that PNA-lectin positive signals could be found inside the green IRBP-GFP labelled RPE cell layer.

To verify that the positive signals obtained were actually parts of the photoreceptor segments, we used whole-mount *in situ* immunohistochemistry with a rhodopsin antibody after fixation of the 1-day-old co-cultures. A co-localization of the green PNA-lectin and the red rhodopsin-positive signals could be identified as yellow signals in Figure 16b.

Further, also in this setup, we aimed to visualize formation of early endosomes as a sign of an ongoing early phagocytotic process and as it could be observed with bovine outer segments out-of-chip before. Therefore, RPE cells were labeled with an early-endosomes-GFP construct before cells were used for on-chip-culture and co-culture with ROs was initiated for 1 day. The projection of an optical sectioning after immunohistochemistry for rhodopsin showed a co-localization of the GFP- and rhodopsin-positive signals inside the layer of RPE cells that were marked with a phalloidin-antibody (Figure 16c). Co-localizations are indicated with arrows.

Finally, phagocytosis in the cell will also lead to changes on an ultrastructural level. Therefore, we aimed to verify the results using electron microscopy after co-cultivation over a period of 7 days. Phagocytotic vesicles containing parts of photoreceptor outer segments, that can be identified by dense membrane-disks, were found inside the RPE cells, together with vesicles containing electron-dense material as indication of an ongoing digestion of lipid-membranes or debris digestion (Figure 16d).

Taken together, these results indicate that inside the RoC setup the RPE cells indeed have the ability of phagocytotic uptake of shed photoreceptor outer segments from the ROs.

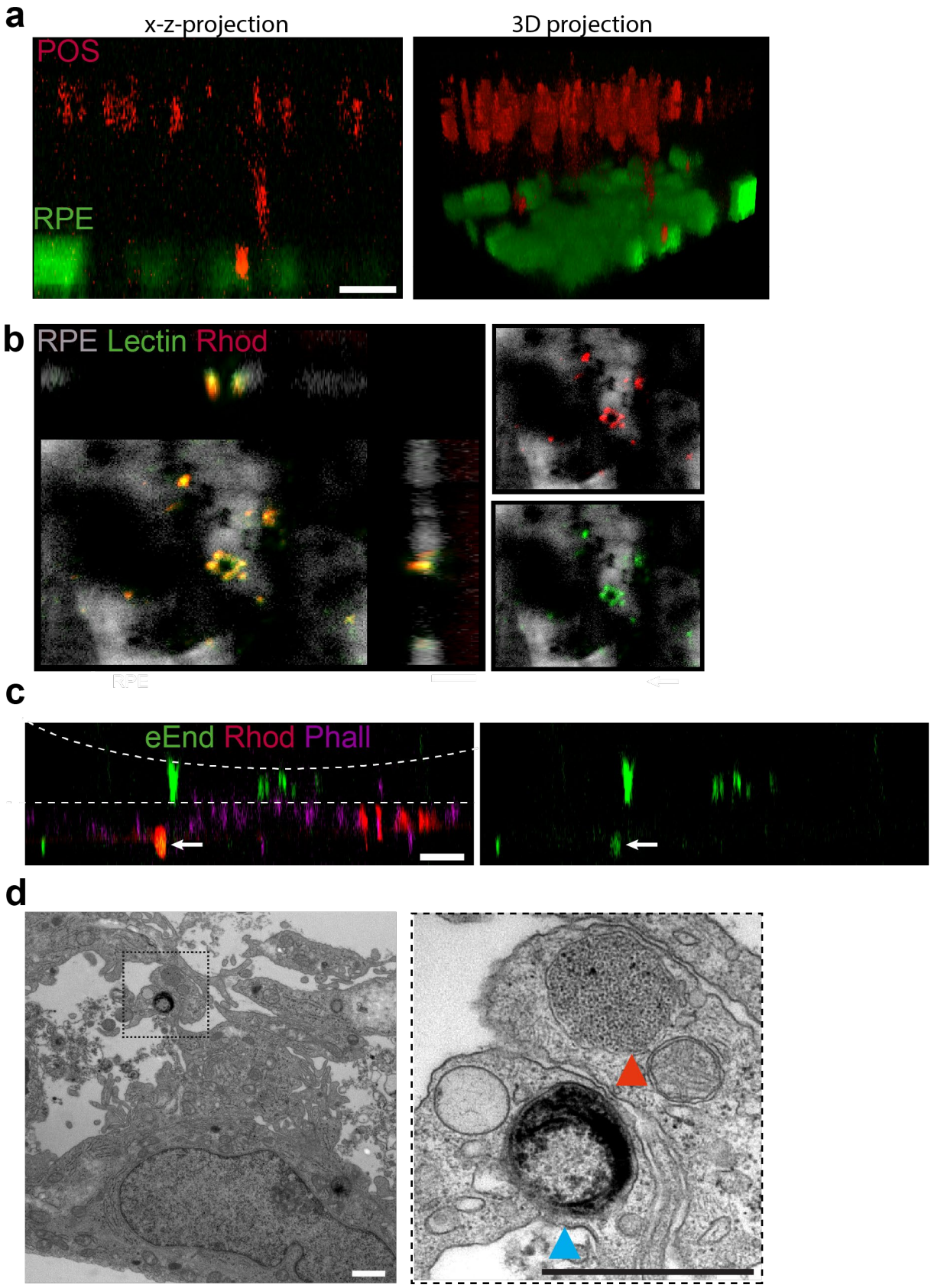

Figure 16: Functional analysis of the co-culture in the RoC using phagocytosis assay.

Co-cultures of ROs and RPE in the RoC setup were analyzed for signs of phagocytotic activity of the RPE. a) Photoreceptor outer segments (POS) of ROs were labeled with PNA-lectin (red), while RPE cells were

labeled with IRBP-GFP (green) before chip cultivation. After 1 day, live-cell imaging was used and both tissues are represented as x-z-projection, as well as 3D-projection to discriminated positions of POS vs. RPE cells. b) Immunohistochemistry of co-cultures from a), stained with PNA-lectin (green) as a photoreceptor segment marker, as well as with rhodopsin-antibody for rod photoreceptors (red). The IRBP-GFP signal of the RPE cells is depicted in white. c) Whole mount staining of day 1 co-cultures with RPE marked with early-endosomes constructs (green) before chip culture was initiated and subsequent immunohistochemistry was performed for rhodopsin (red, rods) and phalloidin (magenta, cytoskeleton of RPE cells). d) After co-cultivation of ROs in the RoC for 7 days, electron microscopy of RPE cells was performed. Signs of phagocytotic vesicles containing membrane stacks are marked with red arrows. Signs of phagocytotic vesicles containing electron-dense material as indication of an ongoing digestion of lipid-membranes or debris digestion are marked with blue arrow. Scale bars are a) 10 µm, c) 50 µm, d) 1 µm. Figure adapted from Achberger, Probst and Haderspeck et al., 2019 (CC BY 4.0).

5.5. Proof-of-principle study: the retina-on-a-chip as drug-testing device

5.5.1. Chloroquine

As a proof-of-concept study to test whether the RoC can be used as a drug testing device, we chose 2 chemicals with known retinopathic side effects.

Chloroquine is an anti-malaria drug that is known to lead to retinopathy if patients are treated long-term (Elman et al., 2009). The retinopathic effect was shown in literature to be at least partially associated with lysosomal dilation, leading to lysosomal dysfunction (Chen et al., 2011; Mahon et al., 2004; Rosenthal et al., 1978).

As a preliminary experiment to assess the necessary concentrations, we analyzed the effect of increasing concentrations (0, 20, 40, 80 µg/ml) of chloroquine on hiPS-RPE out-of-chip in standard dish-cultures (grown on coated coverslips) (Figure 17). These concentrations were known from literature for the treatment of ARPE-19 cells (Chen et al., 2011). After 24 h of treatment, we found clear signs of vacuolization to be observed under the phase-contrast microscope in a dose-dependent fashion (Figure 17a).

Cells on coverslips were then stained using immunohistochemistry against cleaved caspase 3 (CASP3) to assess a potential apoptotic effect and stained against the lysosomal membrane protein lysosome-associated marker protein 2 (LAMP2) to assess the impact on lysosomes in the cells (Figure 17b). Already the lowest concentration tested (20 µg/ml) led to a clear increase in LAMP2 signal (Figure 17b) indicating an increase in lysosome size that also corresponds to previous phase contrast images (Figure 17a). At higher concentrations, the effect increased gradually. Only at the highest concentration (80 µg/ml) however, an

elevated CASP3 signal could be detected, indicating apoptosis of the respective cells (Figure 17b). Consequently, we chose the lowest (20 µg/ml) and highest (80 µg/ml) concentration to be then tested in the RoC setup.

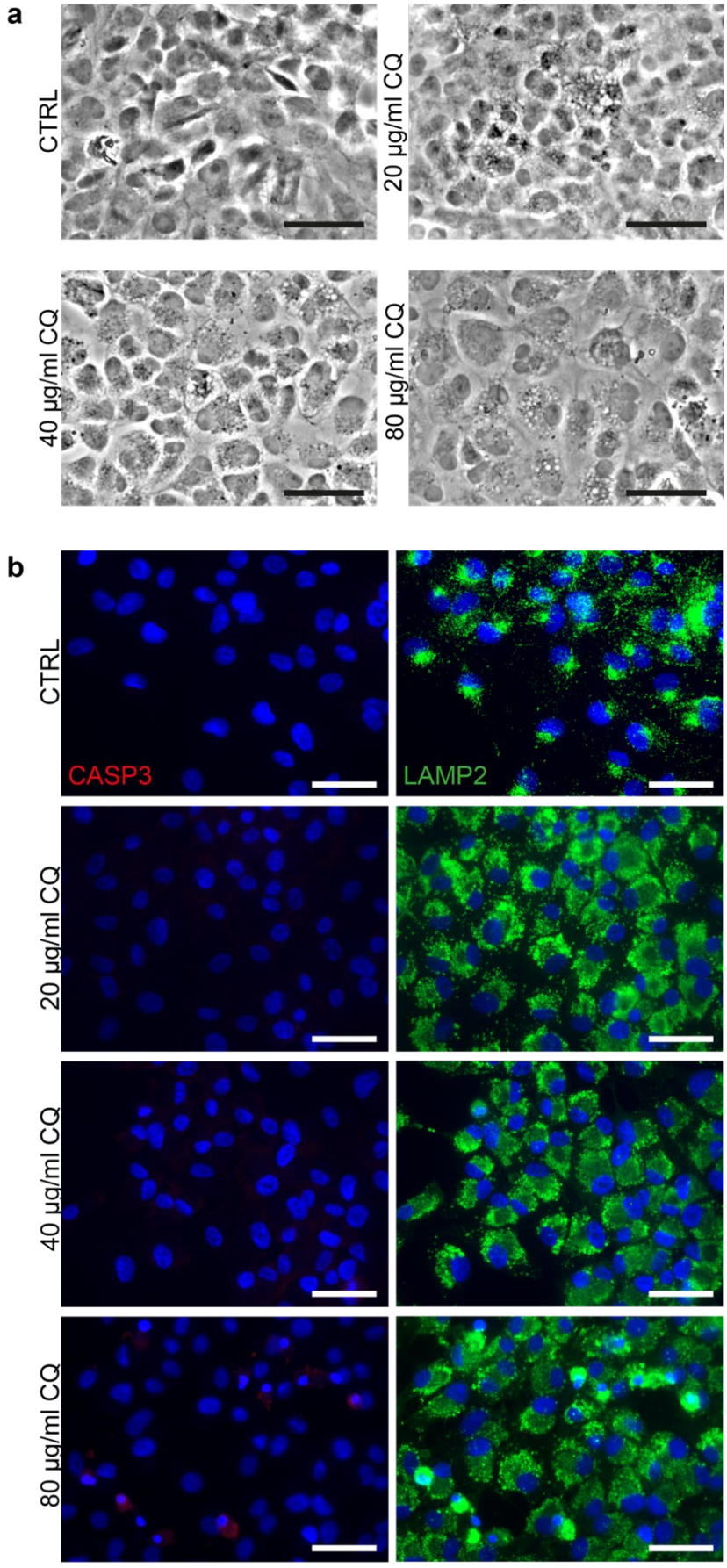

Figure 17: Effect of increasing concentrations of chloroquine on RPE cultured in the dish.

a) *hiPS-derived RPE that had been cultured on coverslips in 24-well plates was treated over 24 h with CQ at 20, 40 or 80 µg/ml and compared to untreated wells in the same plate (CTRL). a) Phase-contrast images of treated cells. b) Cells were fixed and stained using immunohistochemistry against the markers cleaved caspase 3 (CASP3, red) and against the lysosomal-membrane protein LAMP2 (green). Nuclei were marked with DAPI in blue. Scale bars: 40 µm. Figure adapted from Achberger, Probst and Haderspeck et al., 2019 (CC BY 4.0).*

Co-culture chips that had been cultured for 3 days were treated with chloroquine at 20 µg/ml and 80 µg/ml over a period of additional 3 days. Already under light-microscopic observation, morphological changes in the organoid could be monitored, since the shape became less round, the borders less sharp and the outer layer increasingly blurry (Figure 18a). To verify this observation, the drug-induced retinopathy was analyzed using propidium iodide (PI) staining since CASP3 staining did not seem sensitive enough in previous experiments (Figure 17b). PI is a dye marking dead or dying cells since their plasma membrane becomes leaky, allowing the dye to enter the cell (Crowley et al., 2016). The PI-signal intensity was quantified and compared to a non-treated control cultured over the same period of time. Whereas for the low concentration (20 µg/ml) of chloroquine, no obvious increase in PI signal could be observed, there was a significant increase after treatment with the high concentration (80 µg/ml) of chloroquine (Figure 18b). Moreover, the PI signal intensity from the area only covered by RPE was analyzed. Also in this case, a significant increase in signal intensity compared to the RPE-only area in control chips could be observed.

The treated co-culture chips where then stained using immunohistochemistry against the marker LAMP2. Whereas for the low chloroquine concentration, only a minor increase in LAMP2 signal could be monitored, the high concentration led to a strong lysosomal dilatation, since the LAMP2-marked vesicles became greater in size and a strong signal was visible (Figure 18c). The positive LAMP2 signal was visible in the RPE as well as in the RO. Consequently, the retinopathic, as well as the lysosomotropic effect of the drug can be recapitulated *in vitro* in the RoC setup.

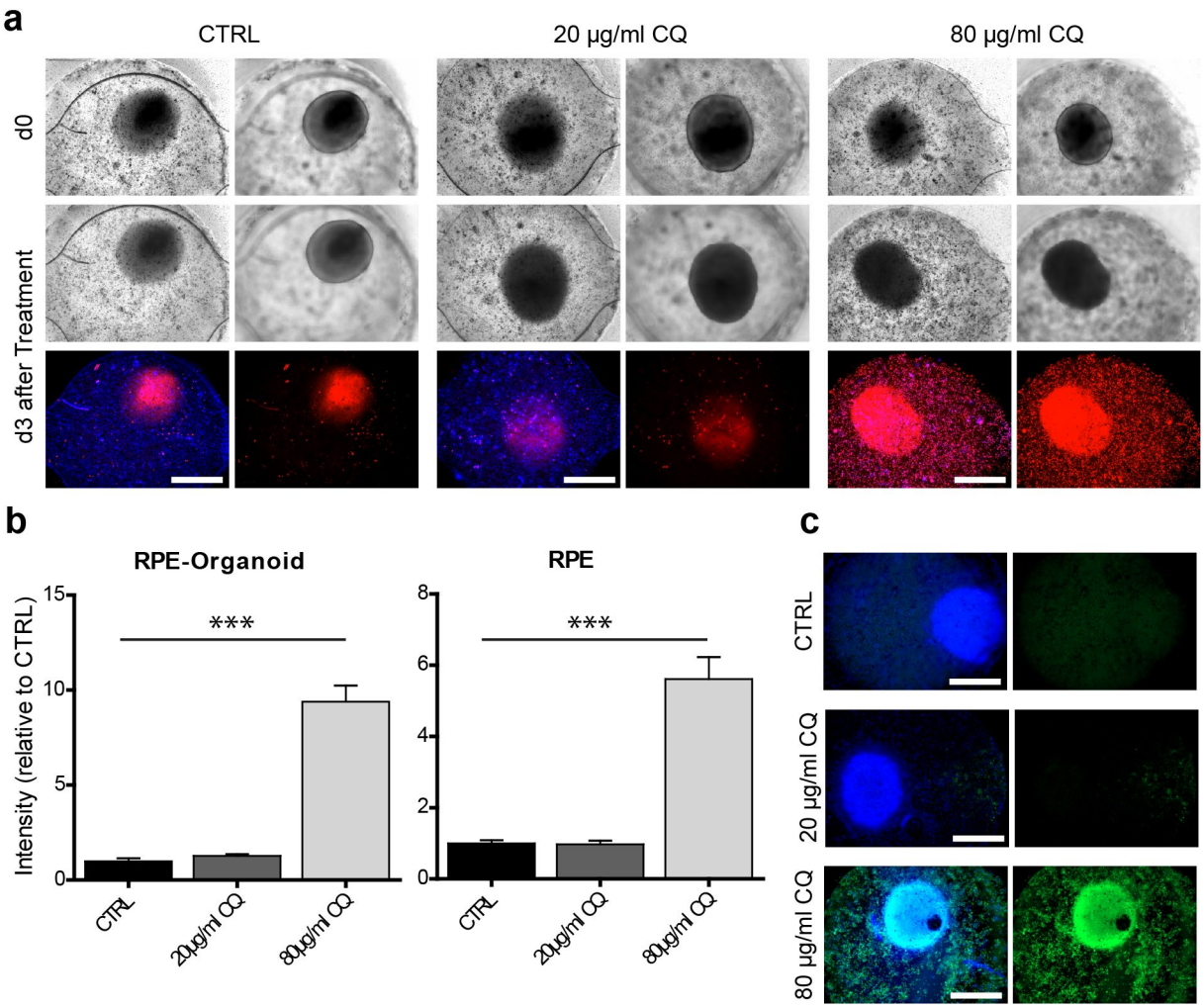

Figure 18: Effect of chloroquine treatment on the retina-on-a-chip.

*Retinal organoids (d243-260) and RPE were cultured in the RoC and treated over a period of 3 days with chloroquine (CQ) at 20 or 80 µg/ml. An untreated control (CTRL) was used as reference. a) On day 3, chips were stained with propidium iodide (PI, red, cell death) and live-cell fluorescence imaging of different treatment conditions was performed. Bright-field images and fluorescence-images were taken at different focus-levels: first, focusing on the RPE level (left) and second, focusing on the organoid level (right). Nuclei were stained with HOECHST (blue). b) Quantification of the PI signal intensity in the control (CTRL), the 20 µg/ml, and 80 µg/ml condition, as calculated relative to the control and shown for the combined RPE-organoid signal, and for the RPE-only signal (n=6-11 chip chambers per condition, 3 independent experiments). Statistically testing was performed of treated vs. control-intensities. c) Chloroquine-treated RoC were fixed and stained against the lysosomal marker LAMP2 (green) using immunohistochemistry. Nuclei were stained with HOECHST (blue). Error bars: S.E.M. ***p-value<0.001 (one-way-ANOVA with Dunnet post-hoc test). Figure adapted from Achberger, Probst and Haderspeck et al., 2019 (CC BY 4.0).*

5.5.2. Gentamicin

Gentamicin is an antibiotic drug used for example for the treatment of endophthalmitis (Hancock et al., 2005). We used this drug as another proof-of-concept to replicate known pharmacologic side-effects. Again, the effect of the drug treatment was analyzed using PI

staining to visualize drug-induced retinopathy with live-cell imaging (Figure 19a). Two different concentrations (0.5 mg/ml and 2.5 mg/ml) of gentamicin that had been previously verified, were used to treat RPE with ROs in the co-culture chip over a period of 6 days. The treated conditions were compared to non-treated controls in medium with diluent solution. Further, also ROs cultured in the RoC without RPE and treated with the same concentrations of gentamicin were compared to non-treated controls. The intensity of the PI signal was measured and is shown relative to the control-chip intensity in Figure 19b.

The low concentration (0.5 mg/ml) of gentamicin led to no obvious changes in PI signal intensity in the co-culture condition (RO + RPE), whereas in the RO-only condition, a minor increase in cell death could be observed. The high concentration (2.5 mg/ml) of gentamicin however, had a significant effect on cell viability in the co-culture RoC (RO + RPE), as well as in the RO-only setup, confirming a retinopathic effect of the drug *in vitro*.

However, the measured intensities always reflect the combined signals from RO plus RPE in the co-culture condition. To be able to compare the effect that the presence of RPE cells has on treated ROs, the intensities of RPE were subtracted from the combined signals. This revealed that for the 0.5 mg/ml treatment, no obvious effect can be observed if RPE is present as opposed to an increase in cell death if RPE is missing, indicating a protective effect of RPE presence for low concentrations of gentamicin.

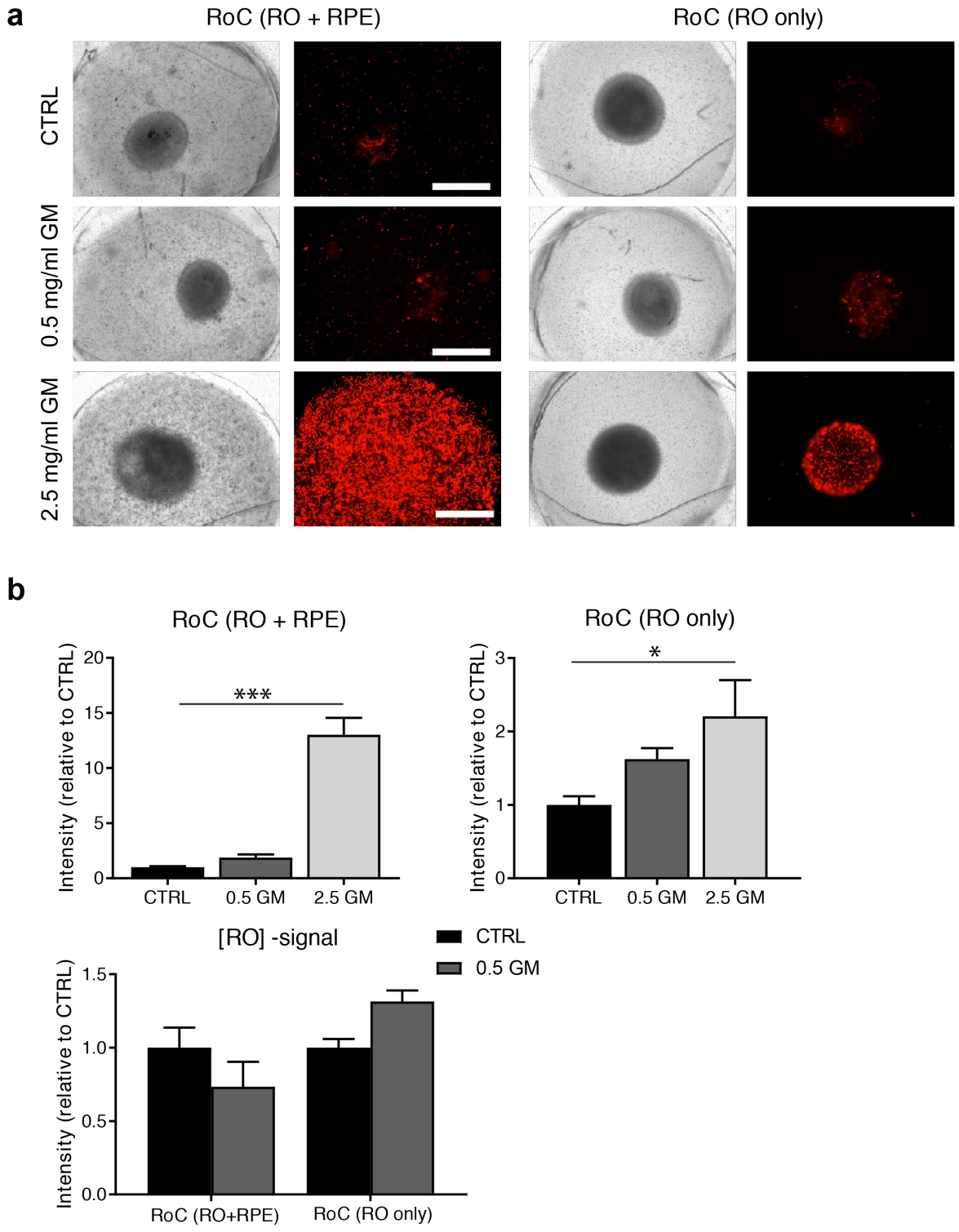

Figure 19: Effect of gentamicin treatment on the retina-on-a-chip.

ROs (d243-260) and RPE were cultured in the RoC and treated over a period of 6 days with gentamicin (GM) at 0.5 mg/ml and 2.5 mg/ml. A diluent-treated control (CTRL) was used as reference. a) Live-cell imaging of different treatment conditions of RoC stained with PI. On the left, the co-culture RoC is shown, including ROs and RPE. On the right, the RoC only contains ROs. Bright-field and fluorescence images are shown. The PI signal (red) was measured for every condition. b) Quantification of the PI signal intensity in the control (CTRL), the 0.5 mg/ml, and 2.5 mg/ml condition, as calculated relative to the control and shown for the combined RO + RPE signal, and for the RO-only signal (n=6-11 chip chambers per condition,

*3 independent experiments). A direct comparison of the signal intensity between the RoC with and without RPE for the low concentration (0.5mg/ml) GM is also provided. Error bars: S.E.M. *p-value<0.05, ***p-value<0.001 (b) one-way-ANOVA with Dunnet post-hoc test c) two-way-ANOVA with Bonferroni post-hoc test). Figure adapted from Achberger, Probst and Haderspeck et al., 2019 (CC BY 4.0).*

6. Discussion

6.1. Individual culture chips

We started the chip design for individual RPE or RO-cultures to make sure that a) individual tissues are cultured in the chip under optimal conditions and b) to establish ideal processes for loading, medium supply and analysis with suitable read-out methods.
As a first step, we verified that RPE cells as well as ROs can survive in the chip-culture and do not change characteristic marker expression as well as morphological characteristics.
After 3 days in the chip system, ROs did neither change morphology and microscopic structures, nor did they change marker expression of different retinal cell types.
Even fine microscopic structures of photoreceptors and their outer segments can still be found after chip-culture which shows that this method of cultivation is suitable to preserve such delicate structures. These results provide a first indication that culture of ROs in the chip system is not inferior to standard dish culture. Nevertheless, the segments initially observed inside the chip can still not clearly be referred to as mature “outer segments” since they are far from the length a photoreceptor outer segment would possess *in vivo*.
For RPE cells, the appearance was more difficult to judge since the confluent cell layer cannot simply be transferred to the chip but has to be dissociated instead. This is necessary to generate a cell monolayer adherent to the membrane integrated inside the chip. However, dissociation of the cells by enzymatic passaging can lead to a change of metabolism which becomes obvious by the fact that RPE cells can lose their pigmentation if passaged at low density (Shang et al., 2018) or if dissociated from a sphere, like in our case. It is known that especially the loss of cell contacts and polarity in this context can lead to loss of pigmentation in these cells (Shang et al., 2018). We have observed that after 1-3 months of culture under serum-free conditions, pigmentation can be restored as it was shown before for ARPE-19 cells (Ahmado et al., 2011; Luo et al., 2006). Of course, this long period of culture is not feasible when transferring the cells into the chip setup. Nevertheless, the initial step of cell dissociation cannot be avoided in this protocol. Therefore, it is essential to culture the cells for several months with addition of the appropriate growth factors (Ohlemacher et al., 2015) prior to chip-culture. When transferring the RPE cells into the chip, they then have to be passaged at high cell density to avoid loss of pigmentation and loss of

hexagonal shape (Shang et al., 2018). Using this method however, it is possible to generate RPE monolayers inside the chip that have both, the typical hexagonal shape and pigmentation (see Figure 3e and Figure 4c).

On mRNA level, all analyzed markers of ROs and RPE were expressed in the chip at least to a similar level compared to standard dish-culture. One marker to highlight here was ZO1, that was significantly higher expressed in chip conditions for the RPE and well as for the RO-chips. This molecule is part of tight-junctions at cell-to-cell borders, responsible for forming a tight barrier in epithelial cell types (Campbell et al., 2017). Further, it is part of the outer limiting membrane (OLM) of the neuroretina (Omri et al., 2010). It is possible that under the setting of the chip, especially the cell-to-cell-border formation is improved. This might be due to reduced movement of liquids and reduced shear forces (due to missing pipetting) that otherwise could cause weak junctions to break again.

These results provide indications that inside the chip system, the OLM of ROs is improved and the RPE can form a dense epithelial layer and hence, enabling a more physiological culture.

The goal of these initial experiments was to show that the chip-culture itself is not inferior to standard culture, therefore only short cultivation periods were chosen. If choosing longer periods for future experiments, it is possible that the increased expression of several other markers can be observed, as it was already the case for ZO1.

Taken together, these results indicate that cultivation of RPE cells and ROs inside a defined chip-setup is not inferior, possibly even superior to cultivation in standard dish culture. These findings allowed us to introduce both tissues into a combined chip setting, the retina-on-a-chip.

6.1.1. Immunohistochemistry of RPE cells inside individual culture chips

When analyzing the expression of typical RPE markers on protein level, we found already after 7 days of culture the marker ZO1 as well as MITF to be expressed in the chip-culture. This is in line with previous observations on mRNA level after 7 days of culture.

However, we observed that after 7 days, the marker ZO1 is not as regularly spaced compared to 14 days in culture. This might indicate that RPE cells need this time to regain

their regular quasi-hexagonal shape. As mentioned earlier, RPE cells require a certain time in the chip before they should be used for experiments.
The melanosomal marker Melanoma GP100 was found to be positive in vesicles filling the cell bodies (Figure 4c right). This might be an indication that, even if pigmentation is not clearly visible under the bright-field microscope at that time point, pigmentation markers are still expressed. This observation also verified the results from mRNA expression levels. Consequently, RPE cells show signs of maturity after 14 days in chip-culture.

6.1.2. Polarization of RPE cells inside individual culture chips

Since a functional RPE is of key importance for maintaining the function of the neuroretina (Kay et al., 2013) and therefore, also for a working physiological model system of the retina, we analyzed this tissue in greater detail. One aspect to judge the degree of physiology is a morphological and functional polarization of the RPE cell layer (Kay et al., 2013) which is essential for example for the selective transport of molecules and for the maintenance of different subretinal spaces with specialized chemical compositions (Cao et al., 2018; Kay et al., 2013; Sonoda et al., 2009).
One morphological sign of RPE polarization is the formation of microvilli processes on the apical side, which highly increases the surface and therefore the contact area between RPE and photoreceptor segment tips (Kiser et al., 2014). We analyzed microvilli formation using immunohistochemistry by staining for the marker ezrin, which is a membrane-organizing phosphoprotein and can be used as marker of polarization (Kivelä et al., 2000). Clearly, the ezrin-positive signals could only be found at the apical surface of the RPE cells. This was additionally verified using electron microscopy of the RPE layer which also showed long microvilli processes at the apical side, while at the basal side a dense layer was found that morphologically appeared similar to the basal lamina that would form the RPE's part of the Bruch's membrane *in vivo* (Aisenbrey et al., 2006).
A second indication for polarization of RPE cells is the polarized and directed secretion of certain growth or trophic factors (Kay et al., 2013). We analyzed the secretion of VEGF-A as an angiogenic growth factor secreted predominantly to the basal side of RPE cells since this is the side facing the choriocapillaries (Kay et al., 2013; Witmer et al., 2003). While in transwell cultures of RPE cells, the VEGF-A secretion was significantly higher towards the

basal side, we found a strong tendency but no significant results in the chip environment. This can be due to several factors. It is possible that VEGF-A secretion per se is not as polarized because cells are not as mature and polarized like in the transwell setting. However, it needs to be taken into consideration that measured volumes in the chip setup are much lower than in the transwell setup. Moreover, it was challenging to generate an exact equal volume output from apical and basal channels, since even small resistances in the channels can lead to distortions. While we accounted for volume differences between apically and basally collected volumes by respective calculations, it cannot be excluded that the measurement was not as precise as necessary.

However, if we combine results from ezrin staining, electron microscopy and growth factor secretion, we can conclude that the RPE inside the chip setup is indeed strongly polarized.

6.2. The retina-on-a-chip as a co-culture device for integration of RPE and retinal organoids

Since different methods of loading and cultivation were tested already in individual culture chips, we were able to integrate both tissues into a combined chip, by first loading RPE and - following its attachment to the membrane - loading ROs on the next day.
Our goal was then to analyze if the co-culture RoC actually leads to improved cultivation and more physiological conditions. Therefore, we looked at different aspects of the interaction and interplay of both tissues. Those aspects analyzed were the distance and physiological setup between RPE and ROs as well as an improved photoreceptor segment formation and phagocytosis by the RPE.

6.2.1. Analysis of distance

One aspect to judge a physiological setup inside the RoC is the distance between the RPE and the RO. We used live-cell imaging of labeled ROs and labeled RPE cells within the co-culture RoC setup to analyze the distance between both tissues directly after setup. The mean distance found via this method was 5 µm. It is possible that this method of distance measurement is not precise enough to make a statement on the absolute distance, since it depends largely on the number of optical stacks used and imaging from the side was not possible. However, since 12 different chip compartments were used, we can still conclude that one can find a consistency over different experiments regarding the distance.
In vivo, one would expect to find zero distance between both tissues, since the RPE cell would normally engulf the photoreceptor segments tips with their microvilli processes (Kevany and Palczewski, 2010). Only such a close apposition allows the phagocytotic uptake of cell debris and shed segments, while at the same time supplying the photoreceptor cell with nutrition and keeping up the visual cycle (Kevany and Palczewski, 2010; Sparrow et al., 2010). However, in our RoC setup, we assume that the photoreceptor outer segments from the ROs are not fully mature yet and therefore, do not have the same length as they would have *in vivo*. Consequently, zero distance between ROs and RPE would not allow the segments to grow longer. Indeed, we found that after 7 days of co-culture, the distance between segment tips and RPE seems to be reduced. It needs to be noticed that whole-mount staining was used at this time-point and therefore, a different method of cell labeling,

since labeling with PNA-lectin will not be visible for longer than 3 days. Moreover, rhodopsin signals at this time-point were also found within the layer of RPE cells (as a possible indication of disk shedding), making it difficult to point out segments that are still part of the RO. Therefore, we can conclude that ROs and RPE within the RoC are in very close apposition and that this positioning can be replicated.

6.2.2. Analysis of segment formation

The second aspect to judge a physiological interaction was whether the presence of RPE in the chip and the setup inside the RoC can lead to improved photoreceptor segment formation.

Even though recent publications were able to show that outer segment formation can be achieved in photoreceptors of ROs, these outer segments are still described as rudimentary and developing (Li et al., 2018; Mellough et al., 2019). It is known that the close contact between RPE and photoreceptors can influence the spatial organization of the retina with regard to photoreceptor outer segment differentiation and orientation (German et al., 2008). Therefore, it is possible that bringing both tissues into the required close contact, an improvement of photoreceptor segment maturation can be achieved.

Here, segment formation of the photoreceptors of ROs in the RoC setup was analyzed using immunohistochemistry and electron microscopy. We found indications that not only new segments are formed within the RoC within only 7 days, but moreover the RoC even seems to improve this process compared to standard dish-cultured ROs. This can be due to several factors: First, it can be due to the absence of shear forces in the area around the ROs, while in standard dish-culture, the process of medium change or maybe even movement of the plate itself, might destroy some of the developing segment-structures. Second, the presence of RPE in a physiological setup might help to improve segment formation, since RPE cells produce trophic factors for the photoreceptors and also have the ability to phagocytose shed outer segments as well as debris (Molday and Moritz, 2015; Steinberg, 1985; Strauss, 1995). A combination of these factors could help to provide a physiological environment that allows segments to grow and keep photoreceptors in a close-to-physiological state.

Nevertheless, one needs to take into account that segment formation was not monitored with live-cell imaging here and that preparation of the tissue as microscopic slides (either for

IHC or EM) was necessary. This process can always result in tissue destruction and the actual number of segments in each condition might vary depending on the methods used.
For future experiments, live cell monitoring of segment formation and longer cultivation periods might reveal the full impact that this RoC setup has on outer segment formation.

6.2.3. Analysis of phagocytosis

The third aspect regarding functional interaction between both tissues in the RoC was the analysis of the RPE's ability for phagocytosis of photoreceptor segments. Ingestion and phagocytosis of membranes stacks of the photoreceptor outer segments that continuously shed these structures, is an important function of the RPE during the visual cycle as well as for the renewal of segment structures (Kevany and Palczewski, 2010; Sparrow et al., 2010). To answer whether this functional ingestion can actually be observed in the RoC, we have shown with live-cell imaging and immunohistochemistry that different markers for photoreceptor segments can be found inside the RPE cells after co-cultivation with ROs inside the chip. Even though it provides the strong impression, these results cannot exclude that the identified parts of photoreceptors are only within in the layer of RPE cells but not actually taken up inside a cell. Therefore, in addition, signs of early endosome formation were analyzed, indicating a phagocytotic process which involves fusion of these early endosomes with phagosomes and formation of phagolysosomes during the digestion of particles (Kevany and Palczewski, 2010). The co-localization of early endosomal-bodies with rhodopsin provides an indication that the segment structures have actually been ingested by the cell and have initiated a phagocytotic process. Further, also on an ultrastructural level, morphological signs of phagocytotic bodies could be overserved.
Altogether, these results indicate that a physiological setup and interaction between the ROs and RPE inside the RoC can be achieved and that the RPE generated from hiPSC is capable of a functional digestion. Nevertheless, the rate of phagocytosis vs. disk renewal cannot be observed in this setup to state whether the degree of phagocytotic uptake is close to the physiological setting.

6.3. Proof-of-principle study: the retina-on-a-chip as drug-testing device

One of the goals for developing a retina-on-a-chip system was the possibility to use it as a drug-testing device for the discovery of new drugs as well as for toxicology assessment of existing substances. We analyzed two substances with known retinopathic side-effects suitable for a proof-of-principle study in the RoC: chloroquine and gentamicin.

6.3.1. Chloroquine

Chloroquine as well as its metabolite hydroxychloroquine are well known drugs that are used for the treatment of malaria and rheumatic diseases like rheumatoid arthritis (Ding et al., 2016; Stokkermans and Trichonas, 2019). Both substances can severely affect the retina, by binding to melanin in RPE cells and also by affecting the lysosomal activity in those cells, leading to reduced phagocytosis which can then also affect photoreceptors of the retina (Stokkermans and Trichonas, 2019). The effects include lysosome enlargement due to an accumulation of the drug where it also leads to a change in pH and consequently, to lysosomal dysfunction (Chen et al., 2011).

In the RoC system, we aimed to recapitulate this lysosomotropic effect by visualizing lysosomes after treatment with chloroquine. While treatment of RPE with chloroquine in standard dish culture had a strong effect at already 20 µg/ml, the lysosomal dilation and cell death in the RoC only becomes visible at higher concentrations. This might be due to several reasons.

One technical factor might be the differences in the optical properties of the microscopic setup between chip setup and standard dish culture, including different refraction of light of PDMS as fabrication material, as well as different background fluorescence that makes it difficult to compare between both setups. Further, it is known that PDMS which the chip is primarily made of, is able to absorb substances, depending largely on their chemical properties.

Even though the mentioned reasons might have influence on the necessary drug concentration, is was still possible to replicate the drug's effect on cell viability and lysosomal enlargement in the chip setup. Chloroquine as a drug is used over long periods for the treatment in patients with malaria (Ding et al., 2016). As seen in our RoC, this treatment

can have consequences for the sight of the patient. The usage of the RoC as a drug testing device could be verified by these proof-of-principle experiments.

6.3.2. Gentamicin

The antibiotic drug gentamicin was another candidate to be tested in the RoC system. This aminoglycoside is used for example for treatment of endophthalmitis and anterior segment infections (Hancock et al., 2005). Besides other side effects, local administration can also lead to ocular toxicity, including retinal damage (Hancock et al., 2005; McDonald et al., 1986; Zemel et al., 1995).

We treated the RoC system with the drug over several days and monitored effects by measurement of PI signal intensities. The setup that was necessary for microscopic observation of fluorescence intensities only allowed us to detect combined signals from both, RO and RPE. PI as marker for cell death, also does not allow to distinguish both cell types. Consequently, we had difficulties to state which cell type is primarily affected and also whether the co-culture of both tissues has any effect on cell survival after drug treatment. To account for differences in PI signal between both tissues, we subtracted the observed intensities of the RPE signal in the surrounding area from the co-signal directly underneath the RPE. This could then be compared to an RPE-free condition and gave us a hint, that there might be indeed an influencing effect of the RPE, leading to less cell death in the co-culture condition, although this effect was not significant. A protective effect might either be due to the barrier function of the RPE or to characteristics of the cells themselves. Indeed, it is known from *in vivo* experiments that ocular pigmentation in rabbits can protect them from gentamicin-induced retinal toxicity (Zemel et al., 1995). Responsible for this effect seems to be the binding of gentamicin by melanin (Zemel et al., 1995).

However, this way of quantifying cell death is only indirectly measuring fluorescence intensities from the ROs. To make definitive statements, other ways of cell viability measurement would be necessary, for example live cell microscopy from the side of the chip. Nevertheless, it gives us a hint that also the influence of the RPE-presence can be monitored in our RoC setup which might be of great benefit when monitoring disorders involving primary RPE cell death. Further, known retinopathic effects of the antibiotic

gentamicin known from literature could be replicated, showing again the suitability of the RoC as a drug-testing device.

7. Further development and outlook

Although there have been other publications aiming to introduce single retinal cells (Mishra et al., 2015; Su et al., 2015) or retinal tissue from mice (Dodson et al., 2015b) into a microfluidic device, this is the very first chip system merging organ-on-a-chip technology with retinal organoids derived from human induced pluripotent stem cells.

The microfluidic channels integrated in the chip system enable vasculature-like perfusion. However, the current retina-on-a-chip setup does not include any other cell types (like immune or endothelial cells) that do not originate from retinal progenitors. If endothelial cells would be integrated into a future version of the chip, this might not only help to improve supply with nutrients and oxygen even further, but it can also help to build a full blood-retinal barrier, which requires endothelial parts. The blood-retinal barrier is important to control transport of different substances to and from the retina and therefore homeostasis of the retinal microenvironment (Cunha-Vaz, 1998; Steinberg, 1985).

Several publications reported different attempts to develop a blood-retinal barrier (Chen et al., 2017; Yeste et al., 2018). However, so far none of these have combined their system with a neural retina with all different layer but have been restricted to endothelial and RPE cells. The integration of the blood-retinal barrier into our system would hold great potential for the investigation of the pathomechanisms of several disorders involving a disruption of retinal barrier functions such as diabetic retinopathy. Further, the emulation of a barrier is also essential when analyzing how drugs impact the retina when applied systemically.

Another option for further development can concern the chip fabrication material used. PDMS has some clear advantages that make it a suitable material for chip production especially when several rapid adaptations in prototypes are required. These advantages include biocompatibility, optical clarity, gas permeability, inexpensiveness and ease of handling (Huh et al., 2011). Besides these desirable properties, PDMS also has certain characteristics that can lead to limitations in chip use: It absorbs small hydrophobic molecules and is therefore not suitable for specific experiments with certain drugs or fluorescent dyes (Huh et al., 2011). For

a next generation of chip, the utilization of a different kind of plastic would seem reasonable, such as PMMA for instance, which is also inexpensive and features good mechanical/chemical properties (Liga et al., 2016; Zhang et al., 2009).

The chip as model system for the human retina can bring important insights and is a suitable tool for *in vitro* experiments, despite the aforementioned options for improvement.
In this study, we only used drugs with already known side effects on the retina. However, in future studies, newly developed pharmaceuticals could be tested for retinal effects in such a setup. Those studies would normally require extensive testing in animals, such as mice or rabbits. As described before, the ethical as well as the financial aspects of testing huge numbers of animals for every potential drug, ask for suitable alternatives. In certain aspects the retina-on-a-chip shows some advantages over testing of animals since these species have eyes and retinae with different morphological and physiological characteristics. The testing of human cells and tissues can therefore bring along important insights that could not be gained from other species with different properties.
Further, for many retinal disorders there are still no suitable drugs known to ameliorate the symptoms or cure the disease. Large-scale testing of candidate drugs in a close-as-possible-physiological setup will be necessary to find such urgently needed treatments. This requires disease models that are able to accurately represent the condition in a patient's eye. The retina-on-a-chip is the first step towards solving this problem since it allows to integrate human retinal cells from any background. In this way, either stem cells that originate from patients can be used for differentiation of retinal cells, or the disease can be introduced by genetically engineering the respective stem cells or retinal cells. Even drug-induced disorders can be used as model to help find protective agents.
Lastly, the retina-on-a-chip can help to generate important insights on retinal development itself, as well as on the important interplay of different tissues of the eye, such as the neural retina and the pigmented epithelium of the retina.

8. References

Achberger, K., Haderspeck, J.C., Kleger, A., and Liebau, S. (2019a). Stem cell-based retina models. Adv. Drug Deliv. Rev. *140*, 33–50.

Achberger, K., Probst, C., Haderspeck, J., Bolz, S., Rogal, J., Chuchuy, J., Nikolova, M., Cora, V., Antkowiak, L., Haq, W., et al. (2019b). Merging organoid and organ-on-a-chip technology to generate complex multi-layer tissue models in a human retina-on-a-chip platform. Elife *8*, e46188.

Ahmado, A., Carr, A.-J., Vugler, A.A., Semo, M., Gias, C., Lawrence, J.M., Chen, L.L., Chen, F.K., Turowski, P., da Cruz, L., et al. (2011). Induction of Differentiation by Pyruvate and DMEM in the Human Retinal Pigment Epithelium Cell Line ARPE-19. Investig. Opthalmology Vis. Sci. *52*, 7148.

Aisenbrey, S., Zhang, M., Bacher, D., Yee, J., Brunken, W.J., and Hunter, D.D. (2006). Retinal Pigment Epithelial Cells Synthesize Laminins, Including Laminin 5, and Adhere to Them through α3- and α6-Containing Integrins. Invest. Ophthalmol. Vis. Sci. *47*, 5537.

Alge, C.S., Hauck, S.M., Priglinger, S.G., Kampik, A., and Ueffing, M. (2006). Differential Protein Profiling of Primary versus Immortalized Human RPE Cells Identifies Expression Patterns Associated with Cytoskeletal Remodeling and Cell Survival. J. Proteome Res. *5*, 862–878.

del Amo, E.M., Rimpelä, A.-K., Heikkinen, E., Kari, O.K., Ramsay, E., Lajunen, T., Schmitt, M., Pelkonen, L., Bhattacharya, M., Richardson, D., et al. (2017). Pharmacokinetic aspects of retinal drug delivery. Prog. Retin. Eye Res. *57*, 134–185.

Amrite, A.C., Edelhauser, H.F., and Kompella, U.B. (2008). Modeling of corneal and retinal pharmacokinetics after periocular drug administration. Invest. Ophthalmol. Vis. Sci. *49*, 320–332.

Baden, T., Berens, P., Franke, K., Román Rosón, M., Bethge, M., and Euler, T. (2016). The functional diversity of retinal ganglion cells in the mouse. Nature *529*, 345–350.

Barar, J., Asadi, M., Mortazavi-Tabatabaei, S.A., and Omidi, Y. (2009). Ocular Drug Delivery; Impact of in vitro Cell Culture Models. J. Ophthalmic Vis. Res. *4*, 238–252.

Bartfeld, S., and Clevers, H. (2017). Stem cell-derived organoids and their application for medical research and patient treatment. J. Mol. Med. *95*, 729–738.

Bassett, E.A., and Wallace, V.A. (2012). Cell fate determination in the vertebrate retina. Trends Neurosci. *35*, 565–573.

Baylor, D. (1996). How photons start vision. Proc. Natl. Acad. Sci. U. S. A. *93*, 560–565.

Becerra, S.P., Fariss, R.N., Wu, Y.Q., Montuenga, L.M., Wong, P., and Pfeffer, B.A. (2004). Pigment epithelium-derived factor in the monkey retinal pigment epithelium and interphotoreceptor matrix: apical secretion and distribution. Exp. Eye Res. *78*, 223–234.

Beddington, R.S., and Robertson, E.J. (1989). An assessment of the developmental potential of embryonic stem cells in the midgestation mouse embryo. Development *105*, 733–737.

Bhatia, S.N., and Ingber, D.E. (2014). Microfluidic organs-on-chips. Nat. Biotechnol. *32*, 760–772.

Bjorklund, L.M., Sanchez-Pernaute, R., Chung, S., Andersson, T., Chen, I.Y.C., McNaught, K.S.P., Brownell, A.-L., Jenkins, B.G., Wahlestedt, C., Kim, K.-S., et al. (2002). Embryonic stem cells develop into functional dopaminergic neurons after transplantation in a Parkinson rat model. Proc. Natl. Acad. Sci. *99*, 2344–2349.

Blanks, J.C., and Johnson, L. V (1984). Specific binding of peanut lectin to a class of retinal photoreceptor cells. A species comparison. Invest. Ophthalmol. Vis. Sci. *25*, 546–557.

Bringmann, A., Pannicke, T., Grosche, J., Francke, M., Wiedemann, P., Skatchkov, S.N., Osborne, N.N., and Reichenbach, A. (2006). Müller cells in the healthy and diseased retina. Prog. Retin. Eye Res. *25*, 397–424.

Bundesministerium der Justiz und für Verbraucherschutz (2002). Gesetz zur Sicherstellung des Embryonenschutzes im Zusammenhang mit Einfuhr und Verwendung menschlicher embryonaler Stammzellen (Stammzellgesetz-StZG).

Campbell, H.K., Maiers, J.L., and DeMali, K.A. (2017). Interplay between tight junctions and adherens junctions. Exp. Cell Res. *358*, 39–44.

Cao, L., Liu, J., Pu, J., Milne, G., Chen, M., Xu, H., Shipley, A., Forrester, J. V, McCaig, C.D., and Lois, N. (2018). Polarized retinal pigment epithelium generates electrical signals that diminish with age and regulate retinal pathology. J. Cell. Mol. Med. *22*, 5552–5564.

Carraro, A., Hsu, W.-M., Kulig, K.M., Cheung, W.S., Miller, M.L., Weinberg, E.J., Swart, E.F., Kaazempur-Mofrad, M., Borenstein, J.T., Vacanti, J.P., et al. (2008). In vitro analysis of a hepatic device with intrinsic microvascular-based channels. Biomed. Microdevices *10*, 795–805.

Chen, I.-P., Fukuda, K., Fusaki, N., Iida, A., Hasegawa, M., Lichtler, A., and Reichenberger, E.J. (2013). Induced pluripotent stem cell reprogramming by integration-free Sendai virus

vectors from peripheral blood of patients with craniometaphyseal dysplasia. Cell. Reprogram. *15*, 503–513.

Chen, L.-J., Ito, S., Kai, H., Nagamine, K., Nagai, N., Nishizawa, M., Abe, T., and Kaji, H. (2017). Microfluidic co-cultures of retinal pigment epithelial cells and vascular endothelial cells to investigate choroidal angiogenesis. Sci. Rep. *7*, 3538.

Chen, P.M., Gombart, Z.J., and Chen, J.W. (2011). Chloroquine treatment of ARPE-19 cells leads to lysosome dilation and intracellular lipid accumulation: possible implications of lysosomal dysfunction in macular degeneration. Cell Biosci. *1*, 10.

Clarke, G., Goldberg, A.F.X., Vidgen, D., Collins, L., Ploder, L., Schwarz, L., Molday, L.L., Rossant, J., Szél, Á., Molday, R.S., et al. (2000). Rom-1 is required for rod photoreceptor viability and the regulation of disk morphogenesis. Nat. Genet. *25*, 67–73.

Clevers, H. (2016). Modeling Development and Disease with Organoids. Cell *165*, 1586–1597.

Combes, R.D. (2004). The use of human cells in biomedical research and testing. Altern. Lab. Anim. *32 Suppl 1A*, 43–49.

Cowan, C.A., Atienza, J., Melton, D.A., and Eggan, K. (2005). Nuclear Reprogramming of Somatic Cells After Fusion with Human Embryonic Stem Cells. Science (80-.). *309*, 1369–1373.

Crowley, L.C., Scott, A.P., Marfell, B.J., Boughaba, J.A., Chojnowski, G., and Waterhouse, N.J. (2016). Measuring Cell Death by Propidium Iodide Uptake and Flow Cytometry. Cold Spring Harb. Protoc. *2016*, pdb.prot087163.

Cunha-Vaz, J.G. (1998). Blood—retinal barrier and new perspectives of management of retinal disease. (Springer, Dordrecht), pp. 5–11.

Dacey, D.M., Liao, H.-W., Peterson, B.B., Robinson, F.R., Smith, V.C., Pokorny, J., Yau, K.-W., and Gamlin, P.D. (2005). Melanopsin-expressing ganglion cells in primate retina signal colour and irradiance and project to the LGN. Nature *433*, 749–754.

Dekkers, J.F., Wiegerinck, C.L., de Jonge, H.R., Bronsveld, I., Janssens, H.M., de Winter-de Groot, K.M., Brandsma, A.M., de Jong, N.W.M., Bijvelds, M.J.C., Scholte, B.J., et al. (2013). A functional CFTR assay using primary cystic fibrosis intestinal organoids. Nat. Med. *19*, 939–945.

Denk, N., Misra, V., Sandmeyer, L.S., Bauer, B.B., Singh, J., Forsyth, G.W., and Grahn, B.H. (2015). Development of a murine ocular posterior segment explant culture for the study of intravitreous vector delivery. Can. J. Vet. Res. *79*, 31–38.

Ding, H.J., Denniston, A.K., Rao, V.K., and Gordon, C. (2016). Hydroxychloroquine-related retinal toxicity. Rheumatology *55*, 957–967.

Dodson, K.H., Echevarria, F.D., Li, D., Sappington, R.M., and Edd, J.F. (2015a). Retina-on-a-chip: a microfluidic platform for point access signaling studies. Biomed. Microdevices *17*, 1–10.

Dodson, K.H., Echevarria, F.D., Li, D., Sappington, R.M., and Edd, J.F. (2015b). Retina-on-a-chip: a microfluidic platform for point access signaling studies. Biomed. Microdevices *17*, 114.

Drukker, M., and Benvenisty, N. (2004). The immunogenicity of human embryonic stem-derived cells. Trends Biotechnol. *22*, 136–141.

Dyer, M.A., Livesey, F.J., Cepko, C.L., and Oliver, G. (2003). Prox1 function controls progenitor cell proliferation and horizontal cell genesis in the mammalian retina. Nat. Genet. *34*, 53–58.

Eiraku, M., Watanabe, K., Matsuo-Takasaki, M., Kawada, M., Yonemura, S., Matsumura, M., Wataya, T., Nishiyama, A., Muguruma, K., and Sasai, Y. (2008). Self-Organized Formation of Polarized Cortical Tissues from ESCs and Its Active Manipulation by Extrinsic Signals. Cell Stem Cell *3*, 519–532.

Eiraku, M., Takata, N., Ishibashi, H., Kawada, M., Sakakura, E., Okuda, S., Sekiguchi, K., Adachi, T., and Sasai, Y. (2011). Self-organizing optic-cup morphogenesis in three-dimensional culture. Nature *472*, 51–56.

Elman, A., Gullberg, R., Nilsson, E., Rendahl, I., and Wachtmeister, L. (2009). Chloroquine Retinopathy in Patients with Rheumatoid Arthritis. Scand. J. Rheumatol. *5*, 161–166.

Elstrott, J., Anishchenko, A., Greschner, M., Sher, A., Litke, A.M., Chichilnisky, E.J., and Feller, M.B. (2008). Direction selectivity in the retina is established independent of visual experience and cholinergic retinal waves. Neuron *58*, 499–506.

Estlack, Z., Bennet, D., Reid, T., and Kim, J. (2017). Microengineered biomimetic ocular models for ophthalmological drug development. Lab Chip *17*, 1539–1551.

Evans, M.J., and Kaufman, M.H. (1981). Establishment in culture of pluripotential cells from mouse embryos. Nature *292*, 154–156.

Farrow, K., and Masland, R.H. (2011). Physiological clustering of visual channels in the mouse retina. J. Neurophysiol. *105*, 1516–1530.

Fernandez-Bueno, I., Fernández-Sánchez, L., Gayoso, M.J., García-Gutierrez, M.T., Pastor, J.C.,

and Cuenca, N. (2012). Time course modifications in organotypic culture of human neuroretina. Exp. Eye Res. *104*, 26–38.

Forsythe, S.D., Devarasetty, M., Shupe, T., Bishop, C., Atala, A., Soker, S., and Skardal, A. (2018). Environmental Toxin Screening Using Human-Derived 3D Bioengineered Liver and Cardiac Organoids. Front. Public Heal. *6*, 103.

Foster, J.W., Wahlin, K., Adams, S.M., Birk, D.E., Zack, D.J., and Chakravarti, S. (2017). Cornea organoids from human induced pluripotent stem cells. Sci. Rep. *7*, 41286.

Fuhrmann, S. (2010). Eye Morphogenesis and Patterning of the Optic Vesicle. In Current Topics in Developmental Biology, pp. 61–84.

German, O.L., Buzzi, E., Rotstein, N.P., Rodríguez-Boulan, E., and Politi, L.E. (2008). Retinal pigment epithelial cells promote spatial reorganization and differentiation of retina photoreceptors. J. Neurosci. Res. *86*, 3503–3514.

Grosche, A., Hauser, A., Lepper, M.F., Mayo, R., von Toerne, C., Merl-Pham, J., and Hauck, S.M. (2016). The Proteome of Native Adult Müller Glial Cells From Murine Retina. Mol. Cell. Proteomics *15*, 462–480.

Haderspeck, J.C., Chuchuy, J., Kustermann, S., Liebau, S., and Loskill, P. (2019). Organ-on-a-chip technologies that can transform ophthalmic drug discovery and disease modeling. Expert Opin. Drug Discov. *14*, 47–57.

Hafezi, F., Grimm, C., Simmen, B.C., Wenzel, A., and Remé, C.E. (2000). Molecular ophthalmology: an update on animal models for retinal degenerations and dystrophies. Br. J. Ophthalmol. *84*, 922–927.

Hancock, H.A., Guidry, C., Read, R.W., Ready, E.L., and Kraft, T.W. (2005). Acute Aminoglycoside Retinal Toxicity In Vivo and In Vitro. Investig. Opthalmology Vis. Sci. *46*, 4804.

Haverkamp, S., Haeseleer, F., and Hendrickson, A. (2003). A comparison of immunocytochemical markers to identify bipolar cell types in human and monkey retina. Vis. Neurosci. *20*, 589–600.

Hohwieler, M., Illing, A., Hermann, P.C., Mayer, T., Stockmann, M., Perkhofer, L., Eiseler, T., Antony, J.S., Müller, M., Renz, S., et al. (2017). Human pluripotent stem cell-derived acinar/ductal organoids generate human pancreas upon orthotopic transplantation and allow disease modelling. Gut *66*, 473–486.

Honegger, P. (2001). Overview of Cell and Tissue Culture Techniques. In Current Protocols in Pharmacology, (Hoboken, NJ, USA: John Wiley & Sons, Inc.), p. 12.1.1-12.1.12.

Hoon, M., Okawa, H., Della Santina, L., and Wong, R.O.L. (2014). Functional architecture of the retina: development and disease. Prog. Retin. Eye Res. *42*, 44–84.

Huang, L., Holtzinger, A., Jagan, I., BeGora, M., Lohse, I., Ngai, N., Nostro, C., Wang, R., Muthuswamy, L.B., Crawford, H.C., et al. (2015). Ductal pancreatic cancer modeling and drug screening using human pluripotent stem cell– and patient-derived tumor organoids. Nat. Med. *21*, 1364–1371.

Huh, D., Matthews, B.D., Mammoto, A., Montoya-Zavala, M., Hsin, H.Y., and Ingber, D.E. (2010). Reconstituting Organ-Level Lung Functions on a Chip. Science (80-.). *328*, 1662–1668.

Huh, D., Hamilton, G.A., and Ingber, D.E. (2011). From 3D cell culture to organs-on-chips. Trends Cell Biol. *21*, 745–754.

Huh, D., Torisawa, Y., Hamilton, G.A., Kim, H.J., and Ingber, D.E. (2012). Microengineered physiological biomimicry: Organs-on-Chips. Lab Chip *12*, 2156.

Ito, S., Onishi, A., and Takahashi, M. (2017). Chemically-induced photoreceptor degeneration and protection in mouse iPSC-derived three-dimensional retinal organoids. Stem Cell Res. *24*, 94–101.

Jeon, S., and Oh, I.-H. (2015). Regeneration of the retina: toward stem cell therapy for degenerative retinal diseases. BMB Rep. *48*, 193–199.

Jiang, S.-M., Zeng, L.-P., Zeng, J.-H., Tang, L., Chen, X.-M., and Wei, X. (2015). β-III-Tubulin: a reliable marker for retinal ganglion cell labeling in experimental models of glaucoma. Int. J. Ophthalmol. *8*, 643–652.

Jin, Z.-B., Okamoto, S., Osakada, F., Homma, K., Assawachananont, J., Hirami, Y., Iwata, T., and Takahashi, M. (2011). Modeling Retinal Degeneration Using Patient-Specific Induced Pluripotent Stem Cells. PLoS One *6*, e17084.

Johnson, T. V., and Martin, K.R. (2008). Development and Characterization of an Adult Retinal Explant Organotypic Tissue Culture System as an In Vitro Intraocular Stem Cell Transplantation Model. Investig. Opthalmology Vis. Sci. *49*, 3503.

Kamiya, D., Banno, S., Sasai, N., Ohgushi, M., Inomata, H., Watanabe, K., Kawada, M., Yakura, R., Kiyonari, H., Nakao, K., et al. (2011). Intrinsic transition of embryonic stem-cell differentiation into neural progenitors. Nature *470*, 503–509.

Kaur, G., and Dufour, J.M. (2012). Cell lines: Valuable tools or useless artifacts. Spermatogenesis *2*, 1–5.

Kay, P., Yang, Y.C., and Paraoan, L. (2013). Directional protein secretion by the retinal pigment epithelium: roles in retinal health and the development of age-related macular degeneration. J. Cell. Mol. Med. *17*, 833–843.

Kels, B.D., Grzybowski, A., and Grant-Kels, J.M. (2015). Human ocular anatomy. Clin. Dermatol. *33*, 140–146.

Kevany, B.M., and Palczewski, K. (2010). Phagocytosis of retinal rod and cone photoreceptors. Physiology (Bethesda). *25*, 8–15.

Kim, D., Gu, Y., Ishii, M., Fujimiya, M., Qi, M., Nakamura, N., Yoshikawa, T., Sumi, S., and Inoue, K. (2003). In vivo functioning and transplantable mature pancreatic islet-like cell clusters differentiated from embryonic stem cell. Pancreas *27*, e34-41.

Kiser, P.D., Golczak, M., and Palczewski, K. (2014). Chemistry of the retinoid (visual) cycle. Chem. Rev. *114*, 194–232.

Kivelä, T., Jääskeläine, J., Vaheri, A., and Carpén, O. (2000). Ezrin, a membrane-organizing protein, as a polarization marker of the retinal pigment epithelium in vertebrates. Cell Tissue Res. *301*, 217–223.

Kolb, H. (1995). Gross Anatomy of the Eye. In Webvision: The Organization of the Retina and Visual System [Internet]., N.R. Kolb H, Fernandez E, ed. (Salt Lake City (UT): University of Utah Health Sciences Center; 1995-. Available from: https://www.ncbi.nlm.nih.gov/books/NBK11534/), p.

Kolb, H., Linberg, K.A., and Fisher, S.K. (1992). Neurons of the human retina: A Golgi study. J. Comp. Neurol. *318*, 147–187.

Kompella, U.B., Kadam, R.S., and Lee, V.H. (2010). Recent advances in ophthalmic drug delivery. Ther. Deliv. *1*, 435–456.

Kurihara, T., Westenskow, P.D., Gantner, M.L., Usui, Y., Schultz, A., Bravo, S., Aguilar, E., Wittgrove, C., Friedlander, M.S., Paris, L.P., et al. (2016). Hypoxia-induced metabolic stress in retinal pigment epithelial cells is sufficient to induce photoreceptor degeneration. Elife *5*.

Lamb, T.D., Collin, S.P., and Pugh, E.N. (2007). Evolution of the vertebrate eye: opsins, photoreceptors, retina and eye cup. Nat. Rev. Neurosci. *8*, 960–976.

Lamba, D.A., McUsic, A., Hirata, R.K., Wang, P.-R., Russell, D., and Reh, T.A. (2010). Generation, Purification and Transplantation of Photoreceptors Derived from Human Induced Pluripotent Stem Cells. PLoS One *5*, e8763.

Lancaster, M.A., and Knoblich, J.A. (2014). Organogenesis in a dish: Modeling development and disease using organoid technologies. Science (80-.). *345*, 1247125–1247125.

Lancaster, M.A., Renner, M., Martin, C.-A., Wenzel, D., Bicknell, L.S., Hurles, M.E., Homfray, T., Penninger, J.M., Jackson, A.P., and Knoblich, J.A. (2013). Cerebral organoids model human brain development and microcephaly. Nature *501*, 373–379.

Lerea, C.L., Bunt-Milam, A.H., and Hurley, J.B. (1989). α transducin is present in blue-, green-, and red-sensitive cone photoreceptors in the human retina. Neuron *3*, 367–376.

Li, G., Xie, B., He, L., Zhou, T., Gao, G., Liu, S., Pan, G., Ge, J., Peng, F., and Zhong, X. (2018). Generation of Retinal Organoids with Mature Rods and Cones from Urine-Derived Human Induced Pluripotent Stem Cells. Stem Cells Int. *2018*.

Li, H., Tierney, C., Wen, L., Wu, J.Y., and Rao, Y. (1997). A single morphogenetic field gives rise to two retina primordia under the influence of the prechordal plate. Development *124*, 603–615.

Li, L., Anand, M., Rao, K.N., and Khanna, H. (2015). Cilia in photoreceptors. Methods Cell Biol. *127*, 75–92.

Liga, A., Morton, J.A.S., and Kersaudy-Kerhoas, M. (2016). Safe and cost-effective rapid-prototyping of multilayer PMMA microfluidic devices. Microfluid. Nanofluidics *20*, 164.

Linta, L., Stockmann, M., Kleinhans, K.N., Böckers, A., Storch, A., Zaehres, H., Lin, Q., Barbi, G., Böckers, T.M., Kleger, A., et al. (2012). Rat Embryonic Fibroblasts Improve Reprogramming of Human Keratinocytes into Induced Pluripotent Stem Cells. Stem Cells Dev. *21*, 965–976.

Lumelsky, N. (2005). Generation of Islet-Like Structures From ES Cells. In Stem Cells in Endocrinology, (Totowa, NJ: Humana Press), pp. 147–163.

Luo, Y., Zhuo, Y., Fukuhara, M., and Rizzolo, L.J. (2006). Effects of Culture Conditions on Heterogeneity and the Apical Junctional Complex of the ARPE-19 Cell Line. Investig. Opthalmology Vis. Sci. *47*, 3644.

Mahon, G.J., Anderson, H.R., Gardiner, T.A., McFarlane, S., Archer, D.B., and Stitt, A.W. (2004). Chloroquine causes lysosomal dysfunction in neural retina and RPE: Implications for retinopathy. Curr. Eye Res. *28*, 277–284.

Malik, N., and Rao, M.S. (2013). A review of the methods for human iPSC derivation. Methods Mol. Biol. *997*, 23–33.

Marmorstein, A.D., Marmorstein, L.Y., Rayborn, M., Wang, X., Hollyfield, J.G., and Petrukhin,

K. (2000). Bestrophin, the product of the Best vitelliform macular dystrophy gene (VMD2), localizes to the basolateral plasma membrane of the retinal pigment epithelium. Proc. Natl. Acad. Sci. *97*, 12758–12763.

Marquardt, T. (2003). Transcriptional control of neuronal diversification in the retina. Prog. Retin. Eye Res. *22*, 567–577.

Marquardt, T., Ashery-Padan, R., Andrejewski, N., Scardigli, R., Guillemot, F., and Gruss, P. (2001). Pax6 is required for the multipotent state of retinal progenitor cells. Cell *105*, 43–55.

Martin, G.R. (1981). Isolation of a pluripotent cell line from early mouse embryos cultured in medium conditioned by teratocarcinoma stem cells. Proc. Natl. Acad. Sci. U. S. A. *78*, 7634–7638.

Masland, R.H. (2012). The neuronal organization of the retina. Neuron *76*, 266–280.

Massey, S.C. (2006). Functional Anatomy of the Mammalian Retina. In Retina, (Mosby Copyright © 2006 Elsevier Inc.), pp. 43–82.

Mathur, A., Loskill, P., Shao, K., Huebsch, N., Hong, S., Marcus, S.G., Marks, N., Mandegar, M., Conklin, B.R., Lee, L.P., et al. (2015). Human iPSC-based Cardiac Microphysiological System For Drug Screening Applications. Sci. Rep. *5*, 8883.

Mathur, A., Ma, Z., Loskill, P., Jeeawoody, S., and Healy, K.E. (2016). In vitro cardiac tissue models: Current status and future prospects. Adv. Drug Deliv. Rev. *96*, 203–213.

McCaa, C.S. (1982). The eye and visual nervous system: anatomy, physiology and toxicology. Environ. Health Perspect. *44*, 1–8.

McDonald, H.R., Schatz, H., Allen, A.W., Chenoweth, R.G., Cohen, H.B., Crawford, J.B., Klein, R., May, D.R., and Snider, J.D. (1986). Retinal toxicity secondary to intraocular gentamicin injection. Ophthalmology *93*, 871–877.

Mellough, C.B., Collin, J., Queen, R., Hilgen, G., Dorgau, B., Zerti, D., Felemban, M., White, K., Sernagor, E., and Lako, M. (2019). Systematic Comparison of Retinal Organoid Differentiation from Human Pluripotent Stem Cells Reveals Stage Specific, Cell Line, and Methodological Differences. Stem Cells Transl. Med. *8*, 694–706.

Meyer, J.S., Shearer, R.L., Capowski, E.E., Wright, L.S., Wallace, K.A., McMillan, E.L., Zhang, S.-C., and Gamm, D.M. (2009). Modeling early retinal development with human embryonic and induced pluripotent stem cells. Proc. Natl. Acad. Sci. *106*, 16698–16703.

Meyer, J.S., Howden, S.E., Wallace, K.A., Verhoeven, A.D., Wright, L.S., Capowski, E.E., Pinilla, I., Martin, J.M., Tian, S., Stewart, R., et al. (2011). Optic Vesicle-like Structures Derived from Human Pluripotent Stem Cells Facilitate a Customized Approach to Retinal Disease Treatment. Stem Cells *29*, 1206–1218.

Mishra, S., Thakur, A., Redenti, S., and Vazquez, M. (2015). A model microfluidics-based system for the human and mouse retina. Biomed. Microdevices *17*, 107.

Molday, R.S., and Moritz, O.L. (2015). Photoreceptors at a glance. J. Cell Sci. *128*, 4039–4045.

Montagnani, S., Rueger, M.A., Hosoda, T., and Nurzynska, D. (2016). Adult Stem Cells in Tissue Maintenance and Regeneration. Stem Cells Int. *2016*, 7362879.

Mu, X., and Klein, W.H. (2004). A gene regulatory hierarchy for retinal ganglion cell specification and differentiation. Semin. Cell Dev. Biol. *15*, 115–123.

Muñoz-Sanjuán, I., and Brivanlou, A.H. (2002). Neural induction, the default model and embryonic stem cells. Nat. Rev. Neurosci. *3*, 271–280.

Nakagawa, M., Taniguchi, Y., Senda, S., Takizawa, N., Ichisaka, T., Asano, K., Morizane, A., Doi, D., Takahashi, J., Nishizawa, M., et al. (2014). A novel efficient feeder-free culture system for the derivation of human induced pluripotent stem cells. Sci. Rep. *4*, 3594.

Nakano, T., Ando, S., Takata, N., Kawada, M., Muguruma, K., Sekiguchi, K., Saito, K., Yonemura, S., Eiraku, M., and Sasai, Y. (2012). Self-Formation of Optic Cups and Storable Stratified Neural Retina from Human ESCs. Cell Stem Cell *10*, 771–785.

Nguyen, M., and Arnheiter, H. (2000). Signaling and transcriptional regulation in early mammalian eye development: a link between FGF and MITF. Development *127*, 3581–3591.

Ogata, N., Wang, L., Jo, N., Tombran-Tink, J., Takahashi, K., Mrazek, D., and Matsumura, M. (2001). Pigment epithelium derived factor as a neuroprotective agent against ischemic retinal injury. Curr. Eye Res. *22*, 245–252.

Ohlemacher, S.K., Iglesias, C.L., Sridhar, A., Gamm, D.M., and Meyer, J.S. (2015). Generation of highly enriched populations of optic vesicle-like retinal cells from human pluripotent stem cells. Curr. Protoc. Stem Cell Biol. *32*, 1H.8.1-20.

Ohlemacher, S.K., Sridhar, A., Xiao, Y., Hochstetler, A.E., Sarfarazi, M., Cummins, T.R., and Meyer, J.S. (2016). Stepwise Differentiation of Retinal Ganglion Cells from Human Pluripotent Stem Cells Enables Analysis of Glaucomatous Neurodegeneration. Stem Cells *34*, 1553–1562.

Okita, K., Nakagawa, M., Hyenjong, H., Ichisaka, T., and Yamanaka, S. (2008). Generation of Mouse Induced Pluripotent Stem Cells Without Viral Vectors. Science (80-.). *322*, 949–953.

Omri, S., Omri, B., Savoldelli, M., Jonet, L., Thillaye-Goldenberg, B., Thuret, G., Gain, P., Jeanny, J.C., Crisanti, P., and Behar-Cohen, F. (2010). The outer limiting membrane (OLM) revisited: clinical implications. Clin. Ophthalmol. *4*, 183–195.

Orlans, H.O., Edwards, T.L., De Silva, S.R., Patrício, M.I., and MacLaren, R.E. (2018). Human Retinal Explant Culture for Ex Vivo Validation of AAV Gene Therapy. In Methods in Molecular Biology (Clifton, N.J.), pp. 289–303.

Osborne, A., Hopes, M., Wright, P., Broadway, D.C., and Sanderson, J. (2016). Human organotypic retinal cultures (HORCs) as a chronic experimental model for investigation of retinal ganglion cell degeneration. Exp. Eye Res. *143*, 28–38.

Paquette, L.B., Jackson, H.A., Tavaré, C.J., Miller, D.A., and Panigrahy, A. (2009). In Utero Eye Development Documented by Fetal MR Imaging. Am. J. Neuroradiol. *30*, 1787–1791.

Parfitt, D.A., Lane, A., Ramsden, C.M., Carr, A.-J.F., Munro, P.M., Jovanovic, K., Schwarz, N., Kanuga, N., Muthiah, M.N., Hull, S., et al. (2016). Identification and Correction of Mechanisms Underlying Inherited Blindness in Human iPSC-Derived Optic Cups. Cell Stem Cell *18*, 769–781.

Pérez de Sevilla Müller, L., Azar, S.S., de los Santos, J., and Brecha, N.C. (2017). Prox1 Is a Marker for AII Amacrine Cells in the Mouse Retina. Front. Neuroanat. *11*, 39.

Proksch, J.W., Granvil, C.P., Siou-Mermet, R., Comstock, T.L., Paterno, M.R., and Ward, K.W. (2009). Ocular pharmacokinetics of besifloxacin following topical administration to rabbits, monkeys, and humans. J. Ocul. Pharmacol. Ther. *25*, 335–344.

Puleo, C.M., McIntosh Ambrose, W., Takezawa, T., Elisseeff, J., and Wang, T.-H. (2009). Integration and application of vitrified collagen in multilayered microfluidic devices for corneal microtissue culture. Lab Chip *9*, 3221.

Purves, D., and Williams, S.M. (Stephen M. (2001). Neuroscience (Sinauer Associates).

Rehman, I., and Bhimji, S.S. (2018). Anatomy, Head and Neck, Eye.

Resau, J.H., Sakamoto, K., Cottrell, J.R., Hudson, E.A., and Meltzer, S.J. (1991). Explant organ culture: a review. Cytotechnology *7*, 137–149.

Rettinger, C.L., and Wang, H.-C. (2018). Quantitative Assessment of Retina Explant Viability in a Porcine *Ex Vivo* Neuroretina Model. J. Ocul. Pharmacol. Ther. *34*, 521–530.

Roberts, P.A., Gaffney, E.A., Luthert, P.J., Foss, A.J.E., and Byrne, H.M. (2016). Mathematical and computational models of the retina in health, development and disease. Prog. Retin. Eye Res. *53*, 48–69.

Rosenthal, A.R., Kolb, H., Bergsma, D., Huxsoll, D., and Hopkins, J.L. (1978). Chloroquine retinopathy in the rhesus monkey. Invest. Ophthalmol. Vis. Sci. *17*, 1158–1175.

Saari, J.C. (2012). Vitamin A Metabolism in Rod and Cone Visual Cycles. Annu. Rev. Nutr. *32*, 125–145.

Saini, A. (2016). Cystic Fibrosis Patients Benefit from Mini Guts. Cell Stem Cell *19*, 425–427.

Sajgo, S., Ghinia, M.G., Brooks, M., Kretschmer, F., Chuang, K., Hiriyanna, S., Wu, Z., Popescu, O., and Badea, T.C. (2017). Molecular codes for cell type specification in Brn3 retinal ganglion cells. Proc. Natl. Acad. Sci. *114*, E3974–E3983.

Sarthy, V.P., Brodjian, S.J., Dutt, K., Kennedy, B.N., French, R.P., and Crabb, J.W. (1998). Establishment and characterization of a retinal Müller cell line. Invest. Ophthalmol. Vis. Sci. *39*, 212–216.

Sayyad, Z., Sirohi, K., Radha, V., and Swarup, G. (2017). 661W is a retinal ganglion precursor-like cell line in which glaucoma-associated optineurin mutants induce cell death selectively. Sci. Rep. *7*, 16855.

Shafaie, S., Hutter, V., Cook, M.T., Brown, M.B., and Chau, D.Y.S. (2016). In Vitro Cell Models for Ophthalmic Drug Development Applications. Biores. Open Access *5*, 94–108.

Shang, P., Stepicheva, N.A., Hose, S., Zigler, J.S., and Sinha, D. (2018). Primary Cell Cultures from the Mouse Retinal Pigment Epithelium. J. Vis. Exp.

Shapley, R., and Hugh Perry, V. (1986). Cat and monkey retinal ganglion cells and their visual functional roles. Trends Neurosci. *9*, 229–235.

Smukler, S.R., Runciman, S.B., Xu, S., and van der Kooy, D. (2006). Embryonic stem cells assume a primitive neural stem cell fate in the absence of extrinsic influences. J. Cell Biol. *172*, 79–90.

Sonntag, K.-C., Song, B., Lee, N., Jung, J.H., Cha, Y., Leblanc, P., Neff, C., Kong, S.W., Carter, B.S., Schweitzer, J., et al. (2018). Pluripotent stem cell-based therapy for Parkinson's disease: Current status and future prospects. Prog. Neurobiol. *168*, 1–20.

Sonoda, S., Spee, C., Barron, E., Ryan, S.J., Kannan, R., and Hinton, D.R. (2009). A protocol for the culture and differentiation of highly polarized human retinal pigment epithelial cells. Nat. Protoc. *4*, 662–673.

de Souza, C.F., Nivison-Smith, L., Christie, D.L., Polkinghorne, P., McGhee, C., Kalloniatis, M., and Acosta, M.L. (2016). Macromolecular markers in normal human retina and applications to human retinal disease. Exp. Eye Res. *150*, 135–148.

Sparrow, J.R., Hicks, D., and Hamel, C.P. (2010). The retinal pigment epithelium in health and disease. Curr. Mol. Med. *10*, 802–823.

Steinberg, R.H. (1985). Interactions between the retinal pigment epithelium and the neural retina. Doc. Ophthalmol. *60*, 327–346.

Stokkermans, T.J., and Trichonas, G. (2019). Chloroquine And Hydroxychloroquine Toxicity (StatPearls Publishing).

Strauss, O. (1995). The Retinal Pigment Epithelium (University of Utah Health Sciences Center).

Su, P.-J., Liu, Z., Zhang, K., Han, X., Saito, Y., Xia, X., Yokoi, K., Shen, H., and Qin, L. (2015). Retinal synaptic regeneration via microfluidic guiding channels. Sci. Rep. *5*, 13591.

Susaimanickam, P.J., Maddileti, S., Pulimamidi, V.K., Boyinpally, S.R., Naik, R.R., Naik, M.N., Reddy, G.B., Sangwan, V.S., and Mariappan, I. (2017). Generating minicorneal organoids from human induced pluripotent stem cells. Development *144*, 2338–2351.

Tada, M., Takahama, Y., Abe, K., Nakatsuji, N., and Tada, T. (2001). Nuclear reprogramming of somatic cells by in vitro hybridization with ES cells. Curr. Biol. *11*, 1553–1558.

Takahashi, K., and Yamanaka, S. (2006). Induction of Pluripotent Stem Cells from Mouse Embryonic and Adult Fibroblast Cultures by Defined Factors. Cell *126*, 663–676.

Takahashi, K., Tanabe, K., Ohnuki, M., Narita, M., Ichisaka, T., Tomoda, K., and Yamanaka, S. (2007). Induction of Pluripotent Stem Cells from Adult Human Fibroblasts by Defined Factors. Cell *131*, 861–872.

Takasato, M., Er, P.X., Chiu, H.S., Maier, B., Baillie, G.J., Ferguson, C., Parton, R.G., Wolvetang, E.J., Roost, M.S., Chuva de Sousa Lopes, S.M., et al. (2015). Kidney organoids from human iPS cells contain multiple lineages and model human nephrogenesis. Nature *526*, 564–568.

Takebe, T., Sekine, K., Enomura, M., Koike, H., Kimura, M., Ogaeri, T., Zhang, R.-R., Ueno, Y., Zheng, Y.-W., Koike, N., et al. (2013). Vascularized and functional human liver from an iPSC-derived organ bud transplant. Nature *499*, 481–484.

Takebe, T., Zhang, B., and Radisic, M. (2017). Synergistic Engineering: Organoids Meet Organs-on-a-Chip. Cell Stem Cell *21*, 297–300.

Thomson, J.A., Itskovitz-Eldor, J., Shapiro, S.S., Waknitz, M.A., Swiergiel, J.J., Marshall, V.S., and Jones, J.M. (1998). Embryonic stem cell lines derived from human blastocysts. Science *282*, 1145–1147.

Turgut, B., and Karanfil, F.C. (2017). Experimental Animal Models for Retinal and Choroidal Diseases. Adv. Ophthalmol. Vis. Syst. *7*, 1–0.

Valdés, J., Trachsel-Moncho, L., Sahaboglu, A., Trifunović, D., Miranda, M., Ueffing, M., Paquet-Durand, F., and Schmachtenberg, O. (2016). Organotypic retinal explant cultures as in vitro alternative for diabetic retinopathy studies. ALTEX *33*, 459–464.

Viravaidya, K., and Shuler, M.L. (2008). Incorporation of 3T3-L1 Cells To Mimic Bioaccumulation in a Microscale Cell Culture Analog Device for Toxicity Studies. Biotechnol. Prog. *20*, 590–597.

Wetts, R., and Fraser, S.E. (1988). Multipotent precursors can give rise to all major cell types of the frog retina. Science *239*, 1142–1145.

Wilmut, I., Schnieke, A.E., McWhir, J., Kind, A.J., and Campbell, K.H.S. (1997). Viable offspring derived from fetal and adult mammalian cells. Nature *385*, 810–813.

Witmer, A.N., Vrensen, G.F.J.M., Van Noorden, C.J.F., and Schlingemann, R.O. (2003). Vascular endothelial growth factors and angiogenesis in eye disease. Prog. Retin. Eye Res. *22*, 1–29.

Xiang, M., Zhou, L., Macke, J.P., Yoshioka, T., Hendry, S.H., Eddy, R.L., Shows, T.B., and Nathans, J. (1995). The Brn-3 family of POU-domain factors: primary structure, binding specificity, and expression in subsets of retinal ganglion cells and somatosensory neurons. J. Neurosci. *15*, 4762–4785.

Yeste, J., García-Ramírez, M., Illa, X., Guimerà, A., Hernández, C., Simó, R., and Villa, R. (2018). A compartmentalized microfluidic chip with crisscross microgrooves and electrophysiological electrodes for modeling the blood–retinal barrier. Lab Chip *18*, 95–105.

Yin, L., Smith, R.G., Sterling, P., and Brainard, D.H. (2009). Physiology and morphology of color-opponent ganglion cells in a retina expressing a dual gradient of S and M opsins. J. Neurosci. *29*, 2706–2724.

Yu, J., and Thomson, J.A. (2008). Pluripotent stem cell lines. Genes Dev. *22*, 1987–1997.

Yu, J., Vodyanik, M.A., Smuga-Otto, K., Antosiewicz-Bourget, J., Frane, J.L., Tian, S., Nie, J., Jonsdottir, G.A., Ruotti, V., Stewart, R., et al. (2007). Induced Pluripotent Stem Cell Lines Derived from Human Somatic Cells. Science (80-.). *318*, 1917–1920.

Zeiss, C.J. (2013). Translational models of ocular disease. Vet. Ophthalmol. *16*, 15–33.

Zemel, E., Loewenstein, A., Lei, B., Lazar, M., and Perlman, I. (1995). Ocular pigmentation protects the rabbit retina from gentamicin-induced toxicity. Invest. Ophthalmol. Vis. Sci. *36*, 1875–1884.

Zhang, W., Lin, S., Wang, C., Hu, J., Li, C., Zhuang, Z., Zhou, Y., Mathies, R.A., and Yang, C.J. (2009). PMMA/PDMS valves and pumps for disposable microfluidics. Lab Chip *9*, 3088.

Zhong, X., Gutierrez, C., Xue, T., Hampton, C., Vergara, M.N., Cao, L.-H., Peters, A., Park, T.S., Zambidis, E.T., Meyer, J.S., et al. (2014). Generation of three-dimensional retinal tissue with functional photoreceptors from human iPSCs. Nat. Commun. *5*, 4047.

9. List of Figures

10. List of Tables

11. Acknowledgement

First and foremost, I would like to thank my supervisor Stefan Liebau for his support throughout the years, from the very beginning of my bachelor's thesis until now. He was always open for my questions and concerns and provided me with a lot of personal and scientific freedom. I am so thankful for the friendly and relaxed atmosphere within the institute that he created.

Further, I would like to thank the whole committee for evaluating this thesis and also for the support and feedback during my Advisory Board Meetings.

Thanks to all current and former members of the Institute of Neuroanatomy – it has been a blast! Stefanie and Moritz Klingenstein (and of course Raphael!), Kevin Achberger, Virginia Cora, Lena Antkowiak, Leo Linta, Maíra Bertolessi Lourenço: you all made the long years and stressful days in the lab so much more fun. Thank you for all the support, conversations, lunches, barbeques and movie/series nights!
Also many thanks to Sabine Conrad and Clara Misbah, for your help in the lab, great advice and support.

Thanks a lot also to the Fraunhofer group: Peter Loskill, Christopher Probst, Johanna Chuchuy, Julia Rogal: It was so much fun working with you and I am really thankful for your support and providing me insights into the "Chip-world".

Last but not least, I want to thank my family, especially my parents Lilo and Wenzel: Thank you for your emotional and financial support throughout my whole studies. You always encouraged me in every situation. Also thanks to my brother Jens, and to Insa, Matilda and Emil for understanding and supporting me and – most importantly – making my life so much more fun!
And of course, my biggest THANK YOU to Matthias. I know that this must have been even more difficult for you than it has been for me. I could not have done this without you! Thank you for believing in me.